



UNIVERSITY OF AMSTERDAM



ANTON PANNEKOEK
INSTITUTE

Master Thesis

ON THE SEARCH FOR GRAVITATIONAL-WAVE PROGENITORS:
REDUCING THE COMPUTATIONAL COSTS OF BINARY
POPULATION SYNTHESIS USING ADAPTIVE IMPORTANCE
SAMPLING

FLOOR BROEKGAARDEN
10528105

Period:
JULY 2017 – JULY 2018

Degree:
MSC. ASTRONOMY & ASTROPHYSICS

Track:
ASTRONOMY & ASTROPHYSICS

Credits:
60 ECTS

Supervisor & Examiner:
DR. SELMA E. DE MINK, PROF ILYA MANDEL, PROF STEPHEN JUSTHAM

Second Reviewer:
PROF.DR. ALEX DE KOTER

Floor Broekgaarden: *On the search for Gravitational-Wave Progenitors:
Reducing the Computational costs of Binary Population Synthesis using
Adaptive Importance Sampling*, Master Thesis, July 2018

*"The fact that we live at the bottom of a deep gravity well,
on the surface of a gas covered planet going around a nuclear fireball
90 million miles away and think this to be normal is obviously some
indication of how skewed our perspective tends to be."*

— Douglas Adams

PREFACE

Preface

ABSTRACT

Abstract

POPULAR SUMMARY

Popular Summary

CONTENTS

I RESEARCH	1
1 INTRODUCTION	3
1.1 Low Mass X-ray Binaries	3
1.2 Common Techniques	6
1.3 Motivation	9
1.4 Outline	10
2 METHODS	15
2.1 Rossi X-ray Timing Explorer	15
2.2 Data Reduction	16
2.3 Timing Analysis	18
2.4 Spectral Analysis	21
2.5 Targets	21
2.6 Robustness of CHROMOS	22
3 RESULTS	27
3.1 Neutron Stars	27
3.2 Neutron Stars & Black Holes	29
3.3 Effects of Neutron Star Properties	31
4 DISCUSSION	39
4.1 Neutron Stars	39
4.2 Neutron Stars & Black Holes	41
4.3 Effects of Neutron Star Properties	43
4.4 Robustness	46
5 CONCLUSION	55
II APPENDIX	57
A A BRIEF GUIDE TO CHROMOS	59
B SOURCES	65
C POWER SPECTRA	69
D POWER COLOUR-COLOUR DIAGRAMS	79
E HARDNESS-HUE DIAGRAMS	83
F HARDNESS-INTENSITY DIAGRAMS	87
BIBLIOGRAPHY	91

LIST OF FIGURES

Figure 1	Artist's impression of a LMXB	4
Figure 2	Common diagrams for black holes	12
Figure 3	Common diagrams for neutron stars	14
Figure 4	Comparison of Aql X-1 PCC diagrams	22
Figure 5	Neutron stars in a PCC diagram	28
Figure 6	Defining the hue in a PCC diagram	30
Figure 7	Neutron stars in a HH diagram	30
Figure 8	Comparing energy and power colours	32
Figure 9	Comparison of neutron stars and black holes	32
Figure 10	Effect of shifting power colour frequency bands	33
Figure 11	Inclination effects	33
Figure 12	Comparing Atoll and Z sources	35
Figure 13	PCC diagram with Sco- and Cyg-like sources	35
Figure 14	PCCs during intermittent pulsations	37
Figure 15	The effect of spin frequency on PCCs	37
Figure 16	Overview power spectra	54
Figure 17	Power spectra with a hue of 0° - 20°	70
Figure 35	PCC diagrams for 4U to GX	80
Figure 39	HH diagrams for 4U to GX	84
Figure 43	HI diagrams for 4U to GX	88

LIST OF TABLES

Table 1	Object properties	23
Table 2	Alternative source names	67

ACRONYMS

AMSP	Accreting Millisecond Pulsar
ASM	All Sky Monitor
BBN	Broad Band Noise
EA	Event Analyser

ECC	Energy Colour-Colour
EDS	Experiment Data System
EIS	Extreme Island State
FB	Flaring Branch
GTI	Good Time Interval
HB	Horizontal Branch
HEASARC	High Energy Astrophysics Science Archive Research Center
HEXTE	High Energy X-ray Timing Experiment
HH	Hardness-Hue
HI	Hardness-Intensity
HIMS	Hard-Intermediate State
HMXB	High-Mass X-ray Binary
HS	Hard State
ISCO	Innermost Stable Circular Orbit
IS	Island State
LB	Lower Banana
LLB	Lower-Left Banana
LMXB	Low-Mass X-ray Binary
NB	Normal Branch
PCC	Power Colour-Colour
PCA	Proportional Counter Array
PCU	Proportional Counter Unit
QPO	Quasi-Periodic Oscillation
RMS	Root Mean Square
RXTE	Rossi X-ray Timing Explorer
SIMS	Soft-Intermediate State
SAA	South Atlantic Anomaly
SS	Soft State
UB	Upper Banana
VLE	Very Large Event

Part I
RESEARCH

INTRODUCTION

LOW MASS X-RAY BINARIES

The end of stellar evolution can be a violent, explosive affair, resulting in a variety of outcomes (see Benacquista, 2012, for a review). Occasionally these outbursts occur in binaries, potentially resulting in the creation of a compact object. Such a binary is classified as an X-ray binary, due to the relatively large fraction of energy emitted in the X-ray regime. A further distinction can be made by dividing these systems into High-Mass X-ray Binaries (**HMXBs**) and Low-Mass X-ray Binaries (**LMXBs**). The former refer to binaries where the companion star mass is above $\sim 10M_{\odot}$, however the focus of this work is on the latter – binary systems with a companion $\leq 1M_{\odot}$ (Tauris and van den Heuvel, 2006). The mass ratio and orbital separation is crucial in determining whether mass transfer will take place between both objects, and if so, which type. Whereas in **HMXBs** stellar winds are the primary accretion mechanism, in **LMXBs** this primarily occurs via Roche-Lobe overflow (Klein-Wolt, 2004).

Roche-Lobe overflow describes a manner in which matter is accreted from a companion to the primary object via the cusp of a gravitational potential. Rather than directly falling towards the compact object, matter must shed its angular momentum by slowly spiralling inwards in quasi-Keplarian orbits. This process leads to the formation of an accretion disk, in which matter loses angular momentum through friction, radiating away a significant fraction of energy (Frank, King and Raine, 2002). An example of such a system can be found in Fig. 1, showing an artist's impression of these components. Assuming the accretion disk radiates locally as a blackbody, the temperature of the disk T can be related to the radius R with $T \propto R^{-3/4}$ (Shakura and Sunyaev, 1976). As the temperature increases towards the centre of the disk, so does the frequency at which most radiation is emitted. While the outer regions of the accretion disk may radiate primarily in optical, in the centre this emission is in the X-ray regime. Using X-rays therefore allows the innermost regions of an accretion disk to be probed, an area strongly influenced by the central compact object.

The central regions of an **LMXB** are commonly split into two components – a geometrically thin, optically thick accretion disk emitting a multicolour blackbody and a centrally located geometrically thick, optically thin corona emitting a power law. Within the corona

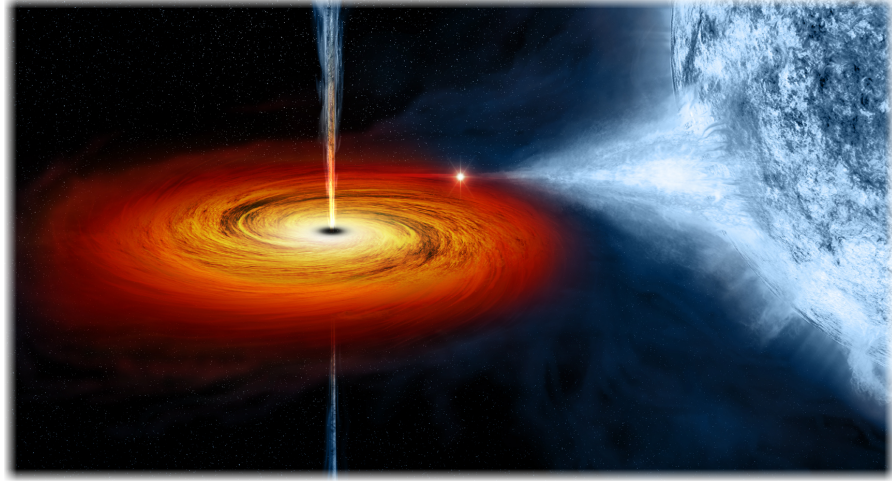


Figure 1: An artist’s impression of a LMXB, showing on a right a companion star from which matter is streaming via Roche-Lobe overflow onto an accretion disk on the left. The inner regions of the disc show jet formation, spewing energy into the surrounding environment. Adapted from NASA, (2014).

soft seed photons from the accretion disk are up scattered to higher energies via inverse Compton scattering (e.g. Done, Gierliński and Kubota, 2007). While at lower energies the power law is curbed by the minimum temperature of the accretion disk, the cut-off at higher energies depends both on the maximum energy a coronal electron can efficiently transfer to a photon and the number of scatterings a photon undergoes. The geometry of the coronal region is as of yet ill-defined, with models ranging from magnetic field-driven geometry (Galeev, Rosner and Vaiana, 1979) to patchy, flaring coronae (Gilfanov, 2010). A widely-accepted view holds the corona as the base of possible jets in such systems (e.g. Markoff, Nowak and Wilms, 2005), but the exact nature and origin of the corona remains unknown.

Black Holes & Neutron Stars

With accretion onto white dwarfs beyond the scope of this project, the focus turns to black holes and neutron stars. The former were predicted as far back as 1916, and in contrast to neutron stars show no surface, but instead an event horizon – the innermost boundary beyond which particles can not escape the gravitational pull of the black hole (Schwarzschild, 1916). Compact objects are thought to be formed during the collapse of star in a supernova, although some theories predict accretion onto white dwarfs as a possible channel for neutron star creation. Neutron stars are prevented from further gravitational collapse by neutron degeneracy pressure, provided the mass remains under the Tolman–Oppenheimer–Volkoff limit of ap-

proximately $3M_{\odot}$ (Oppenheimer and Volkoff, 1939; Rhoades Jr and Ruffini, 1974). With strong magnetic fields, such objects can accelerate particles to near-relativistic speeds. Should the magnetic axis be misaligned with respect to the rotation axis of a neutron star, then this can lead to pulsars, objects showing pulsed emission due to the rapid rotation of highly luminous beams.

The surface of neutron stars causes some distinct changes in observed emission features. Typically the energy spectrum of such systems will show an extra soft component resulting from surface emission, taking the shape of a comptonised blackbody (Done, Gierliński and Kubota, 2007). The extra soft seed photons also affect the higher energies in the resulting spectrum due to their contribution to the illumination of the hot inner flow. Next to the additional component in the energy spectra, neutron star surfaces can lead to additional effects not seen in black holes. Occasionally X-ray bursts in which the observed flux rapidly increases are seen originating from these objects, lasting from seconds to minutes. Bursters can show two types of bursts, type I bursts resulting from thermonuclear fusion on the surface of neutron stars, and type II bursts resulting from accretion instabilities. Occasionally type I bursts will show burst oscillations, presumed to originate from the rotational modulation of a hot spot on the surface of a neutron star (Watts, 2012). These burst oscillations provide a means to determine the spin frequency of the central compact object (pulsar periods being another) (Chakrabarty et al., 2003).

Accretion

There are a number of specific radii which are important to the accretion process. Starting from the centre of a compact object, these radii are often expressed in terms of the gravitational radius $r_g = GM/c^2$, with M the mass of the central object. For black hole LMXBs the most important limit is the event horizon. For non-rotating black holes, this is known as the Schwarzschild radius, located at $2r_g$ (Schwarzschild, 1916). White dwarfs and neutron stars however have surfaces rather than event horizons, affecting the emission from these inner regions. The rotation of a neutron star creates a boundary layer at which the angular velocity of accretion disk must decrease to match that of the neutron star, and is the point at which most kinetic energy is released (Done, Gierliński and Kubota, 2007; Frank, King and Raine, 2002). This difference between black holes and the other compact objects is thought to play an essential role in the observed emission of such systems (e.g. Ghosh and Lamb, 1978; Popham and Sunyaev, 2001; Shakura and Sunyaev, 1988). Further out, the strong gravitational fields of compact objects affect the stability of the inner orbits, resulting in the Innermost Stable Circular Orbit (ISCO) (Misner, Thorne and Wheeler,

¹⁹⁷³). Located at $6r_g$ for non-rotating objects, this boundary presents the innermost limit at which an accretion disk can truncate. White dwarfs and neutron stars can truncate a disk further away depending on the strength of their magnetic field. Within the so-called Alfvén radius, matter is expected to flow along magnetic field lines towards the central object (Lamb, Pethick and Pines, ¹⁹⁷³). Finally, there is the truncation radius of the accretion disk, which varies over time depending on the state of an object. To understand the background behind the various states, a brief overview of common analysis techniques is needed.

COMMON TECHNIQUES

Energy Spectra

Since the discovery of the first extra-terrestrial X-ray source Sco X-1 (Giacconi et al., ¹⁹⁶²) methods have been developed to study these sources. Perhaps the most obvious technique is the energy spectrum, providing information on the relative contributions of various components. Fig. 2a shows an illustration of a simple black hole energy spectrum including various components, with Fig. 3a showing the same for a neutron star. Denoted within the graphs are BB the multicolour disk blackbody, PL the power law emitted by the corona, FL the fluorescent iron line produced by hard coronal photons reflecting off the disk, and for the neutron stars BLBB, the boundary layer blackbody. While extremely simplified versions of energy spectra, especially the reflected component, they show the general shapes of the main components. While energy spectra provide a great deal of information on various components, the rapid change in relative strength of these components is difficult to parametrise. As such, the schematic representation of an black hole energy spectrum as given in Fig. 2a represents a just a single spectral state of the system, in this case a Soft State (SS). Also, while modelling spectra can be done to some accuracy for single and even multiple observations of the same object, it remains difficult to model an entire population of LMXBs.

Hardness-Intensity Diagrams

In order to be able to compare LMXBs with each other and study spectral evolution throughout an outburst, Hardness-Intensity (HI) diagrams were developed, showing the total intensity of an observation against the hardness of an energy spectrum. This latter term refers to the ratio of fluxes measured in two energy bands, with higher over lower energies, similar to how colours work in optical astronomy us-

ing Johnson photometry. Parametrising changes in the energy spectrum with hardness provides an model-independent parametrization of the spectral shape, allowing the spectral evolution to be traced. Fig. 2b shows an schematic diagram of a HI diagram for a black hole, with abbreviations denoting the canonical black hole states. Starting on the right side of the diagram is the Hard State (HS), transitioning in the top into the Hard-Intermediate State (HIMS), the Soft-Intermediate State (SIMS), and then on the left the Soft State (SS), before transitioning back through the SIMS and HIMS . The energy spectral evolution through these states is linked to geometric changes over long time scales. While in the hard state, the disk is thought to be truncated far from the compact object, moving inwards while transitioning into the soft state. The changes in geometry strongly affect the energy spectrum. Where in the hard state the disk blackbody is weak in comparison to the hard powerlaw, in the soft state the disk blackbody dominates with the powerlaw reducing in strength and getting softer. This can be understood in terms of the available soft seed photons from the disk. In the soft state a large fraction of disk blackbody photons are upscattered to higher energies due to their close proximity to the corona, but in the hard state this fraction decreases.

Energy Colour-Colour Diagrams

Although HI diagrams proved useful in describing the evolution of black holes, the evolution of neutron stars is best traced in a colour-colour diagram. To prevent confusion in successive terminology, this will be referred to as a Energy Colour-Colour (ECC) diagram. By analogy with the hardness parameter defined earlier, a softness parameter is defined, probing lower energies. This allows for a classification scheme based on a wider range in spectral shapes. Fig. 3b and 3c display such diagrams, showing ECC diagrams for two types of typical neutron star LMXBs, respectively classified as an atoll and a Z source. The clear distinction in ECC shapes and rapid variability properties, not to mention the high luminosity of Z sources, initially resulted in this division, but later research showed both types of objects could show similar tracks in the ECC diagram (Gierlinski and Done, 2002; Munoz, Remillard and Chakrabarty, 2002). With atolls showing a broad range of luminosities, they remain significantly lower than the luminosities of Z sources, radiating at near Eddington luminosity. The atoll ECC diagram is used to classify the spectral evolution of neutron stars by dividing the track into components, as denoted in Fig. 3b. Starting at the bottom are the banana states, from right to left, the Upper Banana (UB), the Lower Banana (LB) and the Lower-Left Banana (LLB). Increasing in hardness is then the Island State (IS) and finally the Extreme Island State (EIS). The luminosity

The tropical names – atolls, banana etc. – originate from the shape of their ECC tracks. Unfortunately this exotic theme was not extended to Z sources...

generally increases in the direction the track takes from from the **EIS** to the **LLB**. Transitions between these states can take days to weeks, in contrast to Z sources where transitions can be in the order of a few days (Lin, Remillard and Homan, 2009).

Switching to the Z source given in Fig. 3c reveals several branches distinct from atoll sources, notably the Horizontal Branch (**HB**), Normal Branch (**NB**) and the Flaring Branch (**FB**) (Hasinger and van der Klis, 1989). While the **NB** and **HB** show a smooth evolution in timing properties, the **FB** shows a strong discontinuity in timing features. Kuulkers et al., (1994) later subdivided Z sources into two classes, Cyg-like and Sco-like sources. The **ECC** diagram given in Fig. 3c is an example of a typical Cyg-like track, however for Sco-like sources the track is more similar to the shape of a ν . In case of a Cyg-like source the **HB** shrinks and tilts towards the **NB** while the **FB** expands up to the top right. This change in tracks has been to be linked to difference in magnetic fields (Psaltis, Lamb and Miller, 1995).

Power Spectra

In order to capture the timing properties of sources, power spectra can be used. Obtained from Fourier transforms, power spectra vary significantly between spectral states – whether for black holes or neutron stars. Black hole power spectra typically show a number of features, as displayed in Fig. 2c. Denoted with **BBN** is the broad band noise, forming a roughly triangular shape. Additionally there is a Quasi-Periodic Oscillation (**QPO**) alongside its harmonic. The study of QPOs is a field in itself (see van der Klis, 2006, for an overview), although two broad categories exist to explain the origin of these features – geometric and intrinsic models (van den Eijnden, Ingram and Uttley, 2016). While standing shocks in the accretion flow or changes in mass accretion rate were invoked as possible models in past years (e.g. Chakrabarti and Molteni, 1993; Tagger and Pellat, 1999), current studies strongly suggest an geometric origin (see Heil, Uttley and Klein-Wolt, 2015a; Motta et al., 2015, van den Eijnden, 2016, in prep).

Neutron star power spectra show similarities to black hole power spectra, however the presence of a boundary layer and surface make neutron star power spectra more complex (Klein-Wolt, 2004). Fig. 3d gives an schematic example of a neutron star power spectrum, comprising of various components commonly fitted with Lorentzians denoted here with L's. Evolution though spectral states, whether in banana states, or the branches in Z sources, is tied strongly to changes in the power spectrum – with components rising and falling in strength but also shifting in frequency. Previous studies comparing neutron

star with black hole power spectra provide a way to describe various components (e.g. Sunyaev and Revnivtsev, 2000; Wijnands and van der Klis, 1999; van der Klis, 1994), yet a method by which to describe the spectral evolution of LMXBs in a model-independent fashion remains elusive.

Power Colour-Colour Diagrams

The difficulties in tracking the timing evolution of LMXBs led Heil, Uttley and Klein-Wolt, (2015b) to develop Power Colour-Colour (PCC) diagrams. Inspired by ECC diagrams, PCC diagrams plot ratios of integrated power, or variance, of various frequency bands. Fig. 2d shows a schematic example of a PCC diagram, with PC1 showing the ratio of the variance in frequency band C over A on the horizontal axis, and PC2 showing the ratio of the variance in B over D. In this case, the frequency bands A – D refer to consecutive frequency bands in the power spectra, from low to high frequencies. It was discovered that black holes track a near-elliptical path in the PCC diagram, providing a unique manner in which the spectral evolution of black hole systems can be tracked. Denoted in Fig. 2d are the approximate positions of the HS, HIMS, SIMS and SS, showing a continuous path in evolutionary states. Preliminary research into the PCC track of a neutron star suggested parts of the PCC track differed from black holes power colours. Power colours might well help in establishing a single method by which the spectral evolution of both neutron stars and black holes could be described, providing a strong incentive for further study.

MOTIVATION

Compact objects provide insight into the final stage of stellar evolution, and are key to studying the effect of extreme gravitational fields on matter. Timing analysis allows these innermost regions to be observed at a far larger resolution than photometric analysis can achieve. Combining timing information with spectral information gives a trove of information from which a unique level of detailed insight can be gathered, from accretion theory to the properties of compact objects. A number of studies have been conducted into the timing properties of black holes and neutron stars, but require models to determine the evolution over time. With an entire archive of Rossi X-ray Timing Explorer (RXTE) data available, it is now possible to conduct a systematic, model-independent research into the variability of black holes and neutron stars, while testing the applicability of the newly-developed power colour technique.

OUTLINE

While this thesis is intended to be read in full, the possibility arises that earlier sections went unnoticed. As such, this thesis is prefaced by a foreword and several introductory texts. A scientific abstract is available for those working in the field of astronomy, and a popular summary for the general public. With this chapter having presented a brief background to this project, the following chapter describes the methods utilised as part of this thesis. In order to fully understand the intricacies of the data analysis, chapter 2 also gives information on the RXTE spacecraft and the data extraction routines specific to it. Information on the observed population of compact objects can also be found in this section. Chapter 3 then gives a purely phenomenological overview of the results, with interpretations and further discussion provided in chapter 4. The research conducted as part of this thesis is subsequently concluded in chapter 5. Supplementary information is provided thereafter, in part ii. Part ii forms the final part of this thesis, in which software details, nomenclature information and graphs pertaining to individual sources are given when inclusion in the main body of text would have prevented a clear flow of information.

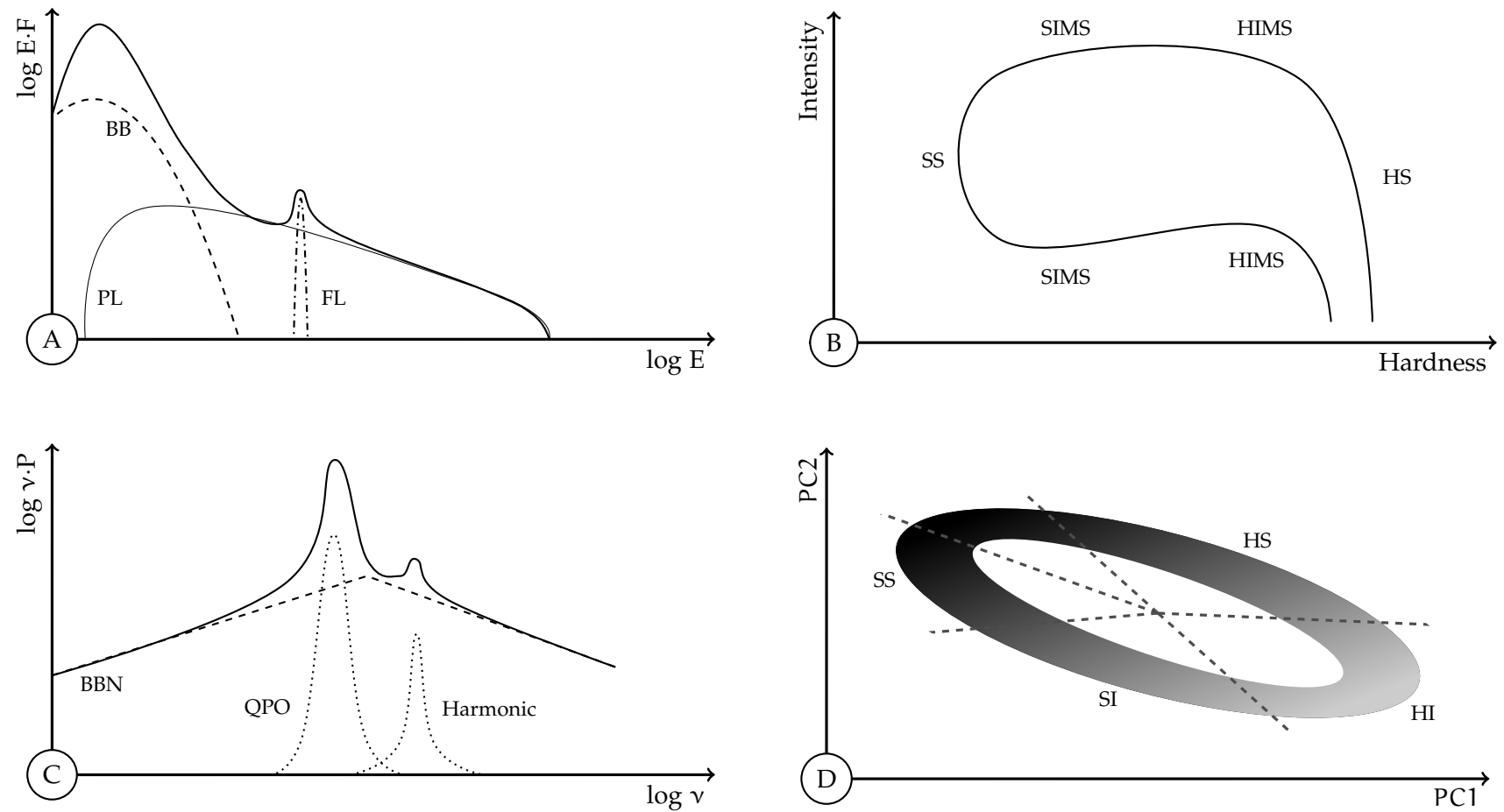


Figure 2: Common diagrams for black holes **UPPER LEFT** (A) A schematic representation of possible energy spectral components, plotted in terms of energy times flux. The disk blackbody BB is denoted by the dashed line, the powerlaw PL by the lower solid line, the fluorescent iron line FL by the dashdotted line, and the total in the upper solid line. With the energy spectra varying over time, these components can pivot and change significantly in intensity (for a full review see Gilfanov and Meroni, 2014). **UPPER RIGHT** (B) A sketch of a HI diagram, showing the general path along which black holes transition. The regions corresponding to canonical spectral states are given in the diagram, with the Hard State (HS), the Hard-Intermediate State (HIMS), the Soft-Intermediate State (SIMS) and the Soft State (SS) (Altamirano, 2008). While in this diagram the transition through the soft states is represented by a smooth line, it commonly is more jagged. **LOWER LEFT** (C) A representative power spectrum showing common components, with the broad band noise (BBN), a Quasi-Periodic Oscillation (QPO) and its associated harmonic. Based on Pahari et al., (2013). **LOWER RIGHT** (D) A schematic PCC diagram, showing the general trend of black hole power colour values. Sources transition along the oval shape, through the various spectral states delineated by the dotted lines. Abbreviations correspond to those adopted in the HI diagram in the upper right plot. The area with no labeling is an overlap of hard and soft states, in which observations can be distinguished with hardness or Root Mean Square (RMS) values. Based on Heil, Uttley and Klein-Wolt, (2015b).

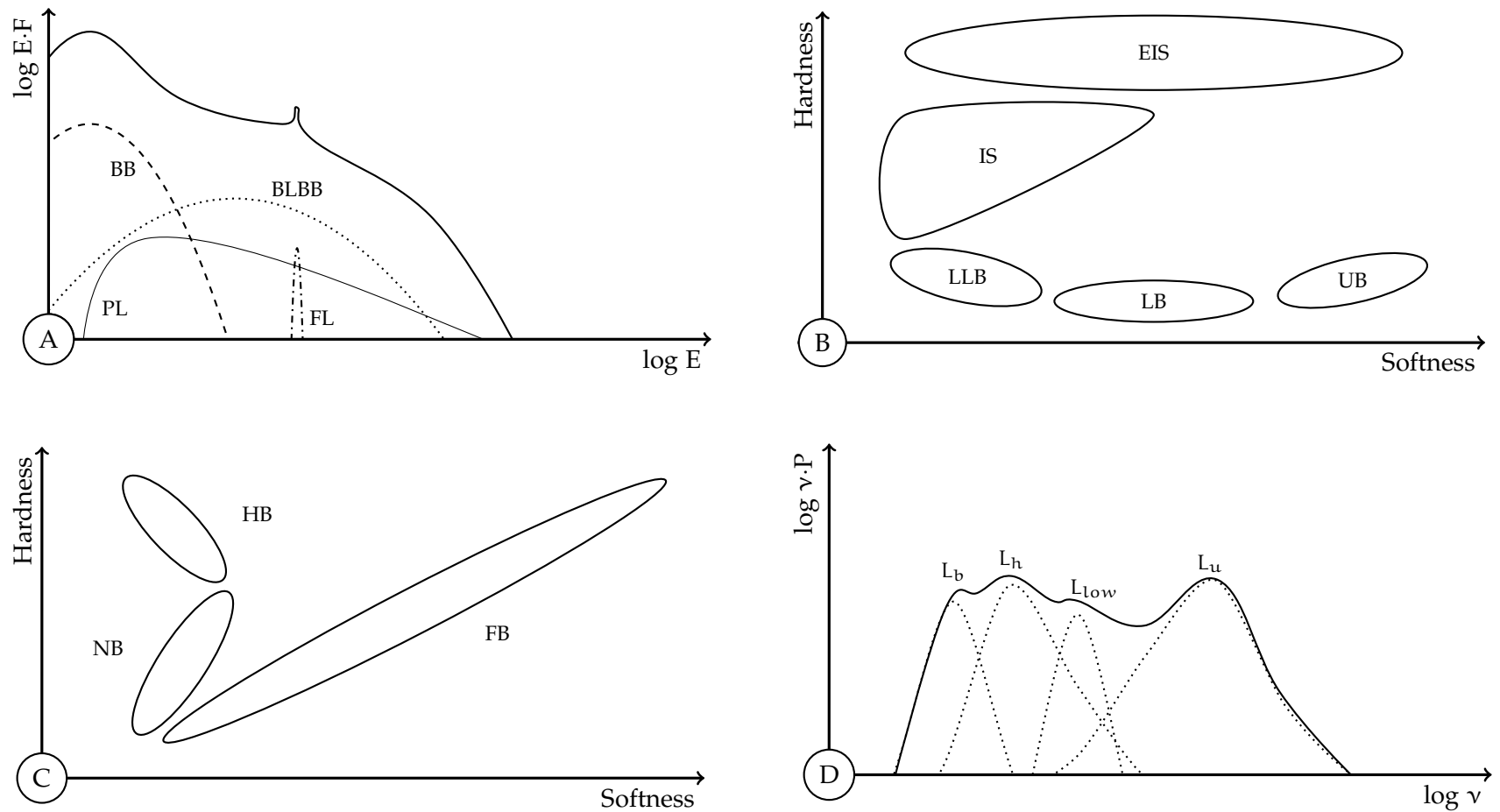


Figure 3: Common diagrams for neutron stars **UPPER LEFT** (A) A schematic representation of an energy spectrum showing the general shape of the main spectral components in terms of energy times flux (see Lin, Remillard and Homan, 2007). The abbreviation BB denotes a multicolour disk blackbody, FL a fluorescent iron line, BLBB the boundary layer blackbody and PL a powerlaw, with the total of all components represented by the upper solid line. **UPPER RIGHT** (B) A schematic **ECC** diagram for an atoll source, with various states denoted. Sources transition around the ‘C’ shape, with starting from the lower right the Upper Banana (**UB**), Lower Banana (**LB**), Lower-Left Banana (**LLB**), then the Island State (**IS**) and Extreme Island State (**EIS**) (Klein-Wolt, 2004). **LOWER LEFT** (C) A schematic **Z** source **ECC** diagram, showing the Horizontal Branch (**HB**), the Normal Branch (**NB**) and the Flaring Branch (**FB**) (Klein-Wolt, 2004). **LOWER RIGHT** (D) A simplified power spectrum of an atoll in the **EIS** state showing various commonly fitted Lorentzian components. These components can rapidly change in number, amplitude, and width over time, while shifting in frequency. Sharply peaked components can emerge at the higher frequencies, referred to as kHz Quasi-Periodic Oscillations (**QPOs**) (see Klein-Wolt, 2004; van Doesburgh, 2014).

2

METHODS

Rossi X-ray Timing Explorer

While a number of X-ray missions have been conducted over the years, RXTE remains a unique mission due to its extraordinary timing resolution (Bradt, Rothschild and Swank, 1993). Operating for more than 16 years from 1995 to 2012, RXTE built up a significant archive of transient X-ray sources, providing a large repository of LMXB observations (NASA, 2015). Using the High Energy Astrophysics Science Archive Research Center (HEASARC) online services, provided by the NASA/Goddard Space Flight Center, data can freely be downloaded for the full length of the mission. With a wide range of data types available, the variety in data products originates in the different instruments carried on board RXTE.

RXTE carried out observations with three observational instruments – the All Sky Monitor (ASM), the High Energy X-ray Timing Experiment (HEXTE) and the Proportional Counter Array (PCA) (Bradt, Rothschild and Swank, 1993). The ASM was designed to survey a large fraction of the sky every 1.5 hours, allowing the intensity and spectrum of more than 75 objects to be monitored. Upon rapid changes in either property, the HEXTE and the PCA could be pointed towards the target typically within a few hours. The energy ranges of the HEXTE and the PCA were designed to be complimentary, with the HEXTE observing from 15-200 keV, and the PCA from 2-60 keV (Jahoda et al., 1996). Both instruments had a 1° field of view, and a minimum timing resolution of $8\mu\text{s}$ for the HEXTE and $1\mu\text{s}$ for the PCA (Rothschild et al., 1998; Zhang et al., 1993).

Only observations conducted with the PCA are used throughout this project, providing an extensive source of data. Comprised of five Proportional Counter Units (PCUs), the PCA allowed energies to be determined to an energy resolution of less than 18% at 6 keV (RXTE, 2006a). Each PCU was filled with a mixture of Xenon and Methane gas, allowing charged particles to ionise the gas, resulting in an electrical pulse proportional to the energy carried by the incident particle (Zhang et al., 1993). An additional layer on top of each PCU contained propane gas in order to reduce the effect of background events. A gradual loss of propane occurred at the start of the mission, leaking through to the Xenon layers (Jahoda et al., 1996). Combined with other effects, this resulted in a gradual change in gain for which gain

epochs have to be defined to correct for these changes (RXTE, 2012b). The loss of the PCU0 propane layer in 2000 required the adoption of an additional calibration epoch. An internal radioactive source allowed for continuous energy calibration (Zhang et al., 1993).

With each active PCU providing data, information was sent to six Event Analysers (EAs) incorporated in the Experiment Data System (EDS) (Jahoda et al., 1996). This phase allows for data processing and compression before telemetry. Two of the EAs were programmed to run in standard configurations, with the others able to run in one of the seven different modes (RXTE, 1999). The sheer number of options, and parameters, needed to extract this data from the different modes requires a large set of extraction tools. With the previous paragraphs giving a brief overview of the hardware behind the observations, additional technical details on the PCA can be found in Zhang et al., (1993). Shifting to the data extraction and analysis side of data reduction requires specialised software, and is explained in the following section.

DATA REDUCTION

In order to conduct a systematic population study, a robust pipeline is needed to run through many scores of observations. While a number of tools are available to help in extracting data, these tools do not lend well to upscaling, often requiring a large number of input parameters for every data mode. To this end, the CHROMOS software pipeline was developed. The technical side of CHROMOS is described in appendix a, in the form of a manual, with information on the underlying methods presented in this section.

The HEASARC online services provides several interfaces for searching and retrieving RXTE data (RXTE, 2000). Using the web-based graphical user interface, a list of ObsIDs can be obtained for each target. ObsIDs are used to classify observations, and are an identification code which changes when a new target is acquired, or when the EA-modes change. ObsIDs follow the format of 'NNNNN-TT-VV-SSX', with NNNNN a five-digit proposal number, TT a two-digit target number, VV a two-digit viewing number, SS a two-digit number to identify different pointings and X a character to denote slewing, configuration changes etc (RXTE, 2000). An FTP-server allows for downloads to be conducted via the command line. Extracting this data requires some knowledge of the available data modes per observation. Two EAs modes should be permanently available, STANDARD1 with no energy information but a 0.125s timing resolution and STANDARD2 data with 129 spectral channels and a 16s time resolution (RXTE,

2013). A whole range of other data modes can also be present depending on the observation. These modes fall into two categories - science array (also known as binned-mode data) and science event format. Both formats require different tools and input to extract the data. Science array format includes data modes such as `BINNED` and `STANDARD2`, and science event format, data modes such as `GOODXENON` and `EVENT` mode. Each data mode can provide diverging timing resolutions depending on the binning method, but files must have a timing resolution higher than $1/128$ s for our subsequent analysis, with the exception of files for spectral analysis and background creation.

To ensure data remains a reliable reflection of the actual target emission, it must be filtered using Good Time Intervals (`GTIs`) (RXTE, 2012d). Following the RXTE cookbooks for science array and science event mode data, the ftool `MAKETIME` is used to set filter criteria (RXTE, 1998a, 2006b, 2012d). To ensure the earth brightness does not contaminate observations, the pointing elevation is set to be above 10° . Additionally, the pointing offset is set to be less than 0.02° and the number of active PCUs set to be greater than one. For all objects save for black holes and Sco X-1, up to 10min since the South Atlantic Anomaly (`SAA`) is removed and an electron count larger than 0.1 is removed to prevent electron contamination. The former sources show sufficiently high count rates to neglect this last criterion, and with current backgrounds able to account for the `SAA` passage, the filtering on time since `SAA` is not required. Using information from standard filter files, the times at which a change in number of PCUs occurs are noted, allowing for 32s around these transitions to be filtered during extraction. This prevents any surge, or change in electrical current, from contaminating the count rate.

The SAA refers to an area in which the Earth's magnetic field is reduced in strength, causing an increase in high energy particle count rates (ROSAT, 2002).

Background files are created from `STANDARD2` files together with standard filter files using the ftool `PCABACKEST` (RXTE, 1998b). This estimated background spectrum also requires a provided model file. With sources showing a net count rate larger than 40 ct/s/PCU, the 'bright' background model can be used for all sources (RXTE, 2012c). Having created background files, the sole step left before extracting the main data files, is determining the correct energy channel ranges. This final part is potentially the most complicated part of CHROMOS, requiring a number of steps. On the basis of the observation date, an initial channel range can be selected using the energy-channel conversion table (RXTE, 2012b). If files are in `EVENT` or `BINNED` mode, then the header of these files will show the channel binning, which can vary from observation to observation. The final channels can be selected using this information, in which channel bins closest to the energy range 2-13 keV are selected while ensuring the lowest energy

channels are omitted (see Gleissner et al., 2004).

Extracting data requires two ftools: `SAEXTRCT` for `EVENT` and `GOODX-ENON` files and `SEEXTRCT` for `STANDARD2` and `BINNED` files (RXTE, 1998d,e). The input parameters can be determined using the files and information generated in the previous steps, with exception of the timing resolution. This is set to $1/128$ s for all files save for `STANDARD2` files, which are extracted with their intrinsic resolution of 16s. A background file is extracted for each subsequent data file to ensure the same filter criteria are applied. `STANDARD2` files are extracted for PCU2 only, the sole PCU with an intact propane layer of the course of the mission, and the most stable one. While the low timing resolution of `STANDARD2` files prevents any high precision timing analysis from taking place, this data is well-suited to spectral analysis. `STANDARD2` files are therefore extracted as both spectra and light curves, rather than just as light curves as all other data modes are.

TIMING ANALYSIS

Light curves must be background corrected, which necessitates the rebinning of background light curves to match the resolution of the original light curve files. This is done on basis of interpolation between each consecutive background data point. Subtracting these values from the light curve count rates produces a light curve suitable for further analysis. To prevent the flares from affecting the general variability trend throughout a single observation, X-ray bursts are identified and removed for all neutron star systems. Tests showed that two consecutive count rates above a Root Mean Square (`RMS`) per observation of 7σ provided a strong indication for an X-ray burst. Numerous methods for automatically identifying the start and end of the bursts were tested, but in the end a choice was made to cut fixed time bins on either side. Approximately 3s was cut before each detection, and 625s afterwards. Further discussion on this method can be found in section 4.4.4.

In order to conduct timing analysis, a switch must be made to the frequency domain. Unless specified elsewhere, all following information is based on work presented in Uttley et al., (2014). While a variety of techniques are available to conduct time-series analysis (e.g. Legg et al., 2012; Maccarone, Coppi and Poutanen, 2000), discrete Fourier transforms are the most prevalent. These transforms can be calculated with

$$X_n = \sum_{k=0}^{N-1} x_k e^{2\pi i n k / N} \quad (1)$$

with X_n the discrete Fourier transform, N the number of time bins and x the k^{th} value of the light curve. X_n is calculated in steps of $f_n = n/N\Delta t$ with Δt the width of a time bin and with $n = 0, 1, 2 \dots N/2$. The maximum frequency is thus 64 Hz due to the $1/128$ s time resolution of the extracted light curves. In order to obtain a power spectrum, the discrete Fourier transform is multiplied with its complex conjugate

$$|X_n|^2 = X_n X_n^* \quad (2)$$

The resulting power spectrum is subsequently normalised with

$$P_n = \frac{2\Delta t}{\langle x \rangle^2 N} |X_n|^2 \quad (3)$$

in which $\langle x \rangle$ is the mean flux of the light curve. This leads to units in terms of fractional variance per Hz (Belloni and Hasinger, 1990). With the exception of perhaps an Accreting Millisecond Pulsar (AMSP), few sources show fully periodic signals over all observations, but will usually show shifting power spectral components. A decision must therefore be made on the total time over which to Fourier transform. With power spectra errors dependent on the number of power spectra over which is averaged, a trade-off is established. Reducing the noise on the final power spectrum requires averaging over many segments, but in the process reduces the sensitivity to varying power spectral components. Following the procedure given in Heil, Uttley and Klein-Wolt, (2015b), a choice is made to take discrete Fourier transforms of each m^{th} segment of 512s in an observation, and average these power spectra:

$$\bar{P}_n = \frac{1}{M} \sum_{m=1}^M P_{n,m} \quad (4)$$

in which M is the total number of segments in an observation. This number is limited not just by the total length of the light curve, but also by gaps due to PCU changes, X-ray bursts etc. The decision to bin across each observation is expanded on in section 4.4.3, where alternative binning methods are also discussed.

With power spectra flattening towards higher frequencies, a correction can be applied by calculating the white noise present in the power spectrum with

$$P_{\text{noise}} = 2 \frac{\langle x \rangle + \langle b \rangle}{\langle x \rangle^2} \quad (5)$$

in which $\langle x \rangle$ is the mean count rate and $\langle b \rangle$ is the mean background count rate in \bar{P}_n . The resulting noise value can be subtracted from the power spectrum. The associated errors on the noise corrected power spectrum are then calculated by dividing each power by \sqrt{M} . As the powers are χ^2_2 -distributed, errors on the power spectrum can be approximated as Gaussian provided a large number of samples are binned.

Power spectral evolution can be parametrised using power colours, as described in section 1.2. These can be calculated using the power spectra obtained for each observation. First, the integrated power, or variance V , can be calculated using

$$V = \Delta\nu \sum_{i=\nu_{\text{low}}}^{\nu_{\text{high}}} \bar{P}_i \quad (6)$$

with $\Delta\nu$ the Nyquist frequency and \bar{P}_i the power in frequency i , running between the four equally spaced frequency bands of 0.0039-0.031 Hz, 0.031-0.25 Hz, 0.25-2.0 Hz and 2.0-16.0 Hz (Heil, Uttley and Klein-Wolt, 2015b). This results in a variance value V for each consecutive frequency band, respectively referred to as V_A , V_B , V_C and V_D . Defining two power colours as

$$\text{PC1} = \frac{V_C}{V_A} \quad \text{and} \quad \text{PC2} = \frac{V_B}{V_D} \quad (7)$$

allows an observation to be placed in a PCC diagram, with PC1 on the horizontal axis and PC2 on the vertical axis. The associated error values can be calculated from the errors on the variance, determined with

$$\text{Err}^2(V) = \frac{(\Delta\nu)^2}{M} \sum_{i=\nu_{\text{low}}}^{\nu_{\text{high}}} \bar{P}_i^2 \quad (8)$$

as given by Heil, Vaughan and Uttley, (2012). Note that the summation is over the average squared power, rather than over the squared average power. Power colour errors can subsequently be calculated with simple error propagation

$$\text{Err}(\text{PC1}) = \text{PC1} \sqrt{\left(\frac{\text{Err}(V_C)}{V_C} \right)^2 + \left(\frac{\text{Err}(V_A)}{V_A} \right)^2} \quad (9)$$

and $\text{Err}(\text{PC2})$ in analogous fashion.

SPECTRAL ANALYSIS

Spectral analysis is conducted with `STANDARD2` files, due to both their energy resolution, and their relative ease of use. The ftool `PCARSP` is run for all files prior to any analysis, allowing response files to be created from energy spectra and filter files (RXTE, 1998c). These response files can be used by the X-ray spectral-fitting program `XSPEC` (Arnaud, 1996) to ensure an accurate representation of count rates in each energy bin after subtracting background values. Energies outside the range 2–13 keV are ignored, before unfolding the energy spectrum around a flat powerlaw. In doing so, the energy spectrum is effectively being divided by the effective area of the instrument response, providing energy spectra independent of long term changes in instrument response (Heil, Uttley and Klein-Wolt, 2015a). The energy spectral hardness is calculated for a variety of energy bands, by integrating the count rate over energy and dividing the resulting flux of the higher energy band by that of the lower energy band. These fluxes are additionally summed, to obtain the relative total intensity.

TARGETS

In order to compare the variability properties of both black hole and neutron star LMXBs, a selection of objects is required. An overview of the chosen objects can be found in Tab. 1 and includes information on various system parameters. The choice of objects was based primarily on the number of RXTE observations available, but also on the system type. These were chosen to ensure a good spread across both atoll and Z sources, as well as various inclinations, accretion states etc. Sources have been divided by compact object, with neutron stars above the centre line, and black holes below. Most columns should be self-explanatory, however `#GOOD` may require additional explanation. This refers to the number of ObsIDs which have power colour ratios with a fractional variance constrained at a 3σ -level in each frequency band. Further discussion on these values can be found in section 4.4.2, in which various selection effects are examined. The object names used in this table and throughout this thesis were selected to reflect the most common name in use. Alternate source names can however be found in Tab. 2, presenting source designations from the 4U, GX, IGR, INTEGRAL1, SWIFT, X and XTE catalogues (SIMBAD, 2016). The choice of black holes systems was made on basis on of PCC diagram coverage as presented in Heil, Uttley and Klein-Wolt, (2015b), providing a representative sample of possible black hole power colour tracks.

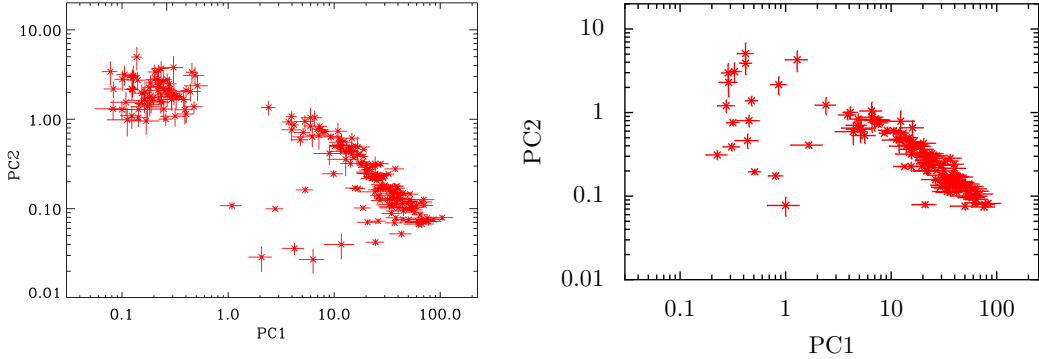


Figure 4: **LEFT** Power colour ratios obtained for Aql X-1 by Heil, Uttley and Klein-Wolt, (2015b). To ensure clarity, the original figure has been adapted by removing power colours from black hole systems. **RIGHT** Power colour ratios obtained with CHROMOS for Aql X-1. Only power colours with a fractional variance constrained at a 3σ level in each frequency band have been included.

ROBUSTNESS OF CHROMOS

Initial tests of the pipeline were conducted by comparing power colours of Aql X-1 with prior results presented in Heil, Uttley and Klein-Wolt, (2015b). Both the results can be seen in Fig. 4, with left showing power colours from Heil, Uttley and Klein-Wolt, (2015b) and right showing results obtained with CHROMOS. Similar tracks are found for Aql X-1 with both methods, save for the top left corner of the PCC diagram where observations are primarily in the soft state. A close inspection revealed differences in noise correction, where (Heil, Uttley and Klein-Wolt, 2015b) used spectral fitting to obtain the white noise, in contrast to the approach taken in this work. Additional binning effects also played a role, and are discussed further in section 4.4.3. The power colours track of black holes obtained with CHROMOS showed only minor differences in comparison to those obtained in Heil, Uttley and Klein-Wolt, (2015b). Further tests were also conducted on parameters related to energy spectra, revealing similar hardness and intensity values in past spectral studies. Suggestions on scientific improvements to CHROMOS are given in the discussion, section 4, with coding recommendations in appendix a.

Table 1: Overview of LMXBs showing system properties and observation details, sorted by compact object type, and then by name. Alternative source names can be found in appendix b, in table 2. Systems are divided into atolls (A), Z sources (Z), accreting pulsars (AP), accreting millisecond pulsars (AMP), and objects showing characteristics of both atoll and Z sources (AZ). A further division is made between persistent accretion-powered pulsars with burst oscillations (P), intermittent ones (I) and burst oscillation sources without detectable accretion-powered pulsations (B) (see Watts, 2012, for a review). Intermittent sources have been assigned to the pulsar or burster group on basis of their timing properties (van Doesburgh, 2014). Spin frequencies have been given where possible, as are inclination angles. #GOOD gives the total number of observations with a significant detected variance at a 3σ -level in all four power colour frequency bands. The total number of available ObsIDs in the RXTE archive are also given per source. References are denoted with numbers, and are given at the bottom of this table.

SOURCE	TYPE	BURSTER / PULSAR	SPIN FREQ. (HZ)	INCLINATION ($^{\circ}$)	#GOOD	#OBSID	REFERENCES
4U 0614+09	A	B	414.7	86	85	502	1,2,2,3
4U 1636-53	A	B	581.9	64	45	1556	4,5,2,6
4U 1702-43	A	B	329		28	210	7,5,5
4U 1705-44	A			51	55	516	8,9
4U 1728-34	A	B	363	50	55	405	7,5,5,10
Aql X-1	A	I/B	550.3	72–79	145	596	4,5,2,11
Cir X-1	AZ			90	52	811	12,13
Cyg X-2	Z			62.5	62	567	8,14
EXO 0748-676	A	B	552.5	75	93	746	15,5,16,17
GX 17+2	Z				4	206	8

SOURCE	TYPE	BURSTER / PULSAR	SPIN FREQ. (HZ)	INCLINATION ($^{\circ}$)	#GOOD	#OBSID	REFERENCES
GX 340+0	Z				5	97	8
GX 349+2	Z				3	142	8
GX 5-1	Z				5	167	8
HETE J1900.1-2455	AMP	I/P	337.3	30	129	361	18,5,19,20
IGR J00291+5934	AMP		599		45	479	21,22
IGR J17480-2446	AP	P	11		42	159	23,5,23
IGR J17498-2921	AMP	P	401		3	129	24,5,24
KS 1731-260	A	B	524		21	82	7,5,5
SAX J1808.4-3658	AMP	P	401	55	25	1337	25,5,25,26
SWIFT J1756.9-2508	AMP	B	182		19	50	27
Sco X-1	Z			30	48	598	8,28
Sgr X-1	A				12	109	8
Sgr X-2	Z				35	88	12
V4634 Sgr	A				119	1008	29
XB 1254-690	A				10	94	30
XTE J0929-314	AMP	B	185		7	46	31,31,22
XTE J1701-462	AZ			60	94	872	12,28
XTE J1751-305	AMP	B	435		21	274	32

SOURCE	TYPE	BURSTER / PULSAR	SPIN FREQ. (HZ)	INCLINATION ($^{\circ}$)	#GOOD	#OBSID	REFERENCES
XTE J1807-294	AMP	P	190		4	112	33,2,22
XTE J1814-338	AMP	P	314		17	93	34,5,22
GX 339-4	BH				391	1401	35
H1743-322	BH				123	558	36
XTE J1550-564	BH				141	423	37

1 Méndez et al., (1997) 2 van Doesburgh, (2014) 3 Schulz et al., (2010) 4 Liu, van Paradijs and van den Heuvel, (2001) 5 Watts, (2012)
 6 Pandel, Kaaret and Corbel, (2008) 7 Galloway et al., (2008) 8 Hasinger and van der Klis, (1989) 9 Di Salvo et al., (2009)
 10 Shaposhnikov and Titarchuk, (2002) 11 Galloway et al., (2016) 12 Fridriksson, Homan and Remillard, (2015) 13 Iaria et al., (2008)
 14 Orosz and Kuulkers, (1999) 15 Homan, Fridriksson and Remillard, (2015) 16 Galloway et al., (2010) 17 Parmar et al., (1986)
 18 Watts et al., (2009) 19 Morgan, Kaaret and Vanderspek, (2005) 20 Papitto et al., (2013) 21 Galloway et al., (2005) 22 Gladstone,
 Done and Gierliński, (2007) 23 Papitto et al., (2011b) 24 Papitto et al., (2011a) 25 Wijnands and van der Klis, (1998) 26 Cackett et al.,
 (2009) 27 Krimm et al., (2007) 28 Crampton et al., (1976) 29 van Straaten, van der Klis and Wijnands, (2005) 30 Bhattacharyya, (2007)
 31 Galloway et al., (2002) 32 Markwardt et al., (2002) 33 Markwardt, Smith and Swank, (2003) 34 Markwardt and Swank, (2003)
 35 Wijnands and van der Klis, (1999) 36 Homan et al., (2005) 37 Homan et al., (2001)

3

RESULTS

NEUTRON STARS

Using CHROMOS, power colours can be obtained for a large number of observations. Applying CHROMOS to the population of neutron stars given in Tab. 1 reveals that most objects follow similar tracks in the PCC diagram. This can be seen in Fig. 5, where a distinct elliptical shape emerges after overplotting these tracks. In this plot PC1 is defined as the variance in (0.25–2.0 Hz)/(0.0039–0.031 Hz) and PC2 as the variance in (0.031–0.25 Hz)/(2.0–16.0 Hz). Only objects with more than three data points were included, and two objects were excluded due to their peculiar behaviours. A full discussion on the nature of those objects can be found in section 4.1. For sake of clarity, only points where the variance is $>3\sigma$ in all four frequency bands are plotted, and error bars are omitted. Typical error bars are on the order of 17% of the power colour values. Individual tracks can be seen more clearly in appendix d, where each object has been plotted with the neutron star PCC tracks in reference.

While using power colours is useful in comparing evolutionary tracks of systems, power colours require two dimensions (PC1 and PC2) to classify the state of a system. Reducing this down to a single parameter can be helpful in comparing the state of a system against other parameters. To this end, the ‘hue’ parameter can be introduced (Heil, Uttley and Klein-Wolt, 2015b). Defined as the angle of a point in the PCC diagram with respect to a central point, hue runs in a clockwise direction from a line in the Northwest direction from 0° to 360° . Following the original classification of the hue centre given in Heil, Uttley and Klein-Wolt, (2015b), a central point with the coordinates (4.51920, 0.453724) is chosen as reference point. An example of this classification can be seen in Fig. 6, where the neutron star PCC diagram has been divided into hue bins of 20° .

These hue bins allow an overview of power spectra to be created per hue bin, showing typical power spectra for a variety of objects. Comprising of various types of neutron star systems, these power spectra can be found in appendix c. Intrinsic scatter in the power, especially at the high frequencies, is reduced by binning data points linear in log-frequency and errors reduced accordingly.

In colour theory, hue is defined as the attribute by virtue of which a colour is red, green, etc (OED, 1976), and is often determined using a colour wheel. This makes hue an excellent analogy to the angle within a PCC diagram.

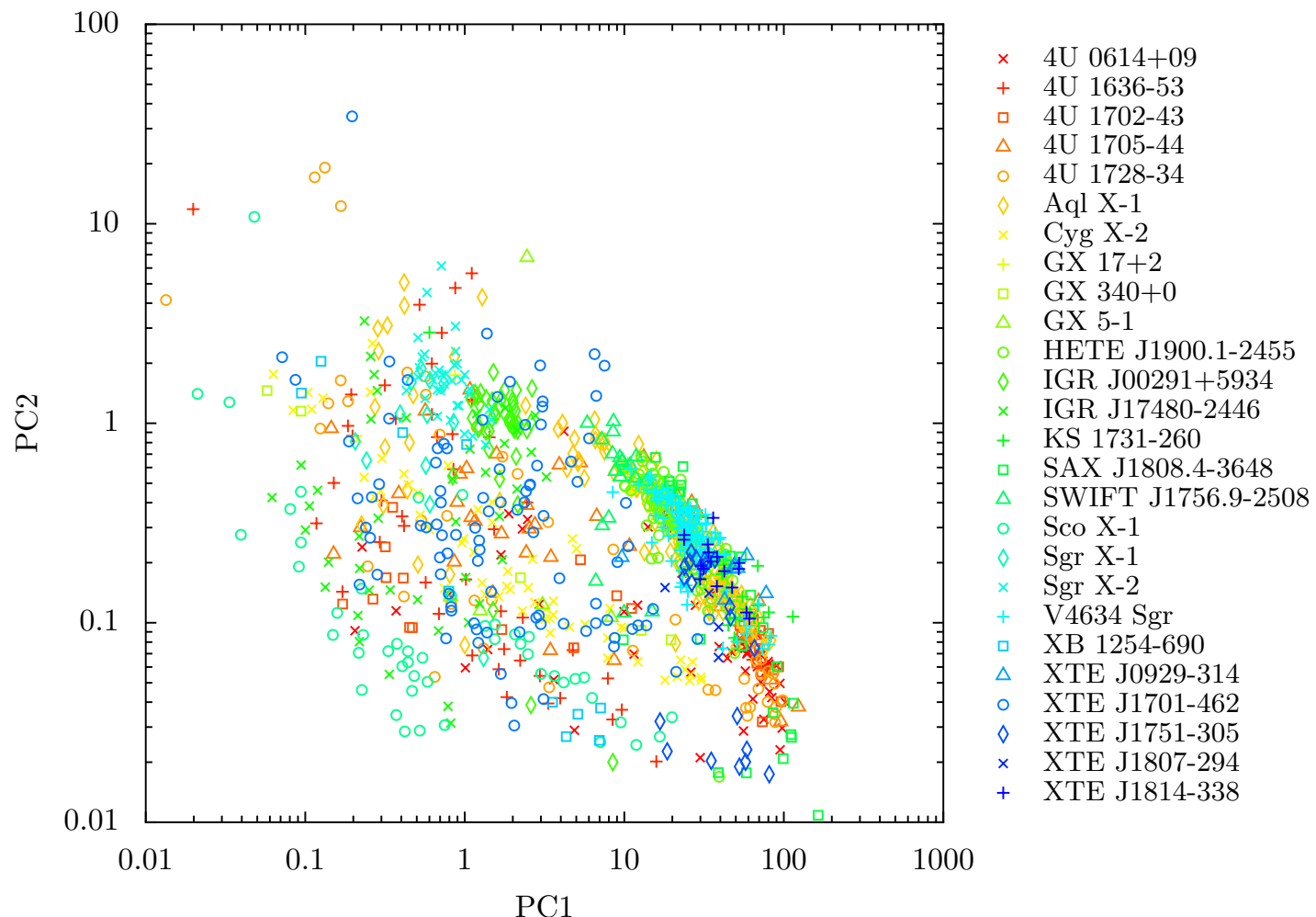


Figure 5: A PCC diagram showing tracks for neutron stars. While providing an excellent overview of the general trend, tracks of individual objects can perhaps be best pursued in appendix d, where PCC diagrams can be found for each system.

An interesting parameter to compare hue with, is the energy spectral hardness. Linking timing information back to spectral information can provide valuable insights into properties of systems such as the relative spectral evolution and therefore changes in inner region structure. A Hardness-Hue (HH) diagram for neutron stars can be seen in Fig. 7, with the hardness defined as the ratio of the total count rate in 9.7-16.0 keV over the total count rate in 6.4-9.7 keV. Next to the selection methods for PCC points described in the first paragraph of this section, only points with a hue-error $< 30^\circ$ are included in this graph, where errors are propagated through from the PCC-errors. In a similar fashion to the PCC diagrams in appendix d, individual HH diagrams can be found in appendix e, allowing the evolution of an object within a HH diagram to be traced against other neutron stars.

An often-used method in X-ray astronomy to trace the overall secular evolution of LMXBs is the HI diagram (e.g. Done and Gierliński, (2003), Klein-Wolt and van der Klis, (2008) or Fridriksson, Homan and Remillard, (2015)). In a HI diagram the energy spectral hardness is plotted against the relative intensity of an object. Appendix f shows HI diagrams for the full population of systems given in Tab. 1, allowing a broad range of tracks to be compared. A number of objects show unusual tracks, a point discussed in more detail in section 4.1.

In order to fully encapsulate the evolution of neutron star LMXBs, ECC diagrams are preferred over HI diagrams. The tracks in the ECC diagram are commonly divided into various states — the EIS, the IS and the banana branch, with the LLB, the LB and the UB. Linking the states of atoll source Aql X-1 with the PCC diagram reveals an interesting link as shown in Fig. 8. Here the softness is defined as the ratio of the total count rate in 3.5-6.0 keV over the total count rate in 2.0-3.5 keV, with the hardness retaining the same definition as earlier. For clarity, error bars on the energy colours have been left off the ECC diagram, typically being small in comparison to the PCC values. A clear distinction can be made in the PCC diagram between sources in the EIS, and sources in the banana states. While the IS does not show up in the PCC diagram, other objects showed this state to be located left of the lower apex, a region with relatively few PCC due to the rapid state transitions.

NEUTRON STARS & BLACK HOLES

In order to conduct a model-independent comparison of accreting black hole and neutron star variability, PCC diagrams can be constructed to show the evolution of both black hole and neutron star systems. In the left panel of Fig. 9, three representative transient black holes have been plotted for comparison with neutron stars, with additional

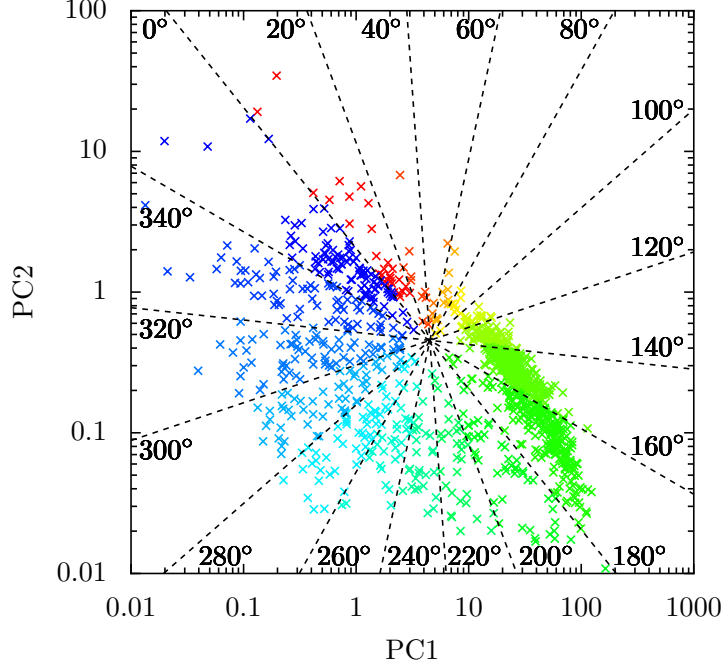


Figure 6: A PCC diagram showing the division of 20° hue bins for neutron star PCCs. The starting angle is defined as the angle at 45° in a counter-clockwise direction from the axes. Based on Fig. 2b from Heil, Uttley and Klein-Wolt, (2015b).

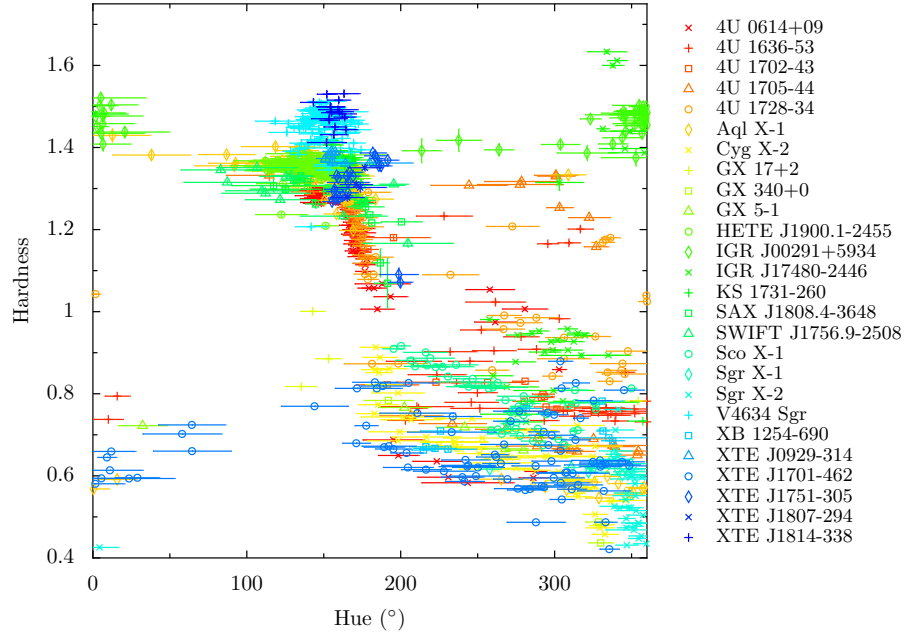


Figure 7: A HH diagram showing the evolution of PCC-tracks for neutron stars through use of the hue. Supplementary HH diagrams can be found in appendix e, showing the tracks of individual objects with neutron star HH tracks as reference.

information on these systems in Tab. 1. Both types of system show similar paths, yet a clear distinction is found on the right-hand side of the diagram where the black holes systematically follow a higher path with respect to the neutron stars. In the right panel of Fig. 9, a HH diagram is shown for the same systems, where the hardness is classified as the same ratio of (9.7–16.0 keV)/(6.4–9.7 keV). With the hue washing out any radial differences in PCCs, in the HH diagram the black holes closely follow the neutron stars albeit with a broader coverage of angles.

While black hole and neutron star LMXBs have similar broad-band spectral shapes, the frequency at which power spectral features occur can be a factor five higher for black holes than for neutron stars (Klein-Wolt, 2004). Thus comparing PCC values of black holes with neutron stars could perhaps best be done by shifting the frequency ranges for neutron star power colours up by a factor of five in the power spectrum. This causes the original frequency band boundaries to shift up to 0.0195, 0.155, 1.25, 10 and 64 Hz, where the final frequency is limited by the resolution in which light curves were extracted. Fig. 10 shows the result of shifting the frequency bands for neutron stars. In the left panel, the original PCC values for neutron stars can be seen in red against the black hole PCC values in grey. In the right panel are respectively the shifted PCC values, shown against the unaffected black hole PCC values. While the shifted PCC values show a greater overlap between neutron star and black hole PCCs, both tracks can still be distinguished.

EFFECTS OF NEUTRON STAR PROPERTIES

Inclination

Power colours present the unique ability to compare various parameters of multiple systems throughout different energy spectral states. Using power colours in such a fashion, Heil, Uttley and Klein-Wolt, (2015a) found black holes systems followed an inclination-dependent track in the HH diagram. Applying the same technique to neutron stars results in Fig. 11, where sources have been split into either a low ($i \leq 60^\circ$) or high ($i > 60^\circ$) binary orbit inclination group using Tab. 1, following the division adopted in Heil, Uttley and Klein-Wolt, (2015a). Errorbars have been omitted for clarity and sources with an undefined inclination plotted in grey. While no particular trend can be discerned from the PCC diagram, the resulting HH diagram shows signs of an offset dependent on inclination, with low inclination sources showing higher hardness per hue than high inclination sources. Implications of this trend are discussed in section 4.3.1, including suggestions on possible origins.

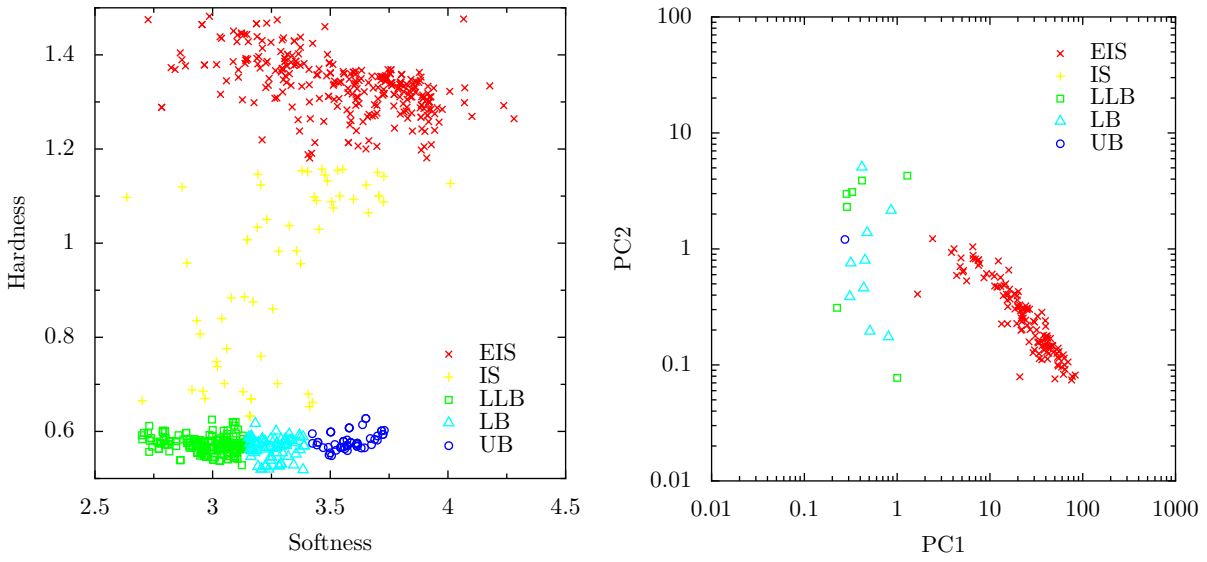


Figure 8: **LEFT** A **ECC** diagram for Aql X-1, showing the commonly-adopted division into various states: the Extreme Island State (**EIS**), the Island State (**IS**) and the banana branch, with the Lower-Left Banana (**LLB**), the Lower Banana (**LB**) and the Upper Banana (**UB**). **RIGHT** A **PCC** diagram showing observations linked to the various states defined using the **ECC** diagram.

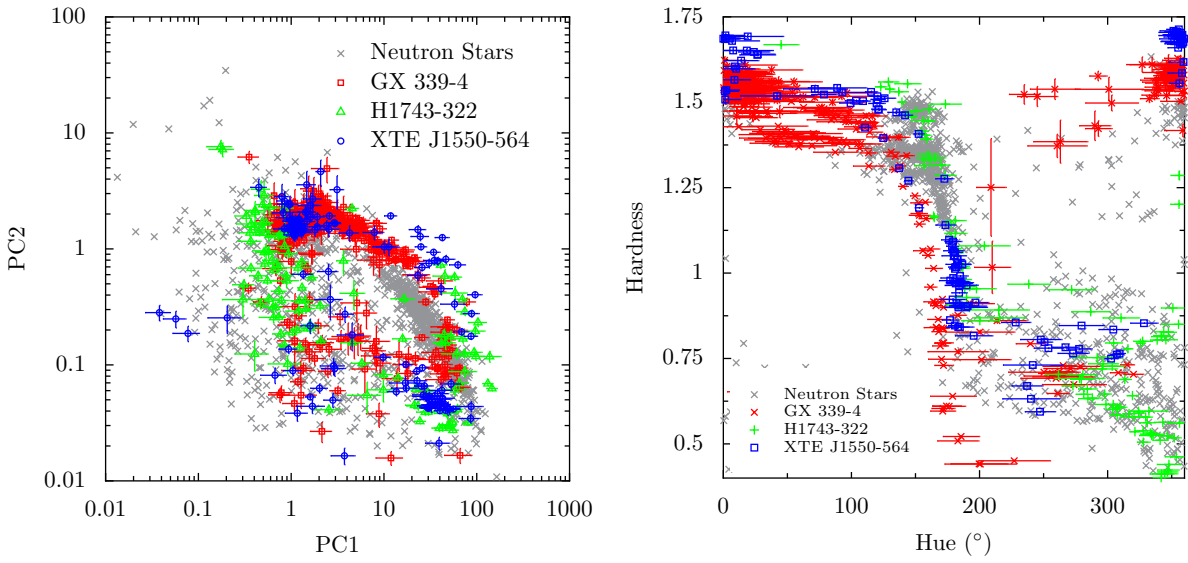


Figure 9: **LEFT** A **PCC** diagram showing black hole systems, with in grey the neutron star **PCCs** in Fig. 5 as reference. **RIGHT** The same systems plotted in a **HH** diagram.

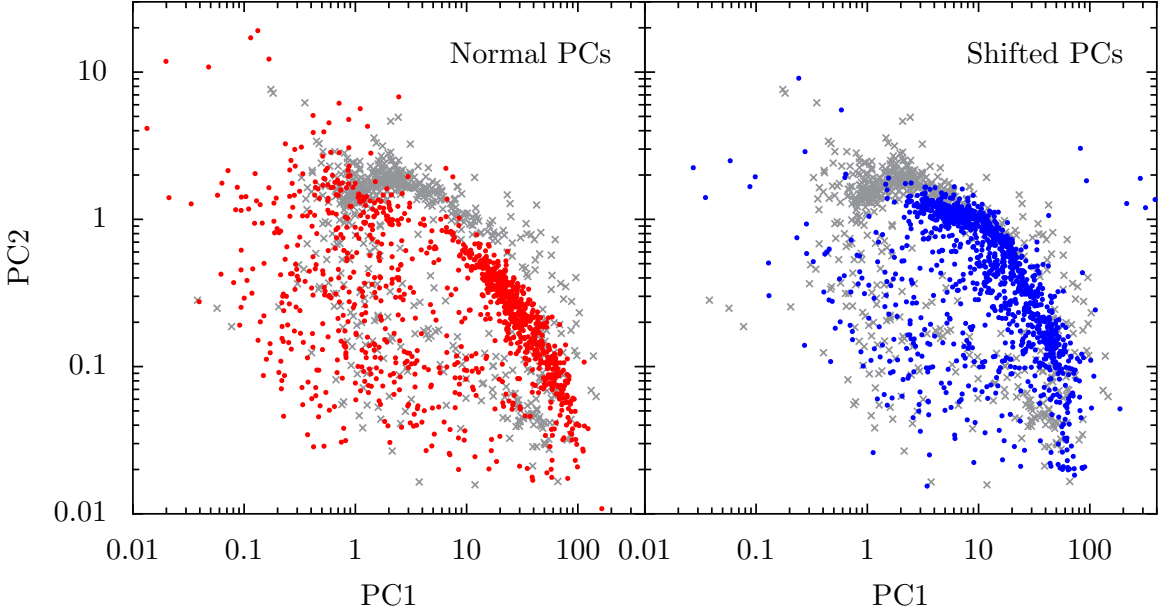


Figure 10: LEFT A PCC diagram showing neutron stars in red against black hole systems in grey. RIGHT PCCs for neutron stars where the frequency bands have been shifted up by a factor of five. The black hole systems in grey have retained the original frequency bands for their PCC values.

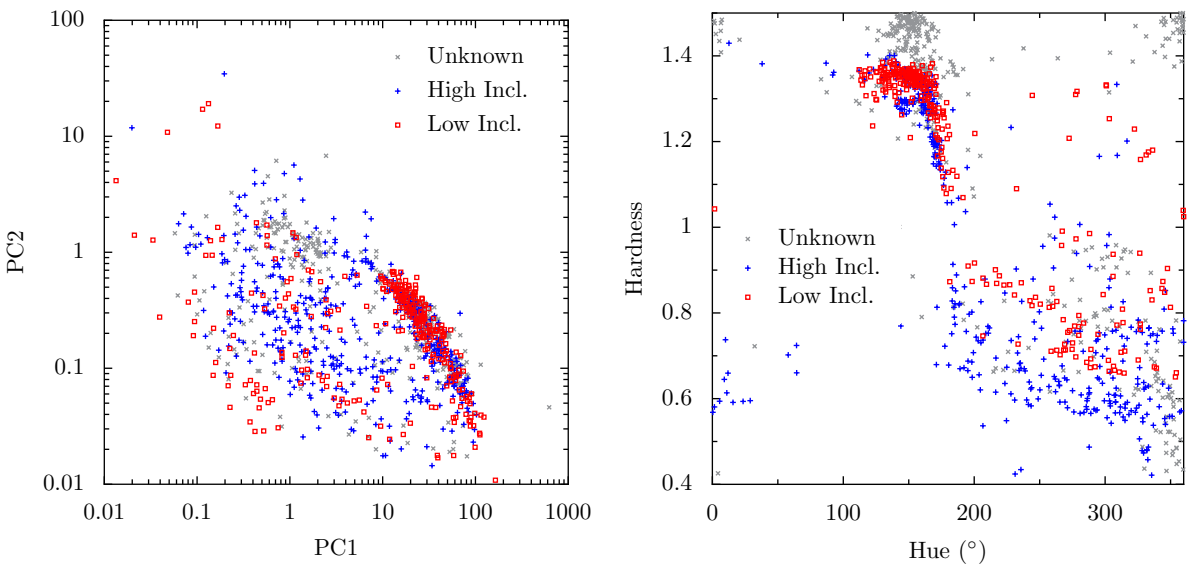


Figure 11: LEFT A PCC diagram with neutron star systems split into high and low inclination groups. Sources with an undefined inclination have been plotted in grey. Details on the inclination of individual sources can be found in Tab. 1. RIGHT A HH diagram with neutron star systems divided in the same manner.

Atoll & Z Sources

Based on the path LMXBs trace out in a [ECC](#) diagram, neutron star systems can be classified into two subclasses: atoll and Z sources (Hasinger and van der Klis, 1989). In Tab. 1, systems classified as either an atoll or a Z source have been denoted with respectively an A or a Z. A comparison of these systems in the [PCC](#) and [HH](#) space can be seen in Fig. 12. Plotted together with unclassified neutron stars, the Z sources in the [PCC](#) diagram rarely cross into the upper-right half of diagram. This is reflected in the [HH](#) diagram, where almost all Z source values remain above a hue of 180° . No particular difference can be discerned between atoll and as of yet unclassified sources, with atoll sources tracing a similar path to the latter.

A further division can be made in Z sources on the basis of spectral and timing behaviour, allowing sources to be split into Cyg- and Sco-like sources (Kuulkers et al., 1997). Nonetheless, there are only a few sources which have been classified as Cyg- or Sco-like sources, as seen in Tab. 1. These can be plotted in a [PCC](#) diagram, as seen in Fig. 13. With Z sources rarely straying beyond the lower left corner, a large degree of scatter is expected, and is found in the [PCC](#) values. It is interesting that there is seemingly a lower degree of scatter for the Cyg-like sources in comparison to the Sco-like sources.

Pulsations & Spin

Since the discovery of the first [AMSP](#) by Wijnands and van der Klis, (1998), systematic searches have revealed fourteen other systems of this nature (see Patruno and Watts, 2012, for a review). One such source, HETE J1900.1-2455, was the first to show ‘quasi-persistent’ activity (Galloway et al., 2006). Believed to be due to a build-up and subsequent suppression of magnetic field through channeling of the accreting flow (e.g. Cumming, Zweibel and Bildsten, 2001), it provides an effective test for a possible correlation between magnetic fields and [PCCs](#). Fig. 14 shows a selection of observations split into time intervals of standard luminosity levels and time intervals with pulsations. Selections were made on basis of the fractional pulse amplitudes between MJD 53520–53690 as given in Galloway et al., (2006). Though the [PCC](#) diagram hints at higher PC₂ values during pulsation periods, no conclusive correlation can be determined, with relatively few observations available to distinguish any trends.

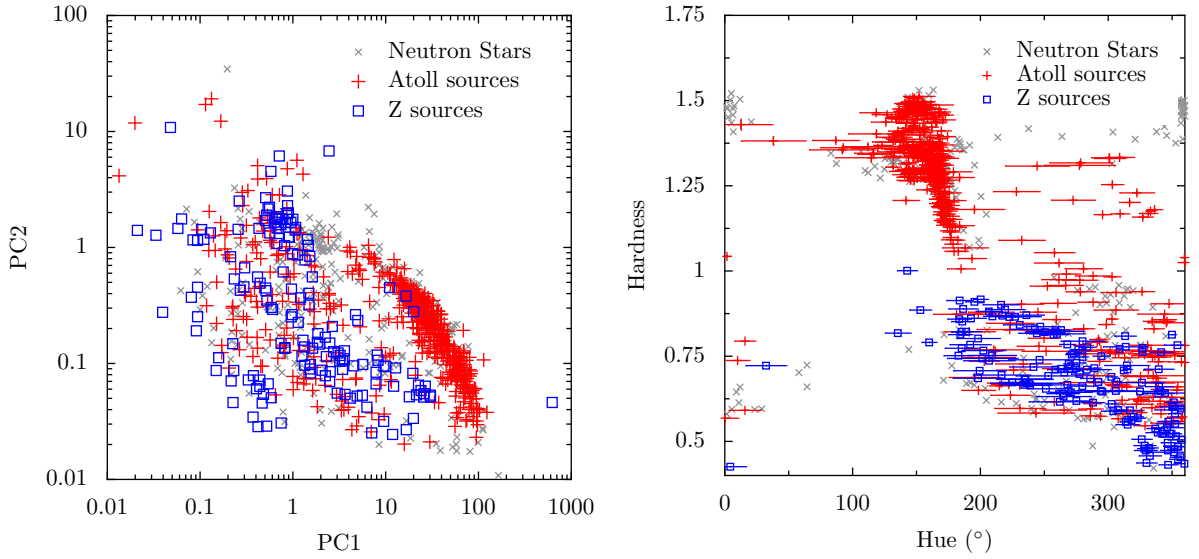


Figure 12: LEFT PCC diagram with systems classified as atoll sources in red, Z sources in blue and unclassified sources in grey. An overview showing the type of each individual system can be found in Tab. 1. RIGHT Replotting the same systems in a HH diagram.

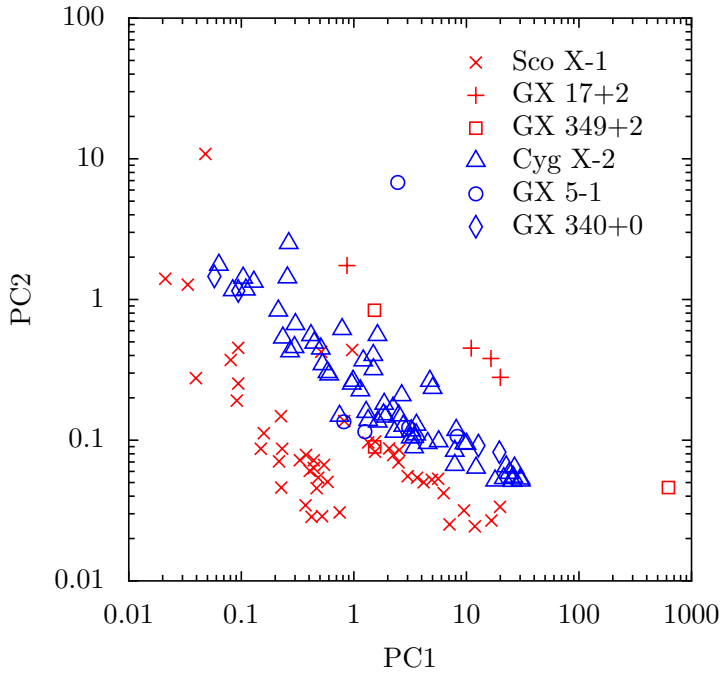


Figure 13: PCC diagram with Z sources. Sco-like sources are plotted in red and with Cyg-like sources in blue. Note the large contributions of Sco X-1 and Cyg X-2 to each respective group.

Pulsations in neutron star LMXBs are commonly used in an attempt to establish the spin frequency of the neutron star, resulting in groups of objects referred to as respectively bursters and pulsars. It is generally accepted that the rapid increase in flux observed in bursters is linked to unstable nuclear burning on the neutron-star surface (e.g. van der Klis, 2000), providing a means to determine the spin frequency of the neutron star through hotspots on the neutron star surface (see Chakrabarty et al., 2003; Strohmayer and Bildsten, 2003). In contrast, pulsars show regular pulsations, resulting in extremely precise spin frequencies. While spin frequencies typically fall far from the frequency bands that power colours probe, some effect of the higher spin frequencies could perhaps be expected to be seen in the lower power colour frequencies. The spin could for instance affect the accretion flow via the pulsar magnetosphere. Coupling spin frequencies with PCCs results in Fig. 15, with objects colour-coded according to their spin frequency. Objects with less than four points have been removed from the sample, to ensure clarity. Bursters show no distinct effects on PCCs, however a tentative link could perhaps be found in pulsar systems where a shift in PCCs according to spin frequency can be observed. An in-depth discussion on this relation can be found in section 4.3.3, as well as an hypothesis on the origin of this tentative relationship.

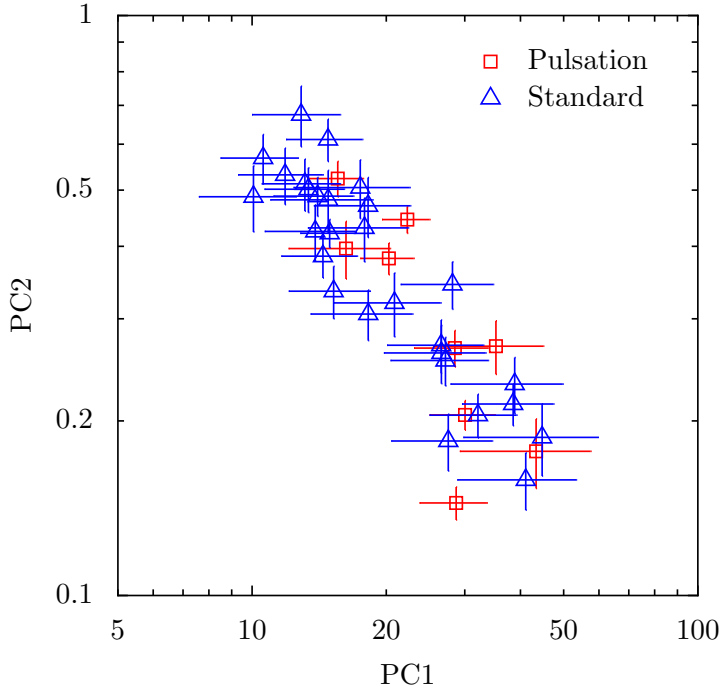


Figure 14: A PCC diagram with observations of HETE J1900.1-2455 split into pulsation time intervals and periods of standard flux-levels. The division between these time intervals was made on basis of information in Galloway et al., (2006).

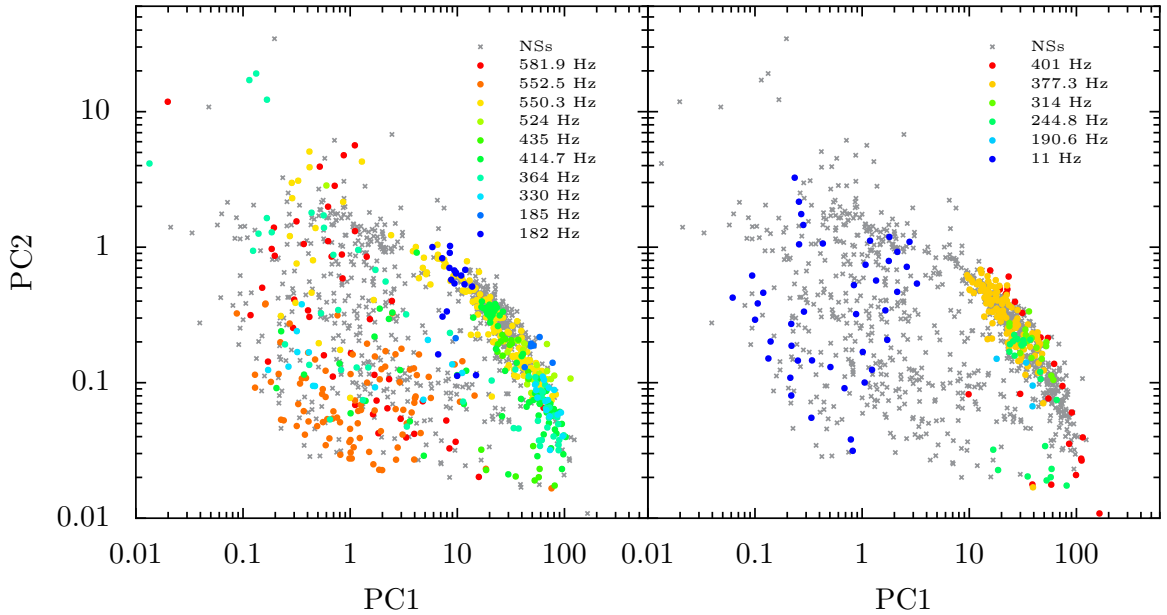


Figure 15: LEFT Bursters plotted in order of frequency, with neutron star LMXBs without a defined spin frequency in comparison. RIGHT PCC diagram showing pulsars per spin frequency together with the PCC values of the other neutron stars.

4

DISCUSSION

NEUTRON STARS

The paths followed by neutron stars in the PCC diagram given in Fig. 5 reveal some interesting points. Firstly, the tracks trace out an elliptical shape, similar to the paths black holes showed in Heil, Uttley and Klein-Wolt, (2015b). Secondly, while the tracks follow a tight track towards the bottom right, a large degree of scatter is found in the left part of the diagram. Thirdly, as visible in appendix d, few sources show a complete oval track across the full PCC diagram, but more often remain confined to particular sections. In order to understand the evolution of neutron stars in the PCC diagram, an in-depth look at the general trend in power spectral properties is warranted. Both Fig. 16 and appendix c show the evolution of power spectra throughout the PCC diagram, with appendix c containing additional power spectra. Similar to the work done previously in Heil, Uttley and Klein-Wolt, (2015b) for black hole systems, the following paragraphs describe the observed trends per spectral state. To help with placing neutron stars in the context of black holes, the choice is made to describe the neutron star evolution in terms of the corresponding black hole states.

HARD STATE With the hard state ranging from a hue angle of approximately 340° – 140° , neutron star power spectra commonly are broad and flat (appendix c; Figs. 17–23). The flat power spectra result in PCC values tending to be located around (1,1) as seen in Fig. 6. Though some overlap occurs between the hard and the soft state in the PCC diagram, a distinction between both states can be made using the energy spectral hardness or the total RMS variability (Heil, Uttley and Klein-Wolt, 2015b). Neutron star power spectra and black hole power spectra are broadly comparable in behaviour at these hues, though errors tend to be smaller in black hole systems. An interesting point is that black hole systems show a relatively well-defined track in the PCC diagram in this state, similar to the neutron stars, as can be seen in Fig. 9. The relative narrowness of the track in comparison to other states seems however to be stronger in neutron stars.

HARD-INTERMEDIATE STATE Transitioning from the hard state at approximately 140° up to about 220° , a broad ‘hump’ gradually starts to emerge at the central frequencies of neutron star power spectra, slowly growing and shifting to higher frequencies (appendix c; Figs. 24–27). While black hole power spectra typically show strong type C

QPOs at these hue values (Heil, Uttley and Klein-Wolt, 2015b), similar **QPOs** in neutron stars tend to be less prominent in comparison to the overall power. Most noticeable are the low frequency **QPOs** appearing in the power spectra of for instance XTE J1701-462 and Cyg X-2. Heil, Uttley and Klein-Wolt, (2015a) showed that removing the type C **QPOs** in this state for black hole systems significantly reduced the scatter in the softer hard-intermediate states. Potentially a similar effect would be expected with neutron stars, whereby **QPOs** partially contribute to the scatter observed at the lower apex. The role of **QPOs** in power colours is discussed further in section 4.3.1, coupling the effects of **QPOs** on power colours with possible **QPO** origins.

SOFT-INTERMEDIATE STATE Ranging between approximately 220° – 300° , neutron star power spectra show increasingly steeper spectra at high frequencies, with additional power emerging at lower frequencies (appendix c; Figs. 28-31). Together with the soft state, observations show a large degree of variability in the power spectra, with sudden troughs and peaks appearing from one observation to the next. While black holes typically show strong variability rapidly reducing in power at high frequencies in this state, neutron stars seem to show only the slightest drop in power at these high frequencies. Extending neutron star power spectra out to higher frequencies would show a rapid drop at kHz frequencies (Klein-Wolt, 2004), but with power colours only probing lower frequencies this plays no role in the analysis. Similar to the black holes, neutron stars show a large degree of scatter in the **PCC** diagram in this state.

SOFT STATE The final canonical spectral state runs from approximately 300° to 20° . Coupled with a high count rate in comparison to observations in the hard state, neutron star power spectra show an increasing likeness to black hole power spectra. Power spectra flatten out fairly rapidly, with power falling away at the highest frequencies (appendix c; Figs. 32-34).

Spectral States

While the evolution of neutron stars across the **PCC** diagram can be understood in terms of power spectral evolution, the strength of power colours lies in their ability to describe the spectral state evolution of black holes. Establishing such a relation for neutron stars spectral states would allow neutron star and black systems with similar states to be compared, and therefore is the primary aspect for which neutron star power colours should be tested. While black holes shows a relation between spectral states and their **PCC** track, this relationship does not necessarily have to hold for neutron stars. Commonly

spectral states in neutron stars are defined on basis of **ECC** diagrams. Similar to power colours, the ratios reduce the influence of shifting energy dependent features and provide a means of classifying sources. Difficulties arise however upon comparing various sources with each other, where Z-shaped tracks can cause atoll sources to be classified as Z sources (see Gierlinski and Done, 2002; Muno, Remillard and Chakrabarty, 2002). As seen in Fig. 8 for Aql X-1, several of these states can be linked to directly to the states exhibited by black holes. A clear relationship can be established between the **EIS** and the hard state in the black holes systems as noted by van der Klis, (1994). While individual banana states do not show distinct paths in the **PCC** diagram, the banana state as a whole is unambiguously related to the soft states of black hole systems. With neutron stars commonly transitioning quickly through the lower apex in the **PCC** diagram, it is difficult to link the **IS** to the intermediate states of black hole systems. Tentative links emerge between these states while looking at **PCCs** with errors slightly larger than the 3σ cut applied to the **PCC** diagrams.

Inspecting the combination of **PCC**, **HH** and **HI** diagrams provides an alternative way to test the link between spectral states and position in the **PCC** diagram. Tests show an excellent agreement between for instance high intensity observations with a high hardness and the position in the **PCC** diagram, located in the area corresponding to hard states in black holes. Such relationships break down however for two objects – Cir X-1 and EXO 0748-676. Since these two sources display differing power colour behaviours by which potential misclassification of spectral states could arise, they were removed from the general overview of neutrons star power colours seen in Fig. 5, and from further analysis. A full discussion on the nature of these sources is given in section 4.4.1.

NEUTRON STARS & BLACK HOLES

Fig. 9 shows the striking similarity between neutron star **PCC** tracks and black hole ones, confirming the power spectral relationships explored in previous studies (e.g. Klein-Wolt and van der Klis, 2008; Sunyaev and Revnivtsev, 2000; Wijnands and van der Klis, 1999). While specific power spectral features vary between neutron stars and black holes, the congruity in **PCC** paths show the broadband components under 16 Hz change in a similar fashion regardless of the compact object.

The second noticeable feature is the clear distinction between both types of objects in the upper-right part of the **PCC** diagram. Originat-

ing from the broad component present in neutron star power spectra, which is absent from black hole power spectra (see Sunyaev and Revnivtsev, 2000), it provides an excellent means of distinguishing black holes and neutron stars in a model-independent way. As explored in earlier studies, the broader power spectra of neutron stars exhibit similar features to black hole power spectra at lower frequencies (Klein-Wolt and van der Klis, 2008). Shifting the power colour frequency bands up for neutron stars might allow for a more accurate comparison to be made between the evolution of neutron stars and black holes. Fig. 10 shows the effect of shifting the frequencies up for black holes - a slight deformation of the original PCC track, and to some degree a larger overlap of neutron star with the black hole systems on the left side. A sharper break can however be seen in the upper right corner, with differences remaining between the tracks in the upper right corner and at the upper apex. With neutron star power spectra showing a larger degree of variability in the low frequencies in the left side of the PCC diagram, it could stand to reason that the scatter is reduced, with the influence of variability in the lower frequencies being suppressed. With neutron star power spectra extending up to several kHz, additional research into the effects of broader frequency bands would be welcomed in order to fully encapsulate power spectral evolution.

The strong relationship between the tracks neutron stars and black holes display in the PCC diagram, as well as the link between canonical neutron star and black hole states provides a strong case for a common geometric model for both types of systems. The comparable variability properties of black holes and neutron stars at low frequencies call for a convergence of accretion models and for a common treatment of LMXBs. This ties into models such as that developed by Lyubarskii, (1997), in which variability originates from propagating fluctuations in the accretion flow. These fluctuations provide a link between variations in mass accretion in the outer regions of a disk on long time scales, and short time scales in the inner regions. Evidence for this model leads from the relationship between the RMS variability and count rate of a source (Heil, Vaughan and Uttley, 2012; Uttley and McHardy, 2001), which is observed over a wide range of time scales (Gleissner et al., 2004). The congruent tracks of black holes and neutron stars follow in the PCC diagram strongly support the Lyubarskii model due their similar evolution in variability.

The tracks traced in the PCC diagram also allow the extent of the role of the compact object type in the timing properties to be probed. Hard states show a clear distinction between black holes and neutron stars, but soft states not, which suggests differences emerge when the accretion disk is truncated further away. As the variability originates

from the accretion disk, the distinction in the hard state must be due to the differences in compact object type. In contrast to black holes, neutron stars have a boundary level, a source of seed photons. The interaction of this emission and the coronal region will change the source emission, and could dampen the variability seen in the inner regions produced by the accretion disk, leading to the shift in power colours as seen in Fig. 9.

EFFECTS OF NEUTRON STAR PROPERTIES

Inclination & QPOs

Using power colours, Heil, Uttley and Klein-Wolt, (2015a) found that sources followed distinct paths in the HH diagram dependent on their inclination. Evidence for a similar relationship in neutron stars is explored in Fig. 11, where objects are split into groups of high and low inclinations. Tentative suggestions of relationship are found between the two groups of neutron stars, with the general trend of low-inclination sources showing higher hardness per hue than high-inclination sources. The clearest distinction emerges at hues around 180° , though at higher hues the high inclination sources show an increase in scatter. Efforts to reduce this scatter would be encouraged, as this could help ascertain whether there a division is present. Currently limited constraints on the inclination angles are in effect, however adopting stronger constraints on this angle could prove beneficial in determining the effects of inclination angles. As systems with an ill-defined inclination close to 60° can blur any potential separation in the HH diagram, further tests could also be conducted only using dippers. These systems with inclinations $> 75^\circ$ would be expected to show the largest deviations from the mean path in the HH diagram and provide a good check for inclination dependence. Other possibilities of examining the inclination-dependence would be to shift the hardness energy bands and check whether the results remain consistent.

The most remarkable point is that this separation in the HH diagram runs counter to the results for black holes, where the behaviour of the high and low group is reversed (Heil, Uttley and Klein-Wolt, 2015a). The black hole systems also show a clearer distinction than found for the neutron star systems. With these systems showing type C QPOs in the hard-intermediate states around the lower apex (Heil, Uttley and Klein-Wolt, 2015a), the split in the HH diagram and the presence of type C QPOs provided evidence for such QPOs to have a geometric origin. Neutron star power spectra show similar low frequency QPOs, but the QPOs are less prominent compared to the broadband noise than in the black hole systems. However, as no

inclination dependence is seen in the PCC diagram, this would imply that if an inclination effect is present in the HH diagram, it would be due to a change in hardness rather than in power colours. This too is surprising, as with relations between low-frequency QPOs and orbital inclination having been established for neutron stars (Homan, Fridriksson and Remillard, 2015), some degree of an inclination dependence in the PCC diagram would be expected.

It would be interesting to explore this relationship between power colours and QPOs further with research into the inclination dependence of neutron stars with shifted PCC frequency bands, able to cover kHz QPOs. Caution should be undertaken however upon shifting the frequency bands to ensure the highest frequency band retains enough power. An interesting possibility for extending the work done in this study would also be to investigate the relationship in general between kHz QPOs and PCC values, not just inclination dependence. With studies suggesting a close link between these QPOs and the surface of neutron stars (e.g. Peille, Barret and Uttley, 2015), combining them with power colours could provide a unique insight into their evolution. Parameters such as the central frequency and width could provide a way to track the evolution of kHz QPOs through the PCC diagram.

Atoll & Z Sources

Z sources systematically show higher luminosities than atoll sources, a point emphasised in Fig. 12, where neutron stars have been divided in atoll and Z sources. In this figure, the Z sources firmly remain in the lower-left side of the diagram, corresponding to the soft states in black holes. With soft states in black holes commonly showing higher luminosities than in hard states, it provides an interesting link between variability and luminosity across both types of compact objects. The right panel of Fig. 12 showing a HH diagram confirms the Z sources remain primarily in the soft states. A difference in energy spectral hardness can however be observed, with the Z sources showing a smaller spread in hardness than the atoll sources. This could possibly be purely down to selection effects, with the number of atolls sources outnumbering Z sources. While island and banana spectral states show strong ties to power colours, limited time prevented similar research into the ties between specific Z source branches and power colours. These branches show strong discontinuities in timing properties (Hasinger and van der Klis, 1989) and hence could be expected to influence PCC values.

Z sources can be further split into Cyg- and Sco-like sources on basis of their behaviour in the HI diagram. Where Cyg-like sources

show a long HB and short FB in the ECC diagram, Sco-like sources show a short HB but long FB (Homan et al., 2007; Kuulkers and van der Klis, 1995). Plotting these groups in a PCC diagram gives Fig. 13, where the Sco-like sources show a far larger spread in values than the Cyg-like source. It must be noted however that both groups are heavily dominated by observations of respectively Sco X-1 and Cyg X-2. To further investigate the difference in scatter, splitting ECC diagrams into the different branches and plotting these groups in the PCC diagram could provide an inroad to understanding the origin in difference between the Cyg- and Sco-like Z sources. It remains curious that while Cyg X-2 shows the largest change in ECC tracks in comparison to Sco X-1, Cyg X-2 shows the tightest PCC track of the two.

Pulsations & Spin

One of the unique properties of neutron star LMXBs are their strong magnetic fields, believed to be capable of channelling the accretion flow close to the surface (see Cumming, Zweibel and Bildsten, 2001; Payne and Melatos, 2006). This is thought to give rise to pulsations which cease upon the ‘burial’ of the magnetic field by the accretion flow. Fig. 14 shows a PCC diagram where observations have been split into time intervals in which pulsations are visible and time intervals with regular flux levels. No notable effects are visible, with only the slightest hint in power colours during pulsation intervals. With observations classified on basis of fractional pulse amplitudes given in Galloway et al., (2006), some degree of error is introduced by manually reading off values. An improved method to check for potential effects of magnetic fields on power colours would be to introduce an automatic detection routine. This would allow PCC values to represent true pulsation intervals, preventing any averaging occurring between pulsation intervals and intervals with no detectable pulsations. With light curve variability arising from accretion rates, it could be expected that this would be reflected in the power spectra, and hence in power colours. As magnetic channelling is suppressed, accretion rates near the surface change, therefore providing a potential change in power colour values. Conceivably this effect might only arise at frequencies beyond those of the PCCs as the process takes place close to the surface of the neutron star. Shifting the power colour frequency bands as described in section 4.2 would allow any effects to be probed in a more direct manner, and should be investigated in future work.

Other properties unique to neutron star LMXBs are the periodic signals originating from their rapidly rotating surface (Watts, 2012). Plotting these frequencies for multiple objects in the PCC diagram gives Fig. 15, where objects have been split into bursters and pulsars.

Bursters show no dependency on spin frequency in the PCC diagram, however pulsars show a tentative link in the hard state. Low number statistics prevents any definitive conclusion as to a potential relationship between an increase in spin frequency and shift in power colours in the hard state, provides grounds for further investigations. Comparing the underlying power spectra shows no particular indication of power spectral changes affecting PC1 more than PC2, or vice versa. With PC2 being related to the uppermost frequency band, it could be hypothesised that the spin frequencies influence these more strongly than the low frequency band. Further research would have to show which frequencies are most affected, and what the exact link between the spin frequency and the lower Fourier frequencies is. It is curious that the bursters show no relationship of this nature, as their peak oscillations having long been established to originate from the surface (Watts, 2012). A key characteristic of pulsars are their strong magnetic fields, which are not necessarily common to bursters. This could affect the truncation radius of the accretion disk, and therefore also the timing properties, but would need significant work before any relation could be confirmed.

ROBUSTNESS

Oddballs

Two objects show differing behaviour to the other sources, in terms of power colours and hardness. Upon examination, these were excluded from further analysis to prevent other trends being obscured. The following paragraphs discuss these sources, and potential reasons for the observed differences.

CIR X-1 The HI diagram of Cir X-1 shows a remarkably broad range of both intensities and hardness values, as shown in Fig. 43. With observations in the lower right of this diagram having a high luminosity and very low hardness, it would be expected that these observations correspond to a soft state. The position of these observations in the PCC diagram show them however to be in the area corresponding to hard states. Fridriksson, Homan and Remillard, (2015) found absorption dips significantly affected the hardness values, complicating the problem further, as absorption would be expected to harden the spectral state since softer photons are preferentially absorbed via photoelectric absorption (Wilms, Allen and McCray, 2000). While beyond the scope of this project, research into the presence of dips would be useful in order to determine to which degree these hard values are indeed affected by dips. Additional research in determining whether potential effects are stronger for soft states or hard states, potentially causing a misclassification in the HI diagram, would also be useful.

EXO 0748-676 The burster EXO 0748-676 reveals the inverse behaviour, with the **HI** diagram suggesting the source remains in a hard state for a substantial amount of time. No trace of this state can be found in the **PCC** diagram, where values firmly remain in the area associated with the soft state. The **HH** diagram confirms the unusual behaviour where values are found to cluster at both high hue and high hardness values. Inspecting power spectra shows the presence of an additional component at low frequencies, causing an upturn in power towards lower frequencies. Low frequency **QPOs** also feature prominently in the power spectra specifically around band C, possibly causing an offset in PC1 values. Research by Homan, Fridriksson and Remillard, (2015) confirms the presence of these features, however even with the presence of **QPOs** it would be difficult to explain the degree of the offset in power colours. Classified as a dipper (Homan, 2012), dips in the light curves of EXO 0748-676 could potentially also affect the power spectra. With dips showing stronger absorption in the energy spectrum at low energies, this will cause an increase in spectral hardness (Wilms, Allen and McCray, 2000), adding complexity to the classification of the state.

While the differing behaviour of these objects is noted, the spread in neutron star types could however show more effects in the **PCC** diagram than discovered over the course of this project and as such, an extended investigation into effects of properties on power colours would be strongly encouraged. Future research into the relationship between canonical neutron star and black hole spectral states is also encouraged, specifically into the **IS** and the banana states where sub-classifications such as **LLB**, **LB** and **UB** show no distinguishing features in the **PCC** diagram.

Selection Criteria

A noticeable property of **PCC** diagrams is the relatively sparse population of data points. Tab. 1 shows the fraction of 'good' observations relative to the total number of observations available in the **RXTE** archive for that object. With typically less than half of the total number of observations for each object usable in the **PCC** diagram, a large amount of data is lost. The largest fraction thereof is down to limited energy channels, with many observation modes starting from energies higher than 2 keV. Using the same energy bands is important if comparing variability in the power spectrum, however the case could be made that using less stringent energy requirements might prove more beneficial than excluding these observations. Studying the distribution of lowest energies per observation could allow energy boundaries to be selected which are represented in most observations. The second

largest fraction contributing to the PCC value sparseness is due to the GTI-filters, primarily caused by the recommended expression for eliminating a high photon count rate. Removing this requirement would result in a significant increase in data points.

Another cause of the low success rate is the fractional variance limit imposed upon PCC values. Requiring the fractional variance to be more than 3σ in all four bands requires both limited variability in power spectra and sufficient segments in the light curves. This is related to binning criteria, a point discussed further in section 4.4.3. Current background models are sufficiently advanced to allow fairly relaxed good time interval criteria, as described in section 2.2, however combined with cuts around the change in the number of active PCUs takes a certain toll on usable observations. Finally, a number of observations fail due to the lack of sufficiently high resolution data modes, or errors in data files. With these last two reasons only having a limited effect on the number of good observations, efforts should focus primarily on energy bands, updating GTI criteria and ensuring power colours are optimally binned.

Binning

A general source of scatter in the PCC diagram could be related to PCC variability within a single observation. Shifting features in the power spectrum, whether QPOs or other strongly peaked components, could shift within the time scale of an observation, affecting PCCs. Examples of such shifts have been demonstrated within black hole systems (e.g. Motta et al., 2012), but subsequently found to affect only a small number of black hole power spectra (Heil, Vaughan and Uttley, 2012). Similar work has yet to be conducted systematically in neutron star systems. In comparison to black holes, strong power spectral features such as QPOs seem suppressed in power spectra, as raised in section 4.3.1. While dividing observations into several parts could potentially reduce any contribution of PCC variations to the scatter, it would significantly increase the errors on each PCC point.

Splitting observations could force the adoption of new binning criteria to ensure minimal errors on PCC values. This ties in to the current selection effects present in the soft states. Typically sources in these states show rapid changes, display larger variability and show an overall increase in error values within power spectra. Combined, they generally result in larger PCC error bars, and hence increase the chance of exclusion from the PCC diagram. Black hole systems show somewhat similar effects, where observations in the soft-intermediate state with variability close to the Poisson noise level show large PCC errors. Heil, Uttley and Klein-Wolt, (2015b) resolved

this issue by manually binning PCC values after comparing power spectra by eye. This introduces a subjective side to power colours and thereby weakens the strength of power colours, in that they are independent of subjective choices such as grouping. Possibly an alternative binning method could be adopted in which PCCs are not calculated according to observation, but by optimally grouping data over time. A drawback could potentially be the inability to group points where fast transitions happen back and forth between states, for instance in between soft states. Further research would have to be conducted to determine which binning method gives the most accurate representation of the data.

Bursts

Another possible selection effect is the filtering of bursts in neutron star light curves, described in section 2.3. This allows the power spectrum to show a more accurate representation of the average variability over the course of an observation, without the influence of outlying data due to a burst. The filtering routine in CHROMOS has been optimized to Aql X-1, and as such very occasionally throws up false positives in other objects. Part of the light curve is subsequently flagged as unusable, resulting in larger error bars on the PCC value. Characteristic flares can show a fast rise over a time scale of seconds, and a subsequent decline over longer time scales of seconds to minutes. A variety of detection tests were conducted, from simple triggering once count rates rose above a particular deviation to triggering only after a sustained period of extreme count rates. Using methods to determine when the count rate returned to a normal level proved difficult and unreliable, so the choice was made to use sustained count rates to detect flares and use fixed time bins to cut flares. The latter currently ensures a flare is completely removed from the light curve, but an optimized cutting routine could improve this technique, ensuring no data is wasted. Future research into the effect of flares on power colours would also be welcome, in order to understand the link between light curve and power spectrum variability.

Hue

The central point from which the hue in the PCC diagram is calculated can be determined in a number of ways. Heil, Uttley and Klein-Wolt, (2015b) adopted a number of constraints to define their coordinates – the hue had to reflect the spectral evolution of an object in a continuous fashion rather than with jarring jumps in hue values and the hue had to ensure an even spread of PCC points across all angles rather than pushing data points into a narrow range. With tracks of neutron star PCCs diverging from black hole PCCs, it could be expected

that ideal placement of the hue centre might be affected. Testing a range of positions for hue centres within the constraints showed little improvement in the spread of hue values. The choice was therefore made to adopt the hue centre coordinates used in Heil, Uttley and Klein-Wolt, (2015b), allowing hues to easily be compared.

It is interesting to note that an increase in hue seems to correspond to an increase in PCC scatter. The rapid transition of objects in the soft-intermediate and the soft state could cause part of the variety in power spectral shapes shown in these states. The wide range of power spectra contributes to a large scatter in PCC values, which could partially explain the increase in scatter with large hues.

Additional selection effects take place in HH diagrams, where values with an error $> 30^\circ$ are omitted. While this is a reasonable criterion to ensure trends remain distinct, the hue error can easily provide a misrepresentation of the significance of a PCC value. The further away a PCC value is from the hue centre, the more accurate the hue is determined, yet the error on the PCC values can be larger than the PCC error on a value closer to the centre which has a correspondingly large margin on its hue. With hue errors dependent on an arctangent after propagation, hue errors can lead to the impression of an ill-defined state, where in reality that point can clearly be associated with a particular state in the PCC diagram.

Hardness Ratio

The hardness ratio bands used in this project range between 6.4-16 keV, however the argument could be made that a hardness ratio spread over a wider energy range might reflect a more accurate representation of the larger changes in the energy spectrum. With RXTE providing an energy range from 1.5 keV all the way up to 117.86 keV (RXTE, 2012b), the chosen energy bands are remarkably narrow. However, sources often tail to near zero counts from 20 keV onwards restricting the available energy bands. At the lower energies calibration issues take effect (see Gleissner et al., 2004), limiting the available energy range. In order to compare results with previous neutron star studies (e.g. Gladstone, Done and Gierliński, 2007), the current energies of 6.4-9.7 keV and 9.7-16.0 keV were chosen. Several tests were conducted on the effects of differing hardness ratio on for instance the HH diagram. While varying the hardness did have the effect of stretching the range of hardness values, no benefit was found in changing the hardness ratio from the values used in prior studies.

Dead Time

Additional contributions to the scatter in the PCC diagram could arise from dead time effects. Using the method to calculate the noise level as given in eq. 5 suffices for sources with a low count rate, however sources with a high count rate should ideally have an additional correction factor to account for dead time (Dennis, 2006; RXTE, 2012a). Dead time, or after which a photon is detected and during which a detector is unable to process another event, causes an overestimate of the noise level if calculated using eq. 5, due to the correlation between dead time events. To reduce the subtraction factor, a correction factor can be introduced as follows:

$$P_{\text{noise}} = 2 \frac{\langle x \rangle + \langle b \rangle}{\langle x \rangle^2} \cdot \frac{P_{\text{cor}}(f)}{2} \quad (10)$$

where the original noise factor (left) has been corrected by a factor dependent on P_{cor} (right). This term can be used not just to correct for dead time effects, but also Very Large Events (VLEs). The latter can be defined as ‘events that exceed the dynamic range … and saturate the amplifier’, and introduce an additional noise component (Jahoda et al., 2006). The correction factor accounting for both effects can be written as a simple addition of these parts

$$P_{\text{cor}}(f) = P_D(f) + P_{\text{vle}}(f) \quad (11)$$

As defined by Jahoda et al., (2006), $P_D(f)$ can be written in Leahy normalization as

$$P_D(f) = P_1 - P_2 \cos \left(\frac{\pi f}{f_{\text{Nyq}}} \right) \quad (12)$$

where if the count rate per PCU is less than 10^4 counts s⁻¹

$$P_1 = 2 \left[1 - 2r_0 t_d \left(1 - \frac{t_d}{2t_b} \right) \right] \quad (13)$$

$$P_2 = 2r_0 t_d \frac{N-1}{N} \left(\frac{t_d}{t_b} \right) \quad (14)$$

leaving $P_{\text{vle}}(f)$ to be defined as

$$P_{\text{vle}}(f) = 2r_{\text{vle}} r_0 \tau^2 \left(\frac{\sin \pi \tau f}{\pi \tau f} \right)^2 \quad (15)$$

The parameters in the equations above are defined as follows:

f	Frequency
f_{Nyq}	Nyquist frequency
r_0	Event rate
t_d	Dead time
N	Number of frequencies
t_b	Bin size
r_{VLE}	VLE rate
τ	VLE window size

While obtaining the values of most parameters is a straightforward task, t_d has an additional dependency:

$$t_d = 10\mu\text{s} \left(\frac{r_{\text{non-VLE}}}{N_{\text{PCU}}} \right) + \tau \left(\frac{r_{\text{VLE}}}{N_{\text{PCU}}} \right) \quad (16)$$

where $r_{\text{non-VLE}}$ and r_{VLE} are respective count rates for non-VLE and VLE events, and N_{PCU} is the number of active PCUs (RXTE, 2012a). $r_{\text{non-VLE}}$ in turn can be calculated from the sum of the count rate for good xenon, propane and coincident events. This just leaves the VLE window size τ , whose value can range between $60 - 500\mu\text{s}$ depending on the setting at the time of the observation. Typically τ will however have a standard setting of $170\mu\text{s}$.

Currently dead time effects are not accounted for in CHROMOS, as most sources show sufficiently low count rates to neglect dead time effects. However, it is expected that the methods given above will be implemented in CHROMOS in the near future to help in reduce errors in high-flux observations. It is not expected to influence the main results of this research, but it could potentially reduce some of the scatter in the soft states.

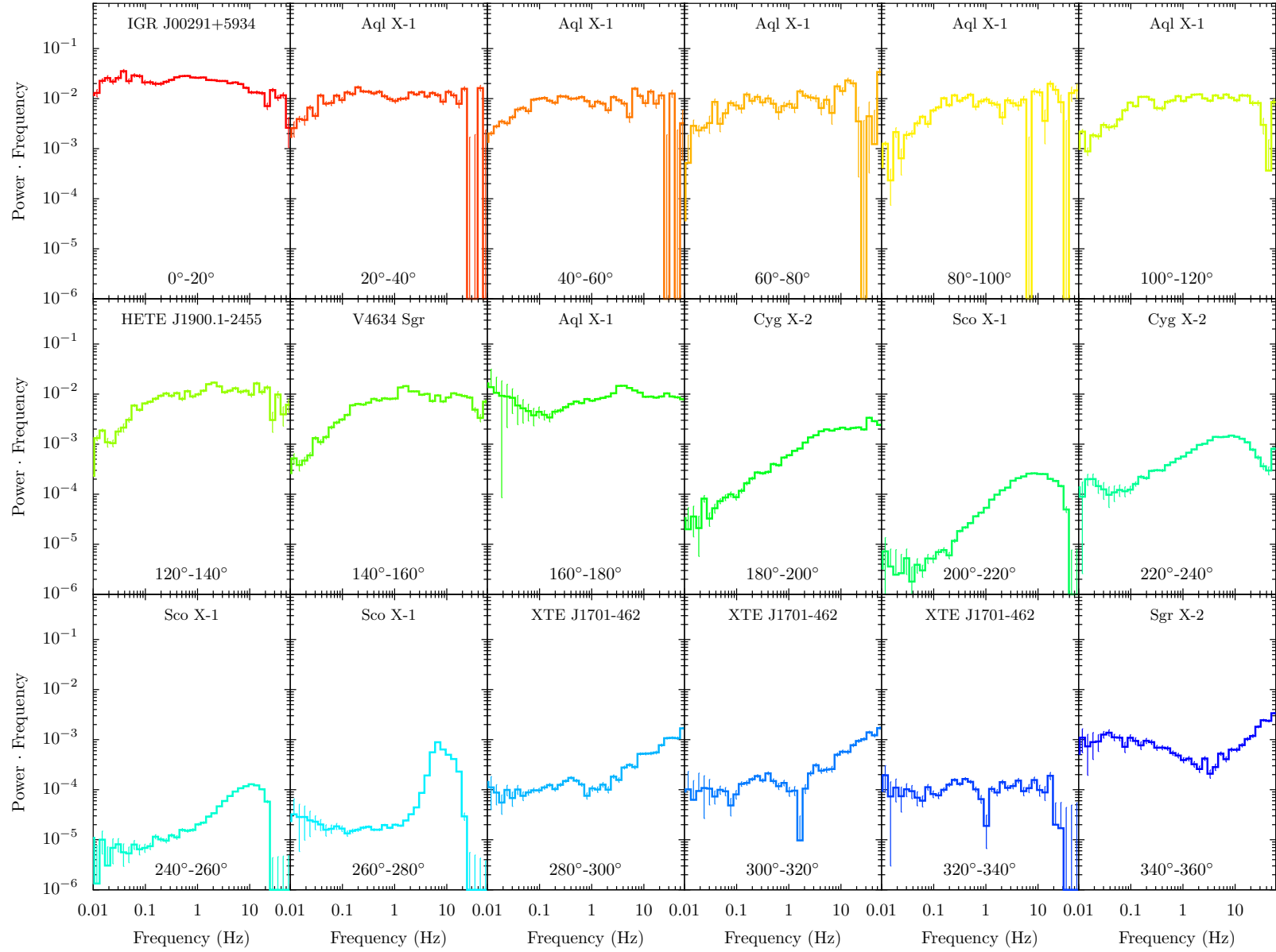


Figure 16: An overview with examples of neutron star power spectra per hue bin. Fig. 6 shows this division in the PCC diagram. Each power spectrum represents a random power spectrum from the source with the most observations in that hue bin. Appendix c contains additional information, showing a larger selection of power spectra per hue bin.

5

CONCLUSION

Using power colours, black hole and neutron star LMXBs have been shown to follow a similar power spectral evolution, providing fresh evidence for a common variability origin from an accretion disk. While significant variability in power spectra can occur over short time scales, power colour tracks show the broad band evolution is relatable and model-independent. Diverging power colour paths additionally allow for the rapid classification of neutron star and black hole LMXBs in the hard states. Further evidence for common behaviour can be found in spectral states, with a link being found between neutron star power colours and the various canonical atoll states, similar to the analogous behaviour discovered for black hole spectral states (Heil, Uttley and Klein-Wolt, 2015b). This allows for a comparison between systems with a similar geometry.

The effect of a number of other LMXB properties on timing properties were also tested. Speculative signs of an inclination dependence of neutron star hardness are found, however they run counter to expectations and require more research. A clear division could be made in the PCC diagram between the population of atoll and Z sources, with the latter remaining firmly in the soft states. Cyg- and Sco-like Z sources showed a tentative difference in power colour spread, however this could be due to observational biases. The effects of pulsations on power colours were also investigated. While bursters showed no particular effects on power colours, a tentative relation between the spin frequency of pulsars and the associated power colour tracks was found. This suggests that strong magnetic fields could affect the timing properties of neutron star LMXBs.

The research conducted in this project could benefit from further research into the effect of broader power colour frequency bands, and into the necessity of various extraction settings, to ensure optimal use of data. While beyond the scope of this project, research into the relationship between power colours and QPOs would be fascinating, potentially allowing the evolution of QPOs to be linked to the broader spectral evolution. A wide range of other parameters from mass to the presence of bursts could also provide new insights into the similarities between black hole and neutron star LMXBs and effects due to the difference in compact object.

Part II
APPENDIX

a

A BRIEF GUIDE TO CHROMOS

This text is intended to introduce users to CHROMOS, a software pipeline written to automate the extraction and analysis of Rossi X-ray Timing Explorer ([RXTE](#)) data. Docstrings and inline commenting should provide additional information for those digging deeper in the exact techniques and calculations used throughout the pipeline. Questions still remaining after studying these resources can be addressed by opening an issue on the [github](#) page of the software, or by contacting the author.

At the time of writing, the source code of CHROMOS is invite-only, pending a publication detailing initial results. The code will be made publicly available some time after publication, however invite requests are welcome. CHROMOS will be released under a [GPL3.0](#) licence, allowing users to modify the code as long as it is open sourced. The primary repository is currently hosted at

https://github.com/astrocoding/master_project

As a brief side note for those who are curious: the name Chromos is an amalgamation of Chroma (GR: colour) and Chronos (GR: god of time). Referring respectively to the power colour analysis CHROMOS is capable of, and the timing capabilities of [RXTE](#), the name is designed to evoke the idea of time and evolution, and form a sense of reliability.

INSTALLING CHROMOS

Software can be installed by cloning the CHROMOS repository, and may need additional supporting software if not present on the user's system. CHROMOS has been designed for use on Taurus, running Ubuntu 14.04.4. A list of required software is documented in [REQUIREMENTS.TXT](#), detailing the recommended version of particular software packages. To ensure the full pipeline works on Taurus, a virtual environment will need to be installed. However, those not doing energy spectral analysis can run CHROMOS without requiring a virtual environment with additional packages.

USING CHROMOS

CHROMOS has been built in modular fashion, allowing for the quick toggling of required components. An overview of some of the current steps in CHROMOS is presented below, showing the order in which the pipeline must be run with `MAIN_PIPELINE.PY`. Parameters for running this file are set in `PATHS.PY`, which can be modified to reflect where data should be stored, under which name etc. The pipeline can be run over multiple sources using scripts in the `MISC` folder, being quick hacks to change the paths file before running the main pipeline. As running CHROMOS on a full set of observations for a single source can take several hours, full CHROMOS runs are best run with `SCREEN`, a command allowing scripts to continue to be run while disconnected from the terminal. The only required information apart from that presented in `PATHS.PY` is a list of ObsIDs over which you wish to run CHROMOS. A list of ObsIDs can be found for each object using the HEASARC archive:

<http://heasarc.gsfc.nasa.gov/cgi-bin/W3Browse/w3browse.pl>

A choice can be made to run CHROMOS for extracting data, calculating power spectra, all the way up to calculating power colours. Additionally energy spectral analysis can also be done, if wished, skipping the whole timing analysis side of CHROMOS. Currently CHROMOS works for `EVENT`, `BINNED`, `GOODXENON` and `STD2` files, extracting all types to allow the choice of data mode to be determined only when necessary.

MODULES

The following paragraphs briefly explain the purpose of each step in CHROMOS, providing a way to choose which components are necessary in your own pipeline. A log of the latest run of each step is automatically saved, allowing for future reference. The abbreviation TA refers to timing analysis scripts, which aren't required to run energy spectral analysis, denoted with SA, and vice-versa.

DOWNLOAD DATA Based primarily on scripts coded by Abbie Stevens, this script checks whether you already have a copy of the required ObsIDs, and if not, will download a copy from the NASA archives to the location specified in `PATHS.PY`

LOCATE FILES Using Phil Uttley's `XTESCAN2`, an overview of data files is created in each 'P-folder', the parent folders to the ObsID directories. This overview contains information on all locations, data types, observation dates etc, for each data file in the folder.

DETERMINE INFO A crucial step in CHROMOS, this code runs through all of the files created in the previous step, creates a database with separate entries of each data file and saves it to a csv file as given in `PATHS.PY`. Despite occasional I/O problems regarding the speed of csv files, the decision for this data storage was made to ensure portability and user-friendliness. All subsequent steps require a database file, and will update it upon completion. If wishing to rerun CHROMOS in its entirety from this step, the database file is best deleted manually to prevent a contamination between previous runs and a new run.

SPACECRAFT FILTERS Following standard steps in the RXTE cookbook, Good Time Interval (GTI) files are made to filter erroneous data such as when the observations are blocked by the Earth.

GOODXENON TO FITS A necessary step in extracting GoodXenon data requires the original data files, consisting of two parts, to be matched together. Ideally this step would still take place, but on a different level, allowing CHROMOS to deal with goodxenon files in the same manner as other data modes.

PCU FILTERS To prevent a surge in current from contaminating data, a cut is made around the time at which the number of PCUs changes.

CREATE BACKGROUNDS Contamination from off-sources photons can be modelled with a background. This step creates background data files which are modelled of basis of the settings of the actual data files. Backgrounds can only be extracted at a maximum time resolution of 16s, and therefore require additional steps after extraction, and before using for analysis.

FIND CHANNELS Perhaps the most intricate part of CHROMOS, this script finds the channels required for the specified energy range. Determining these channels for each data file can currently only be done for one energy range at a time, but can easily be adapted.

EXTRACT LC AND SP The most time-consuming part of CHROMOS, requiring all output of the previous steps to be gathered for input here. Light curves are extracted for all data modes save for STD2 files, for which both light curves and spectra are extracted. The latter are only extracted for PCU2, as it performed the most consistently over the course of the full RXTE mission. Currently all data is extracted at the same resolution, however support has been built to allow for different resolutions per data file, with subsequent files still defined by data mode and maximum possible resolution.

CORRECT FOR BACKGROUND (TA) As background files are only extracted at a 16s time resolution, this script interpolates between values to obtain background rates at the same resolution as the required light curve. This is subtracted from the light curve, and saved to a new file for subsequent steps.

FIND X-RAY FLARES (TA) Code to run through light curves, find when bursts occur and create a new light curve without flares. Can be safely be turned off if wished.

CREATE POWER SPECTRA (TA) Another time-intensive step, this calculates a power spectrum for each observation, which is split up into multiple parts of a predefined length. As an essential step in calculating power colours, this code has been extensively commented.

CREATE POWER COLOURS (TA) The final step in the timing analysis – calculating power colours for as many power spectra as possible. Currently no simple way exists for extracting a simple file with ObsIDs and the corresponding power colours, as this currently requires filtering of the database. Scripts with these filters can be found in the `MISC` folder, allowing power colours to be selected upon 3σ constraints, timing resolution or otherwise.

CREATE RESPONSES (SA) Script allowing response files to be generated for each spectrum, ready for input into `XSPEC`.

CALCULATE HI (SA) Based on Fortran scripts developed by Phil Uttley, this code calculates the hardness and intensity for in predefined energy bands, saving the results, like every other step, to the database.

ACCESSING DATA

All data calculated by `CHROMOS` can be found in the database, apart from in cases when size prohibited inclusion, in which case the path to the file is noted. Logs are also created by `CHROMOS` allowing individual files to be traced back through processing. The sheer size of the database leads to the `PANDAS` package being the recommended package with which to interact with the database. The amount of detail in each database requires substantial filtering on various parameters before running scripts over columns. Investigating the manner in which previous columns were created will be essential if you wish to filter this data yourself. Alternatively, self-made scripts could search for the various files created with `CHROMOS`, which should have recognizable and distinct names.

IMPROVEMENTS

Some large-scale improvements which could be made to CHROMOS are the manner in which it deals with GoodXenon files, which could be substantially simplified, but also an rewrite to adopt a class structure. This would help allow CHROMOS to be more adaptable, giving more freedom for a wider range of extraction parameters. Scripts should also be written to filter the data created by CHROMOS to a simple data files with only the necessary parameters, allowing users to avoid the intricacies of data filtering. A lot of this functionality has already been developed for scripts in the `MISC` folder, or scripts in the `PLOTS` folder. The latter directory is perhaps the best place to start with learning how to obtain the required data from a database file, and will help in checking the data by using pre-coded plotting scripts. Additional suggestions for improving CHROMOS can be found on the github repository, as well as smaller issues and bugs that are continuously changing. It is recommended to always upgrade to the latest version of CHROMOS to avoid potential bugs from affecting scientific results.

b

SOURCES

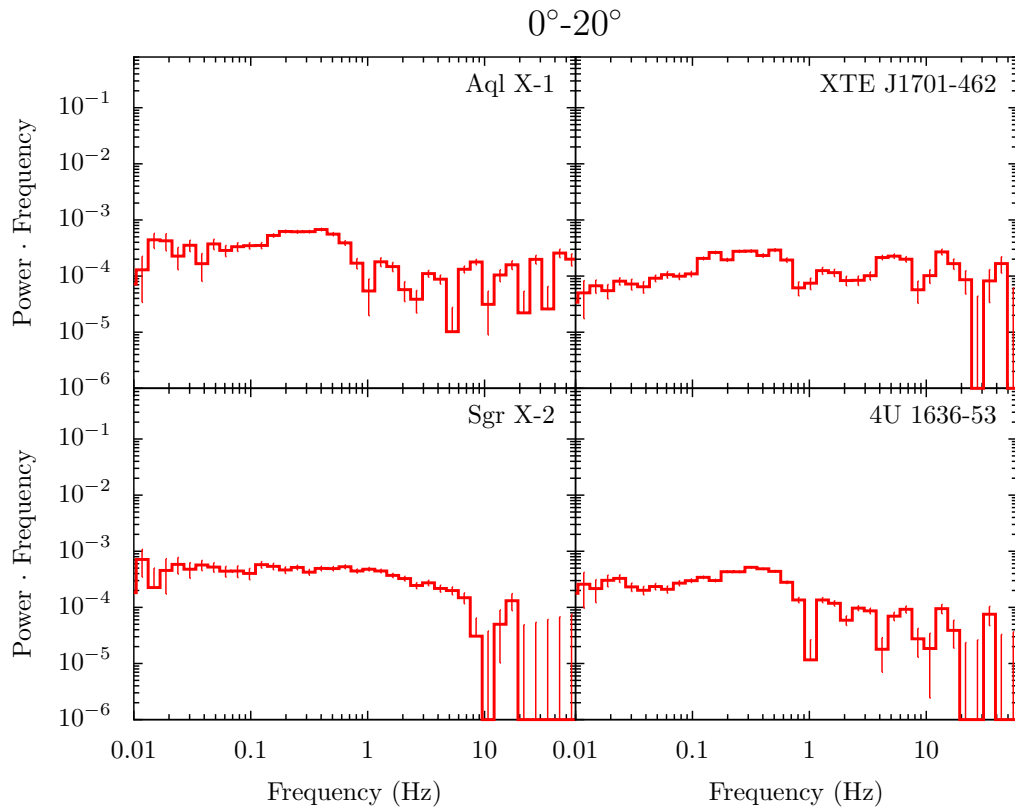
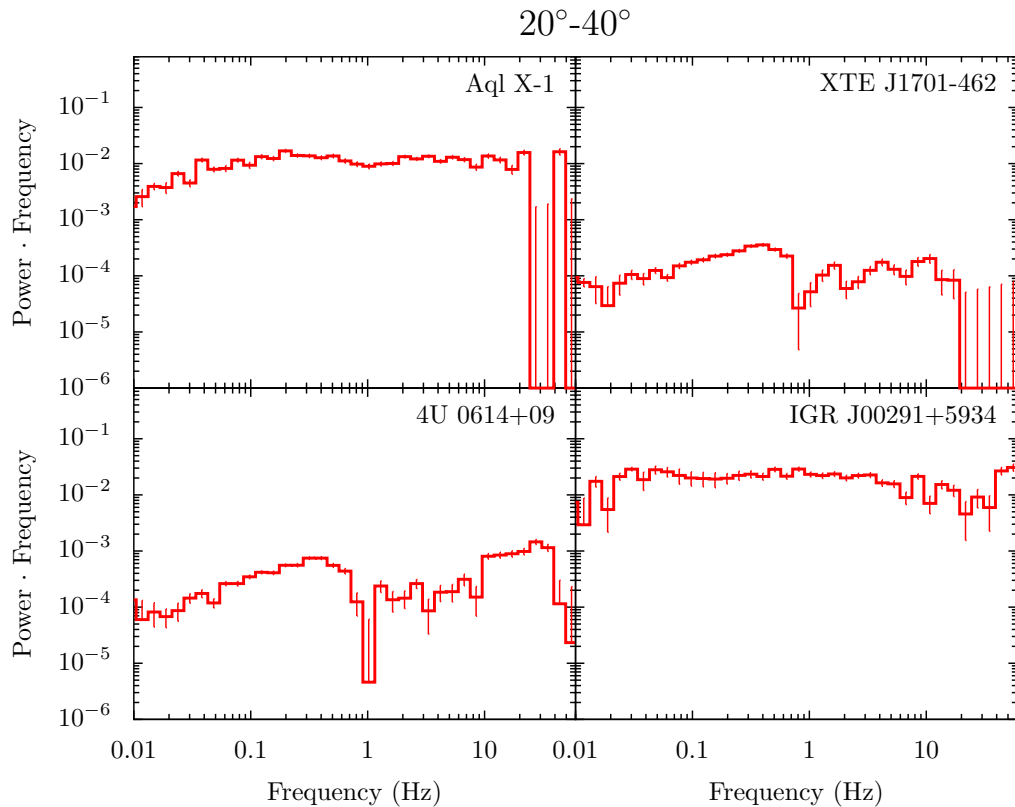
SOURCE	4U	GX	IGR	INTEGRAL 1	SWIFT	X	XTE
4U 0614+09	0614+091			4	J0617.1+0908		
4U 1636-53	1636-5			30	J1640.9-5345		
4U 1702-43	1702-42	340-00		4	J1706.2-4302	Ara X-1	
4U 1705-44	1705-440			43	J1708.8-4406		
4U 1728-34	1728-33	354+00		58	J1731.9-3349		
Aql X-1	1908+00				J1911.2+0034	Aql X-1	
Cir X-1	1516-56			4	J1520.6-5710	Cir X-1	
Cyg X-2	2142+38			22	J2144.6+3819	Cyg X-2	
EXO 0748-676					J0748.5-6742		
GX 17+2	1813-1	17+01		87	J1816.0-1402	Ser X-2	
GX 340+0	1642-45	340+00		32	J1645.8-4536		
GX 349+2	1702-36	349+02		40	J1705.7-3625	Sco X-2	
GX 5-1	1758-25	5-01		78	J1801.1-2504		
HETE J1900.1-2455					J1900.1-2453		
IGR J00291+5934			J00291+5934				
IGR J17480-2446			J17480-2446				
IGR J17498-2921			J17498-2921				
KS 1731-260							

SOURCE	4U	GX	IGR	INTEGRAL 1	SWIFT	X	XTE
SAX J1808.4-3658					J1808.5-3655		J1808-369
SWIFT J1756.9-2508					J1756.9-2508		
Sco X-1	1617-15			2	J1620.1-1539	Sco X-1	
Sgr X-1	1744-26	3+01		73	J1747.9-2633	Sgr X-1	
Sgr X-2	1811-17	13.5		85	J1814.5-1708	Sgr X-2	
V4634 Sgr	1826-2			92	J1829.5-2347		
XB 1254-690	1254-69				J1257.4-6915		
XTE J0929-314							J0929-314
XTE J1701-462					J1700.9-4611		J1701-462
XTE J1751-305							J1751-305
XTE J1807-294				83			J1807-294
XTE J1814-338							J1814-338
GX 339-4	1659-48	339-04		38	J1702.8-4847		
H1743-322			J17464-3213	68	J1746.2-3213		J1746-322
XTE J1550-564				7			J1550-564

Table 2: Overview of various alternative sources names as classified by SIMBAD, (2016), grouped into neutron stars (above the horizontal line) and black holes (below the horizontal line). The leftmost column gives the source names used throughout this work.

C

POWER SPECTRA

Figure 17: Representative power spectra within a hue range of $0^\circ - 20^\circ$ Figure 18: Representative power spectra within a hue range of $20^\circ - 40^\circ$

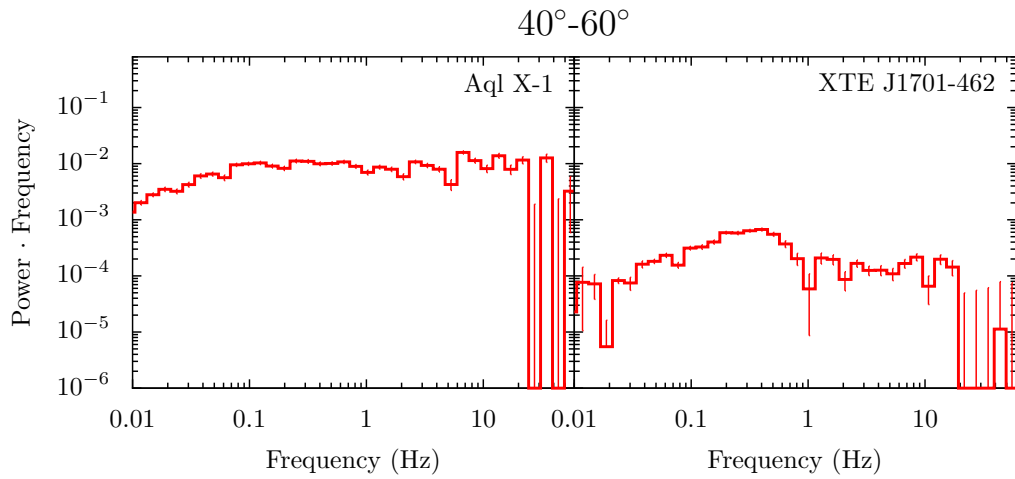


Figure 19: Representative power spectra within a hue range of $40^\circ\text{--}60^\circ$

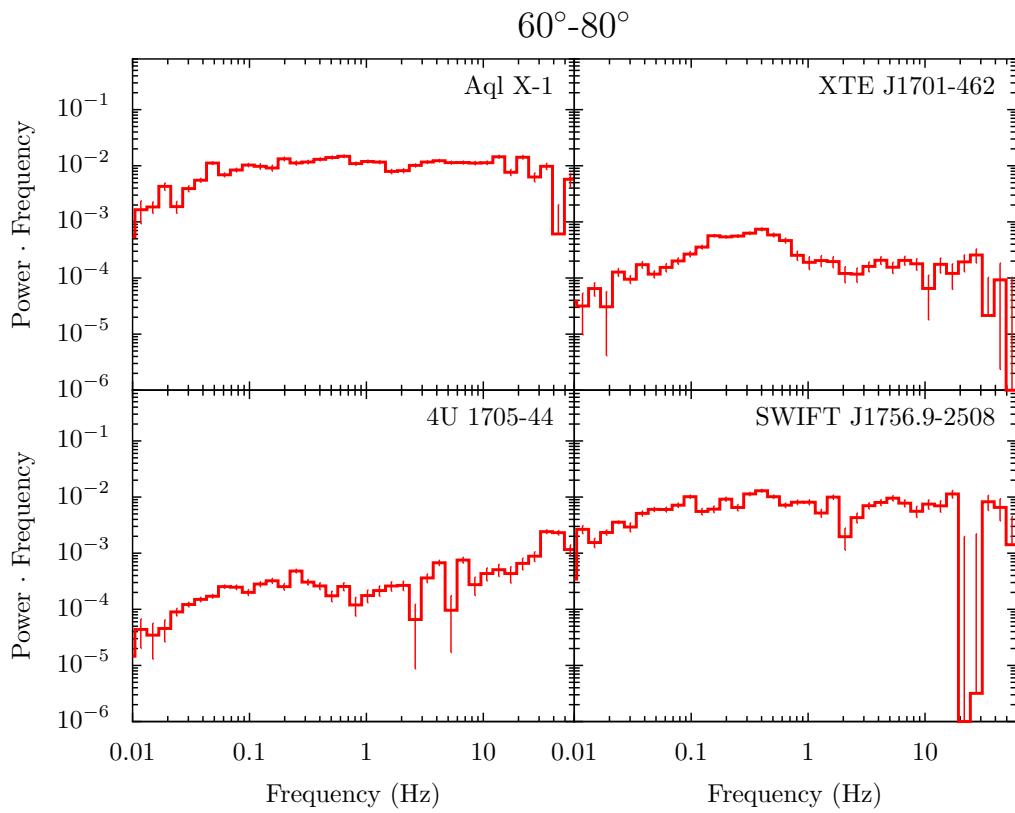
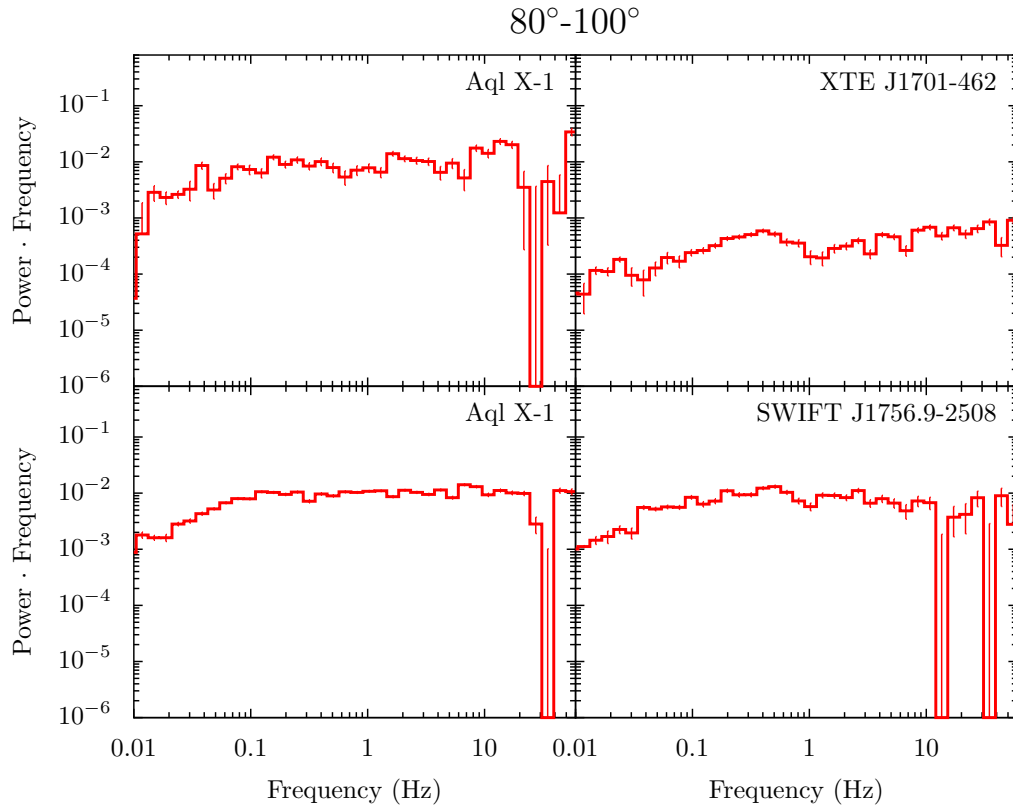
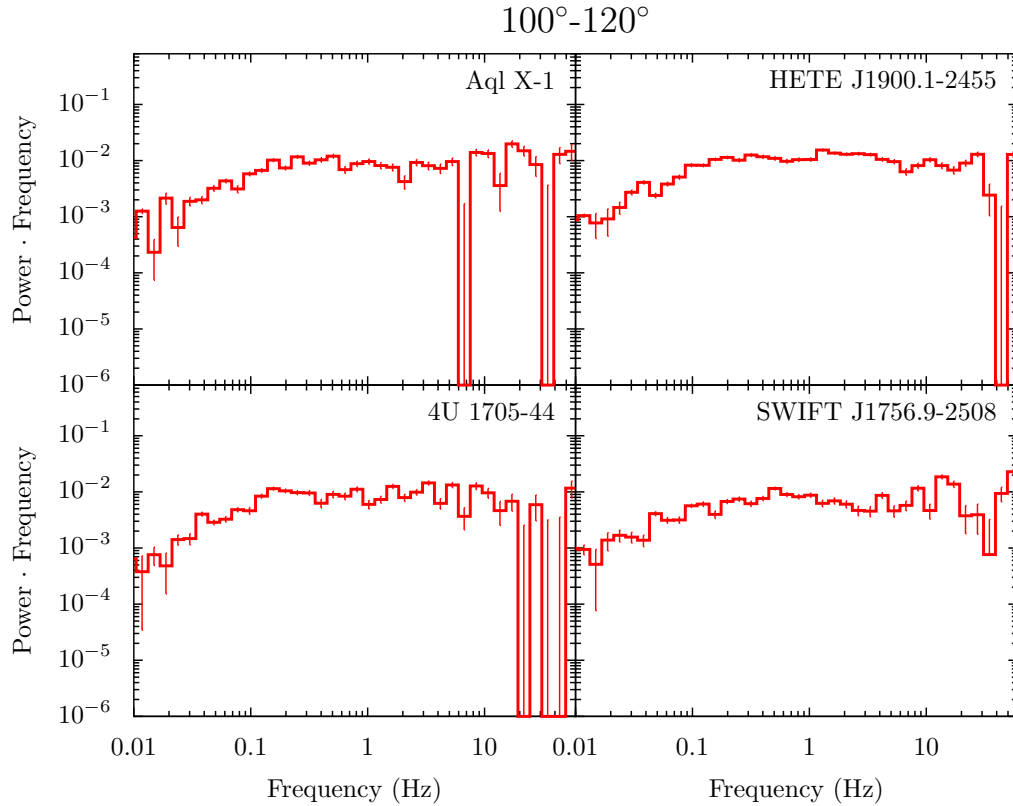


Figure 20: Representative power spectra within a hue range of $60^\circ\text{--}80^\circ$

Figure 21: Representative power spectra within a hue range of $80^\circ\text{--}100^\circ$ Figure 22: Representative power spectra within a hue range of $100^\circ\text{--}120^\circ$

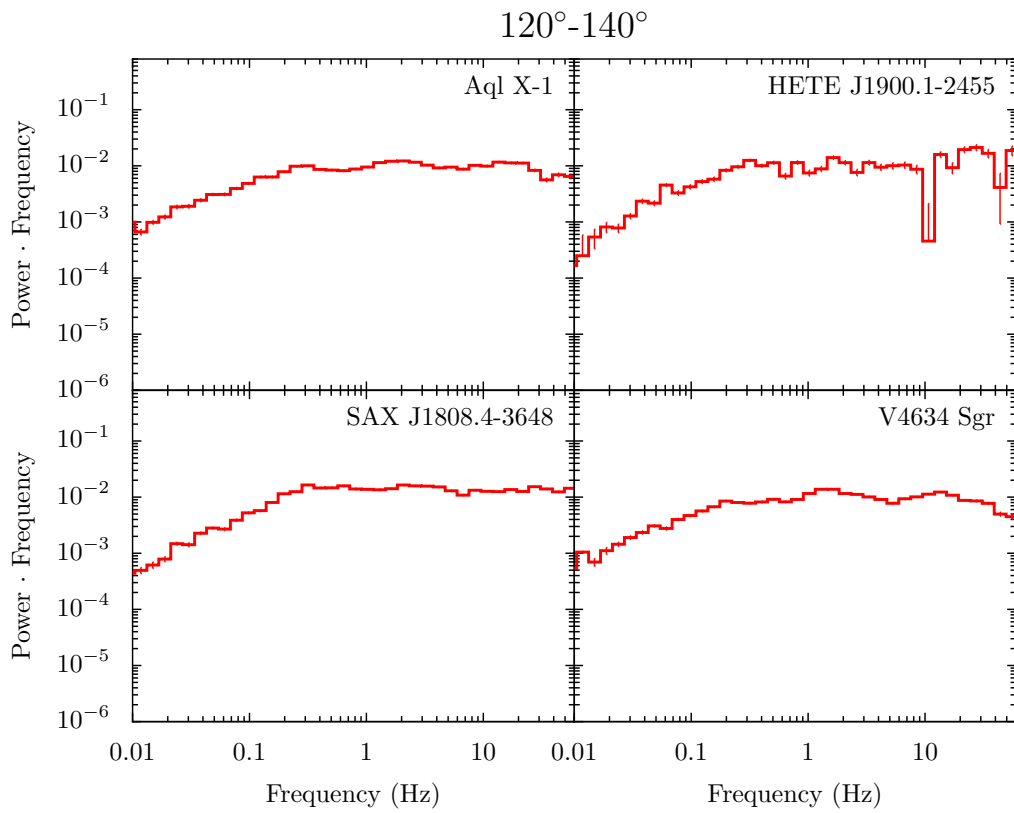


Figure 23: Representative power spectra within a hue range of $120^\circ\text{--}140^\circ$

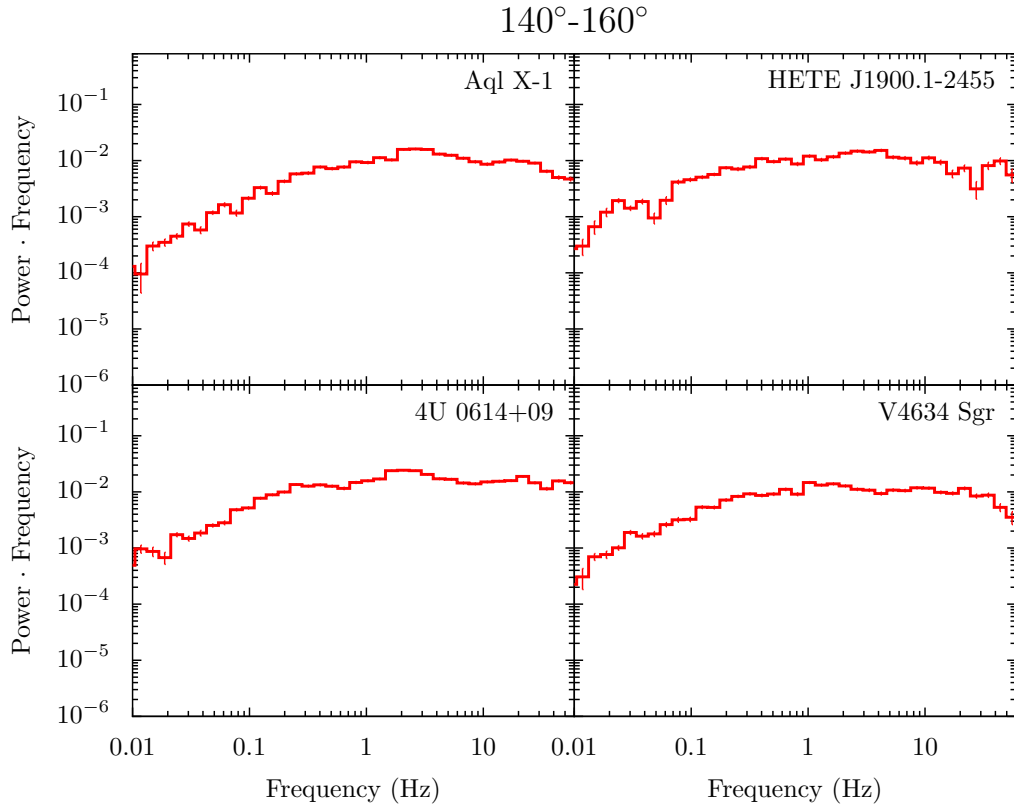
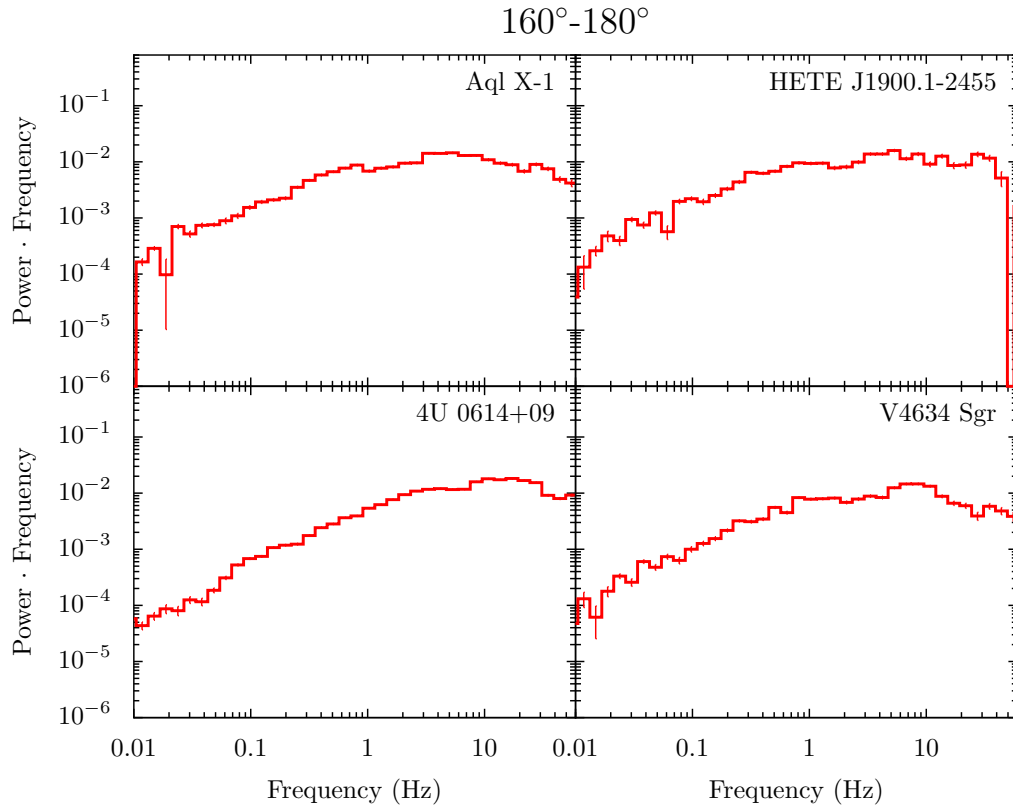
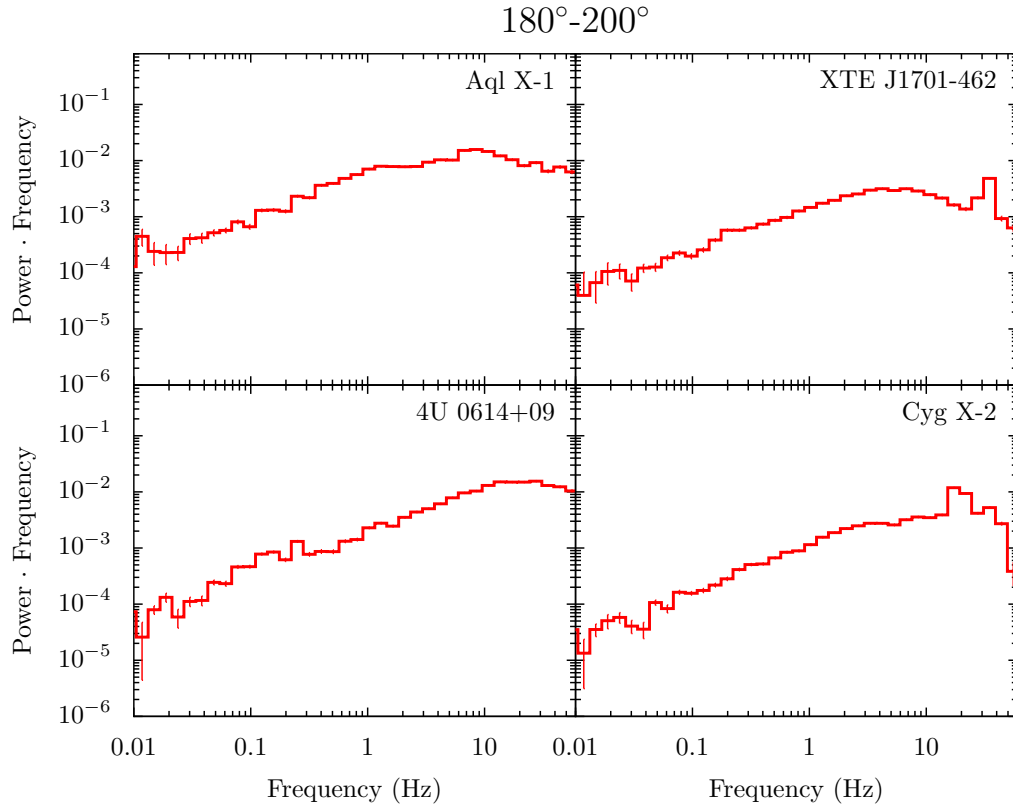


Figure 24: Representative power spectra within a hue range of $140^\circ\text{--}160^\circ$

Figure 25: Representative power spectra within a hue range of $160^\circ\text{--}180^\circ$ Figure 26: Representative power spectra within a hue range of $180^\circ\text{--}200^\circ$

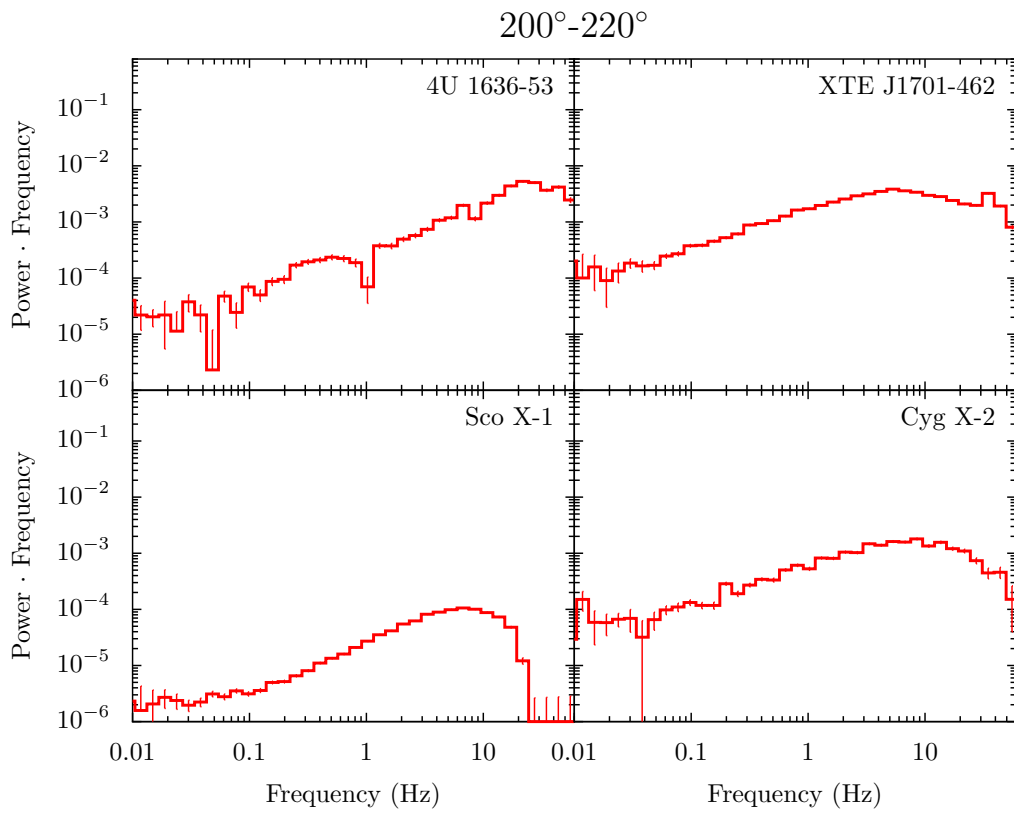


Figure 27: Representative power spectra within a hue range of 200°–220°

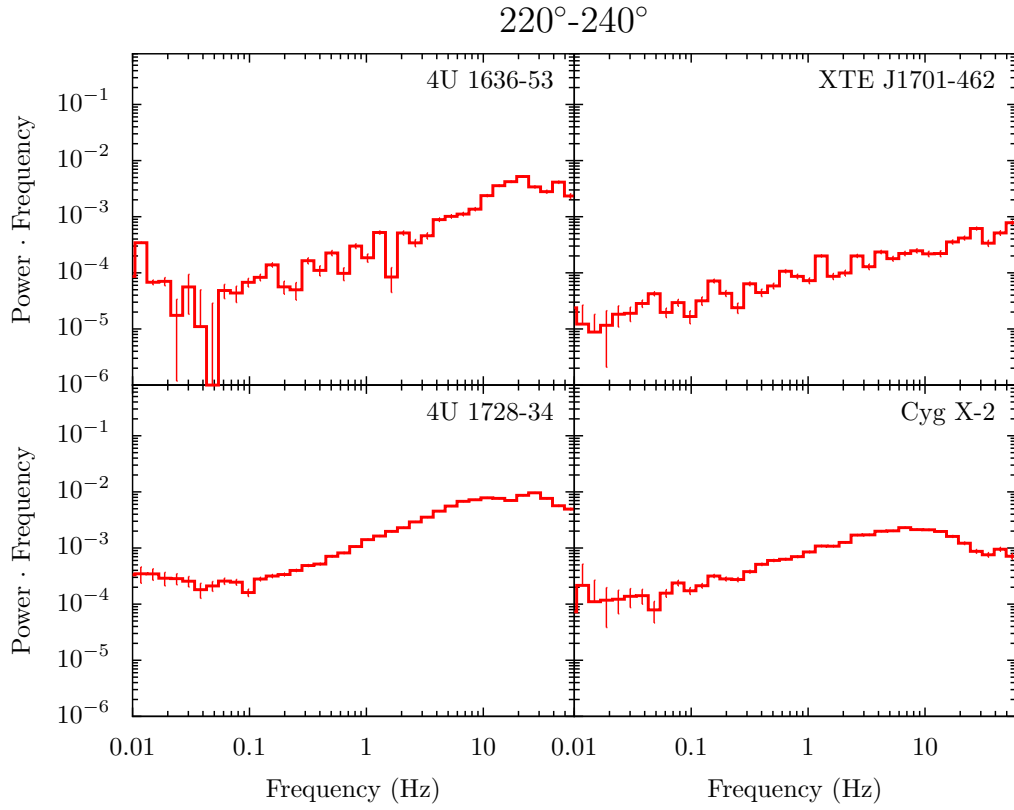
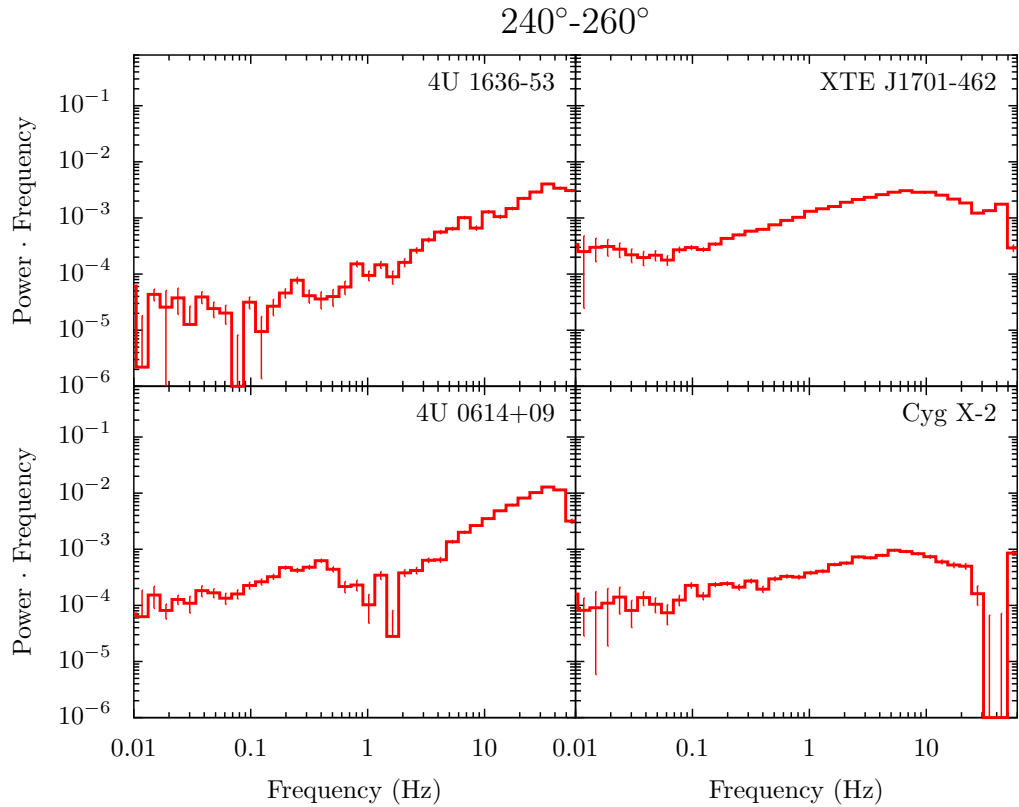
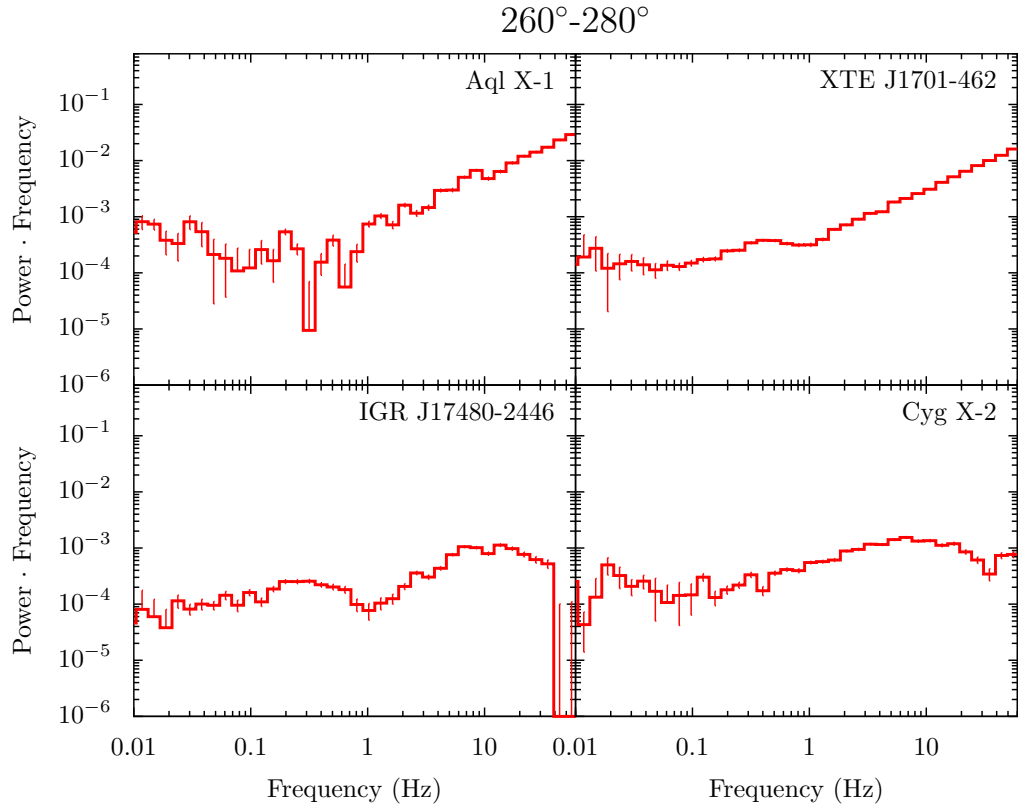


Figure 28: Representative power spectra within a hue range of 220°–240°

Figure 29: Representative power spectra within a hue range of $240^\circ\text{--}260^\circ$ Figure 30: Representative power spectra within a hue range of $260^\circ\text{--}280^\circ$

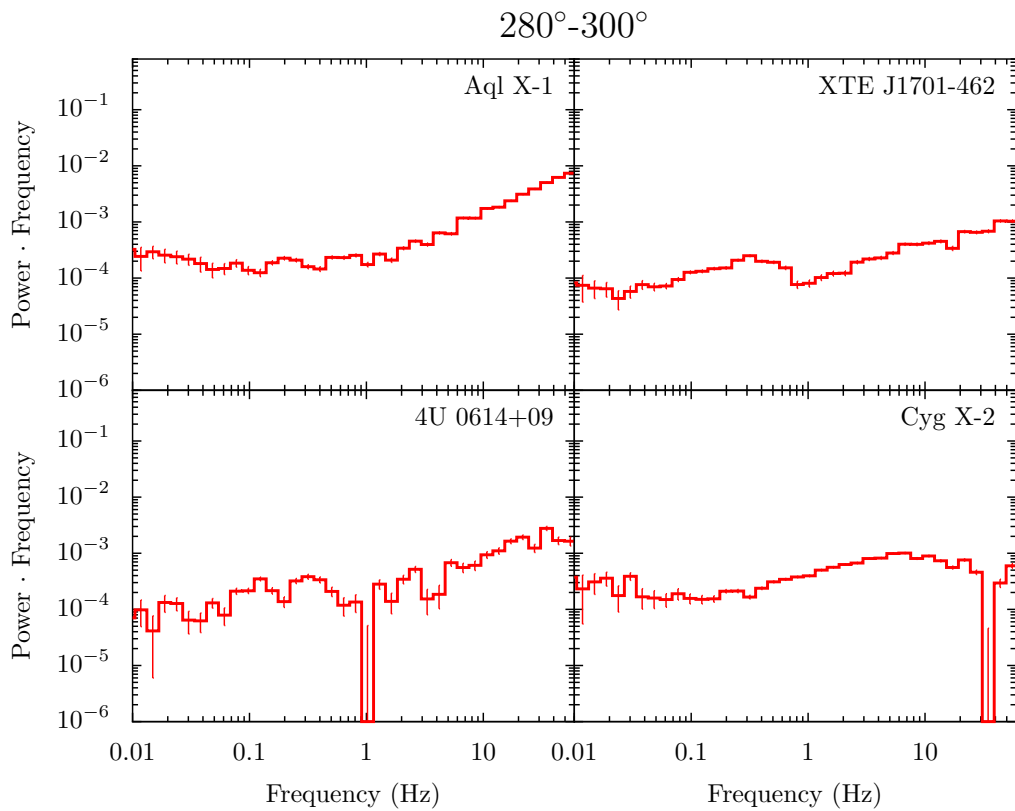


Figure 31: Representative power spectra within a hue range of $280^\circ\text{--}300^\circ$

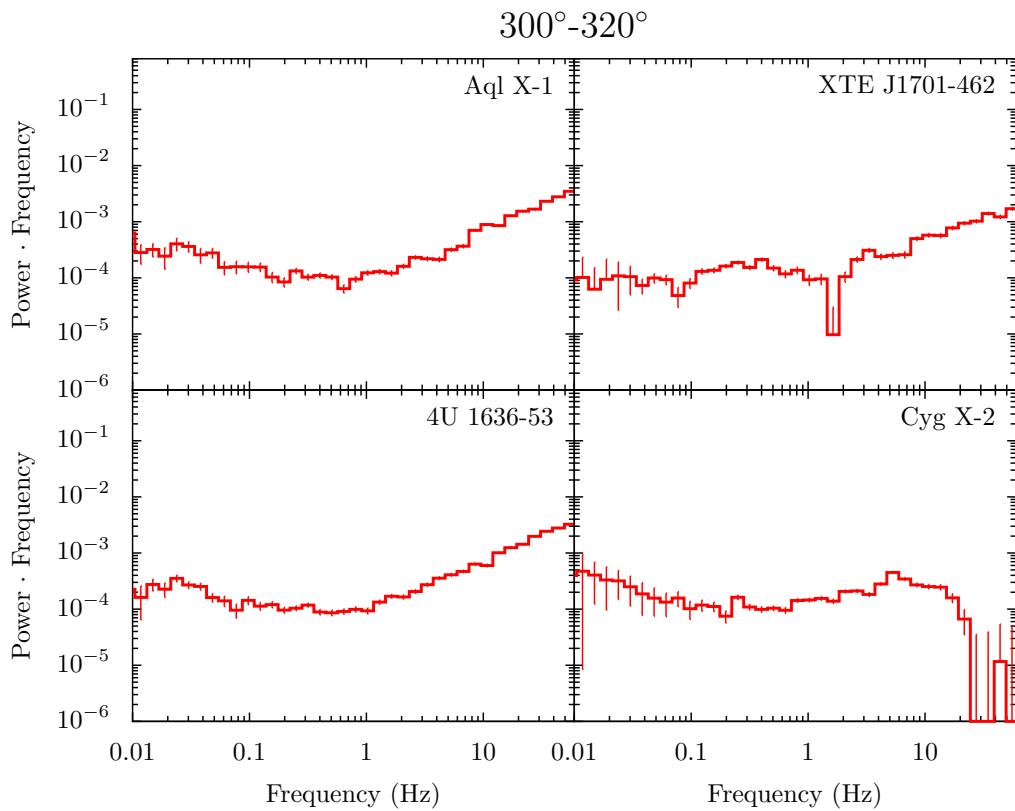
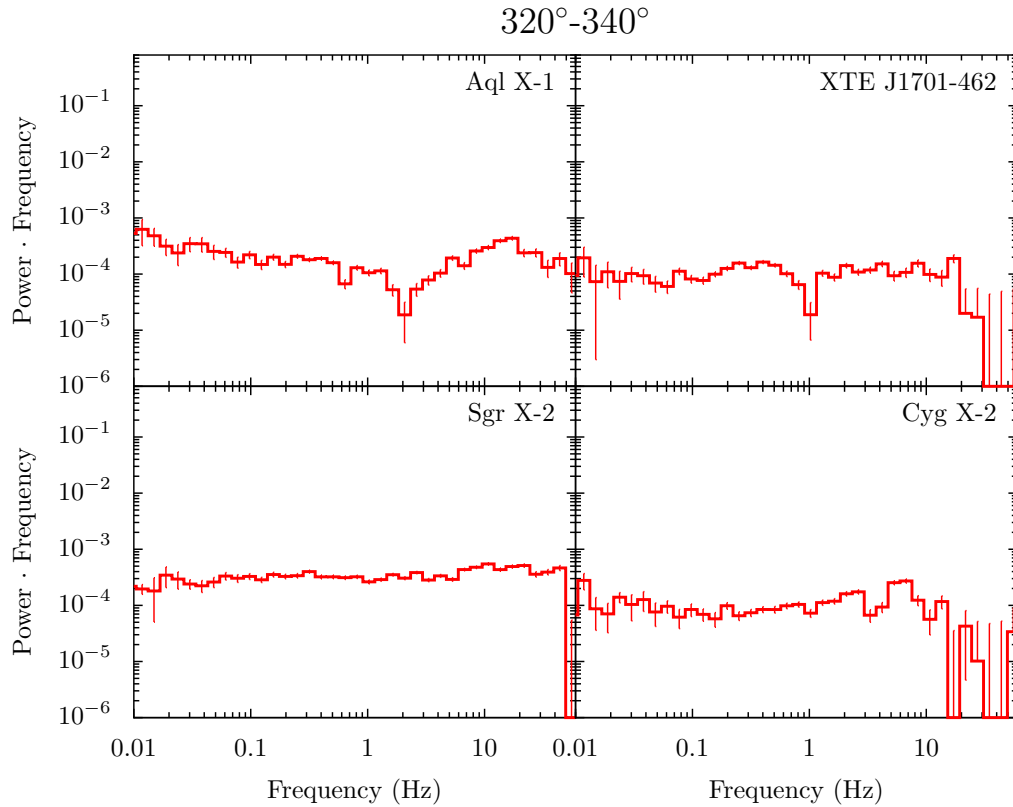
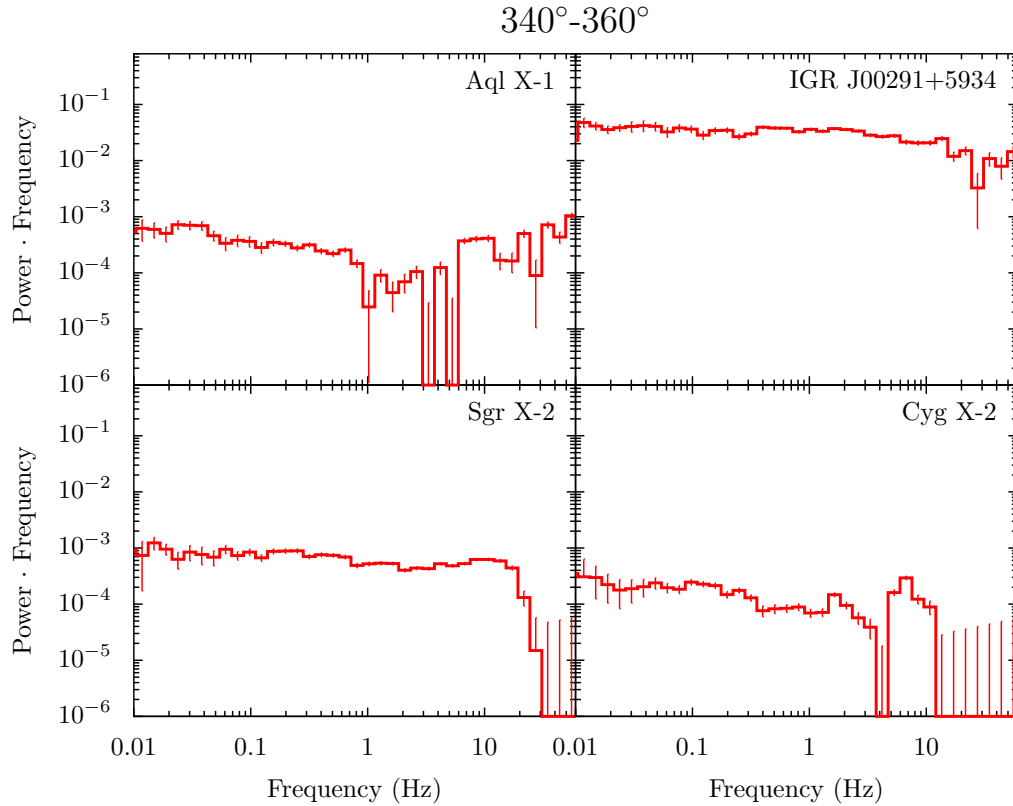


Figure 32: Representative power spectra within a hue range of $300^\circ\text{--}320^\circ$

Figure 33: Representative power spectra within a hue range of $320^\circ\text{--}340^\circ$ Figure 34: Representative power spectra within a hue range of $340^\circ\text{--}360^\circ$

d

POWER COLOUR-COLOUR DIAGRAMS

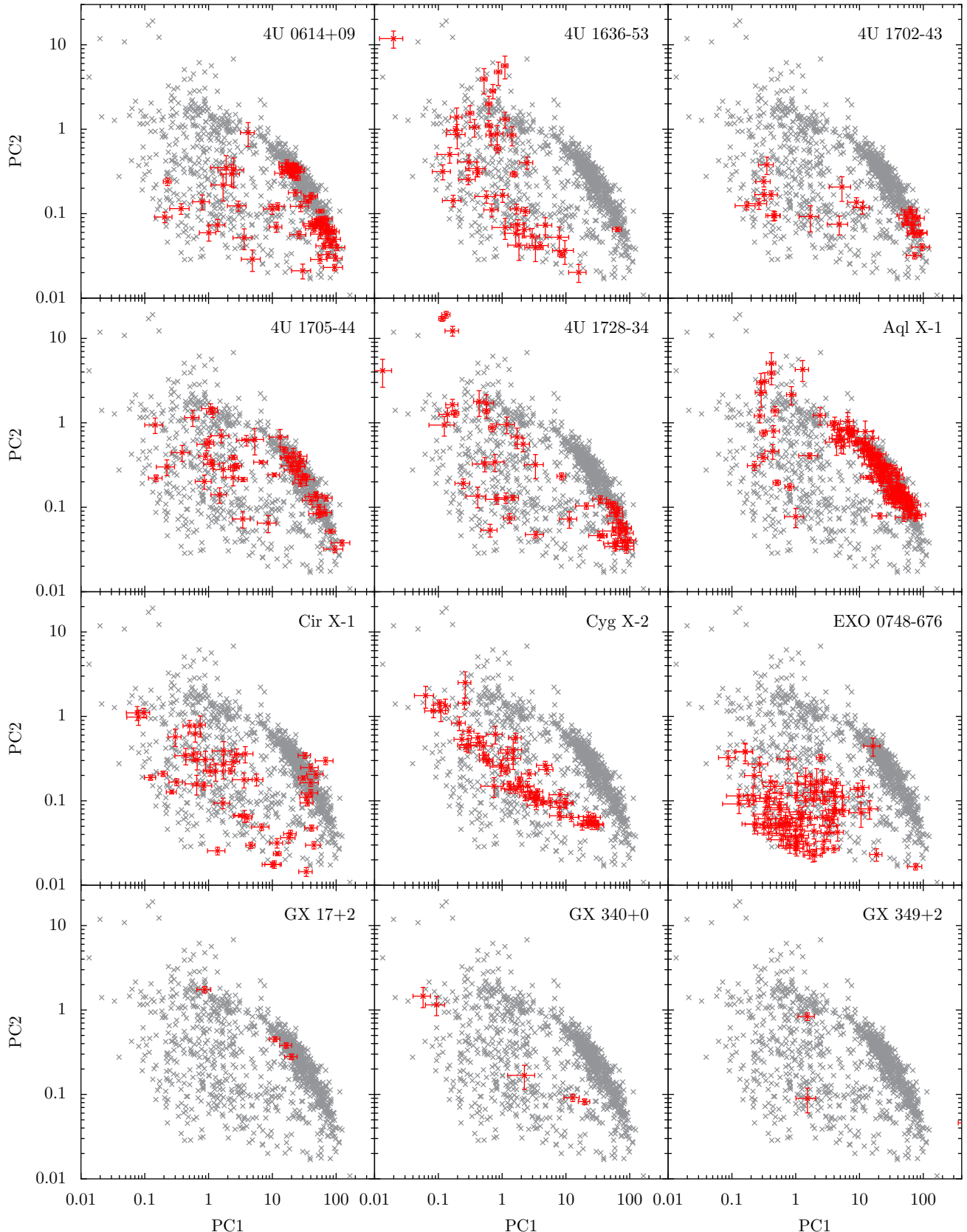


Figure 35: PCC diagrams for 4U to GX

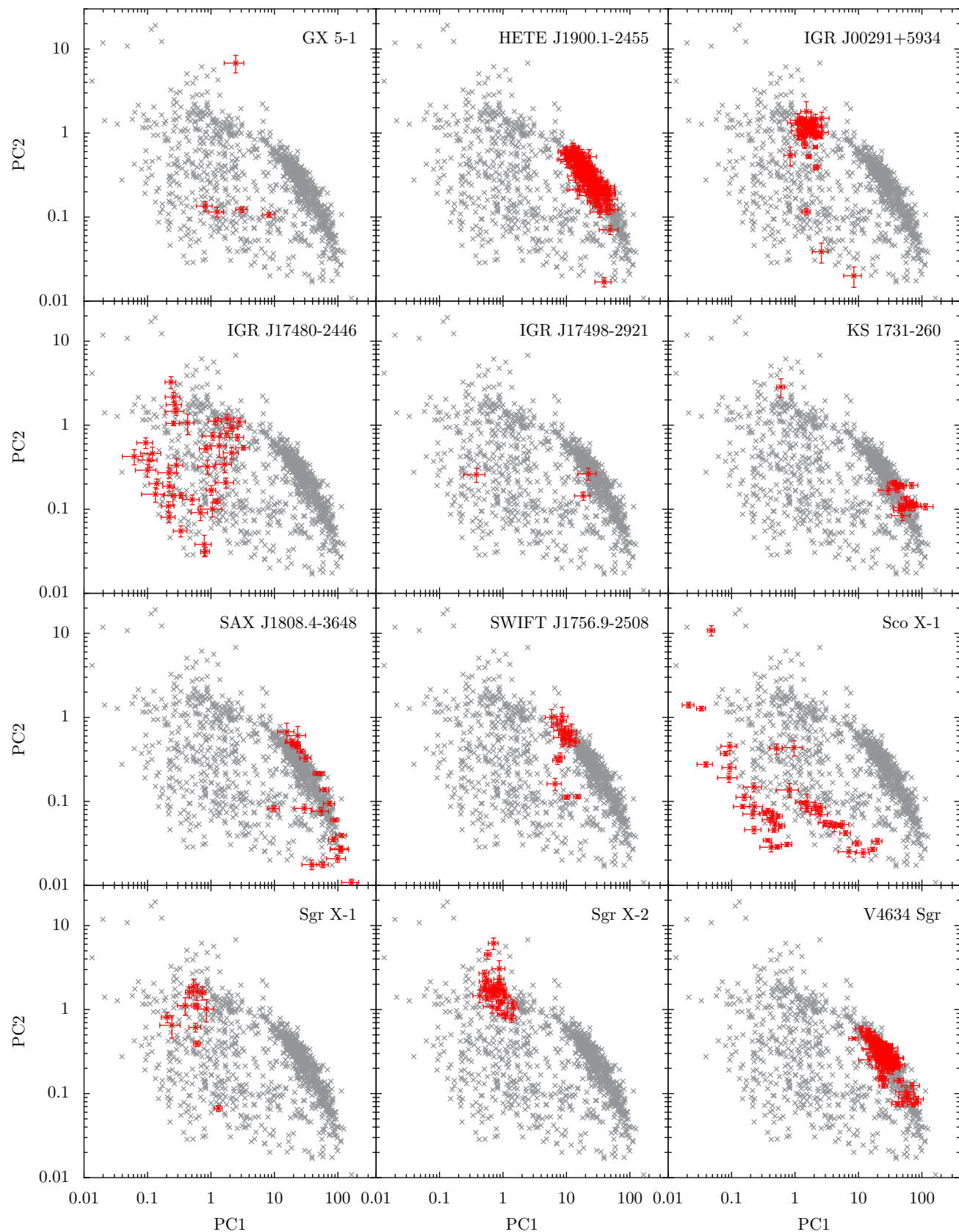


Figure 36: PCC diagrams for GX to V4

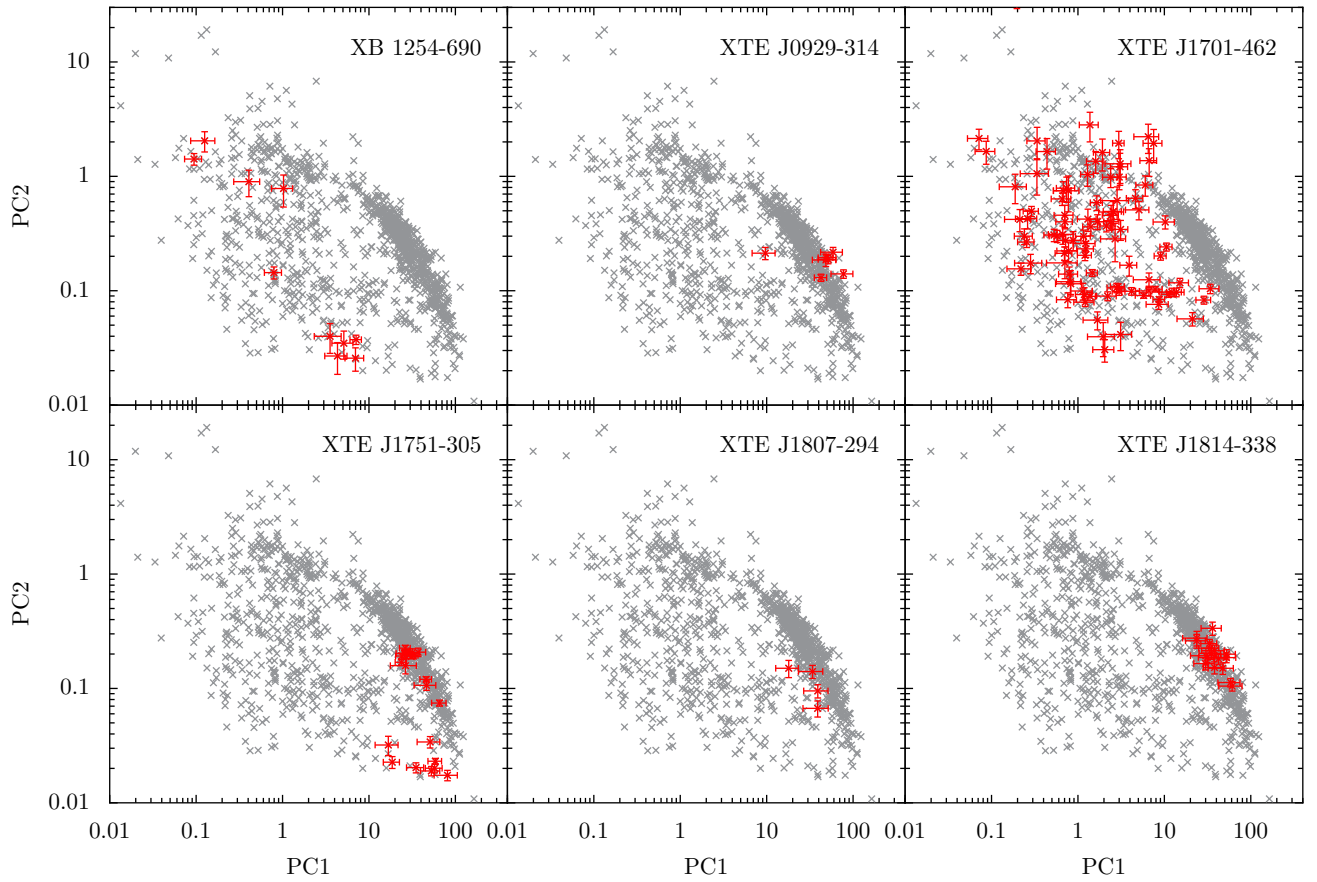


Figure 37: PCC diagrams for XB to XTE

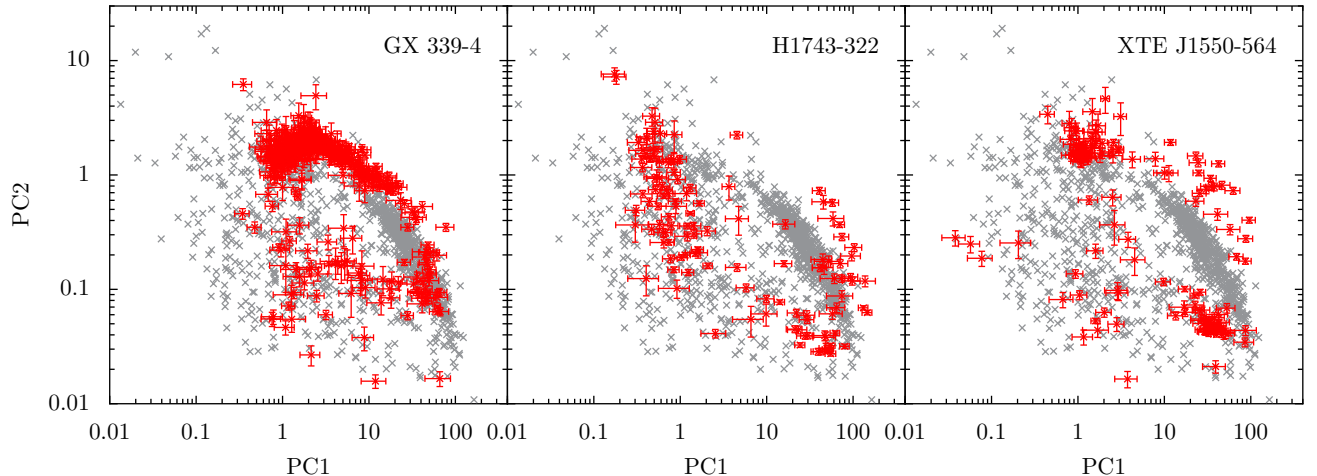


Figure 38: PCC diagrams for black holes

e

HARDNESS-HUE DIAGRAMS

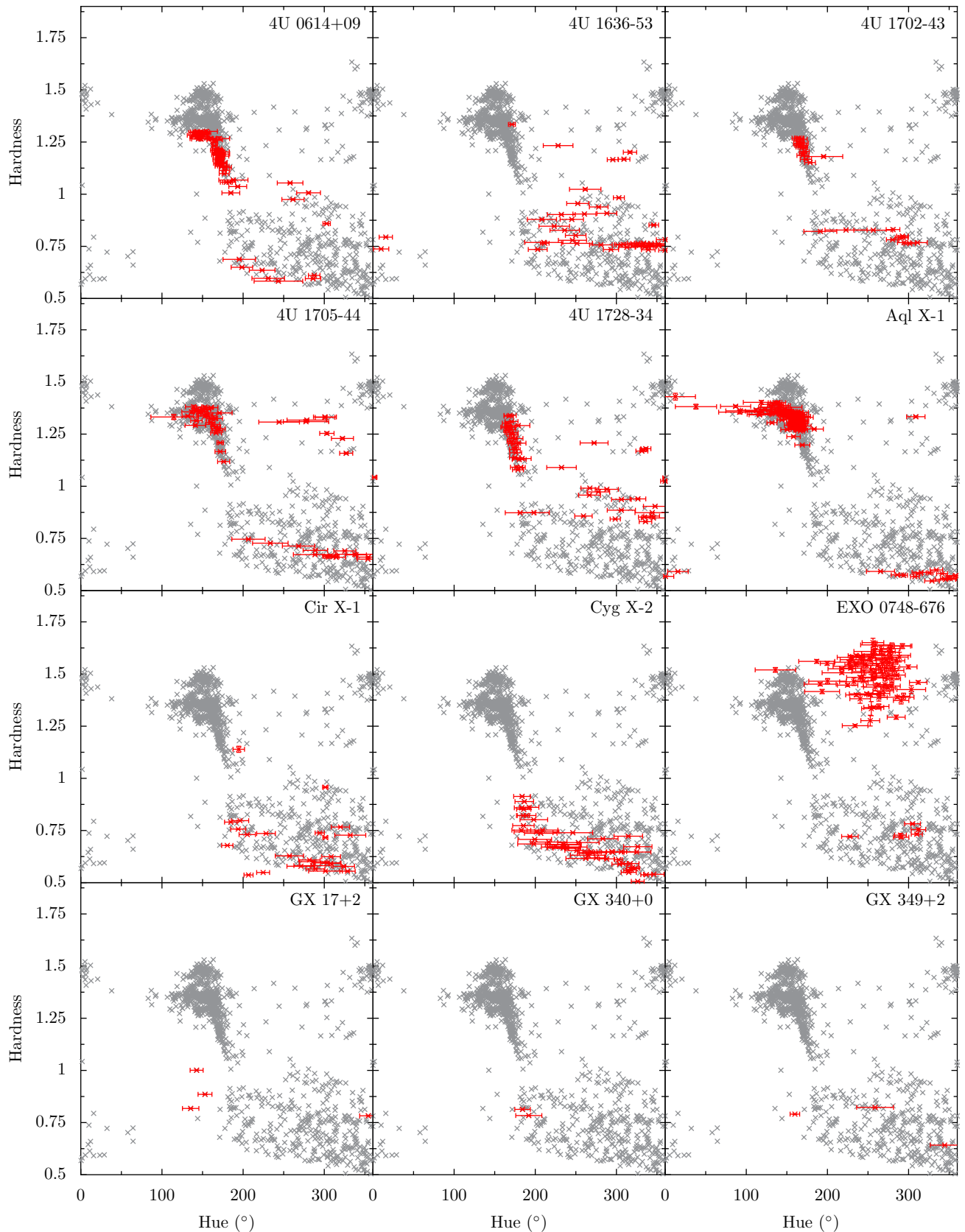


Figure 39: HH diagrams for 4U to GX

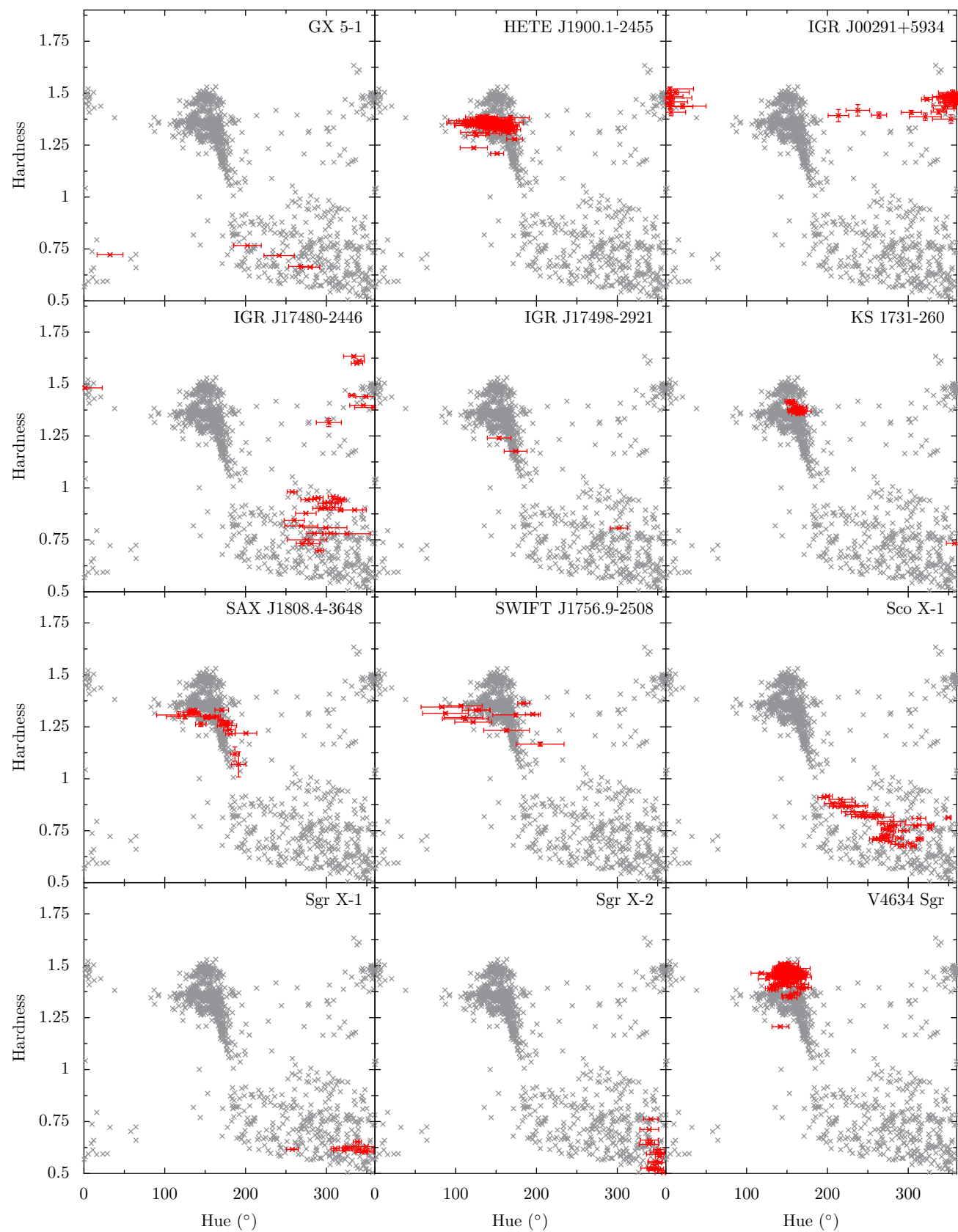


Figure 40: HH diagrams for GX to V4

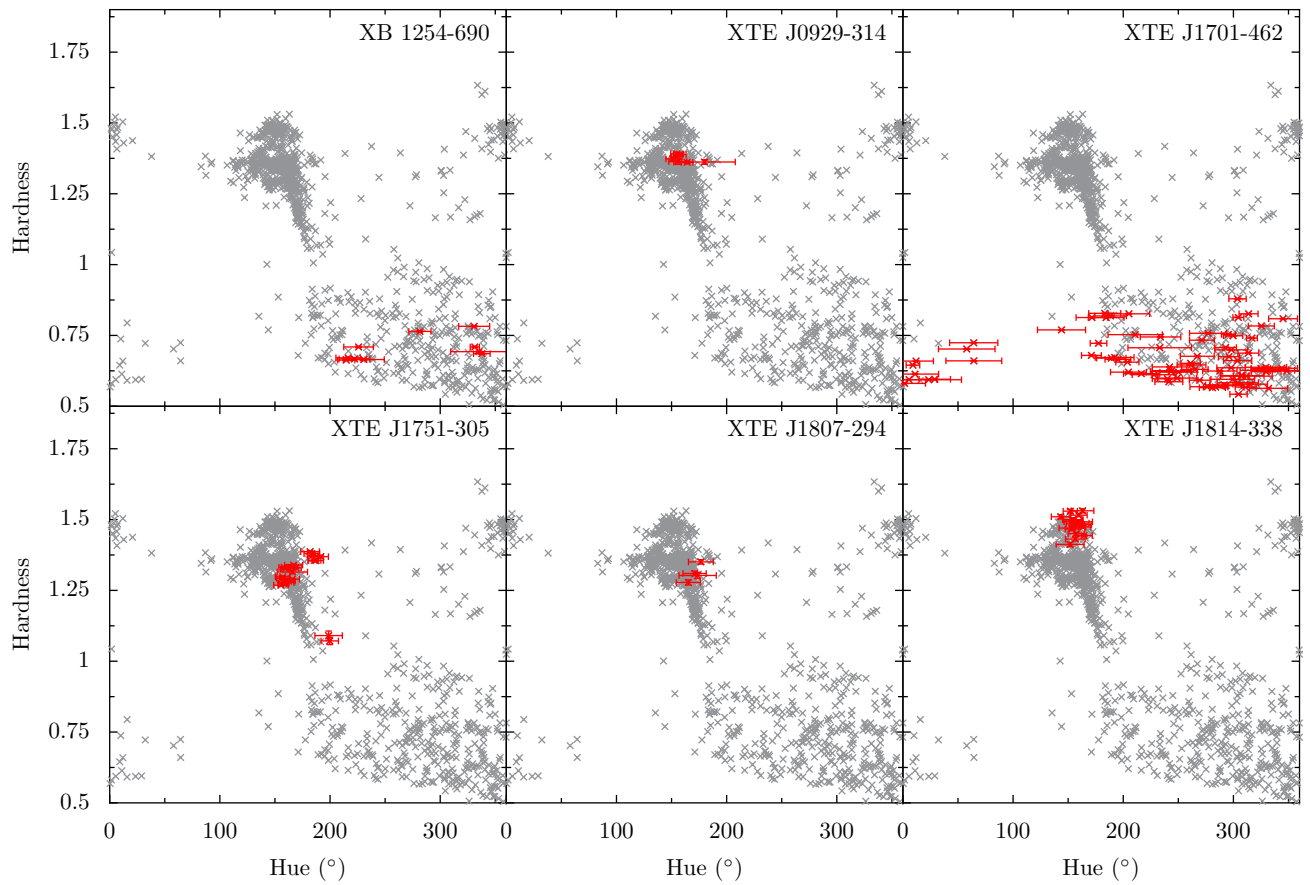


Figure 41: HH diagrams for XB to XTE

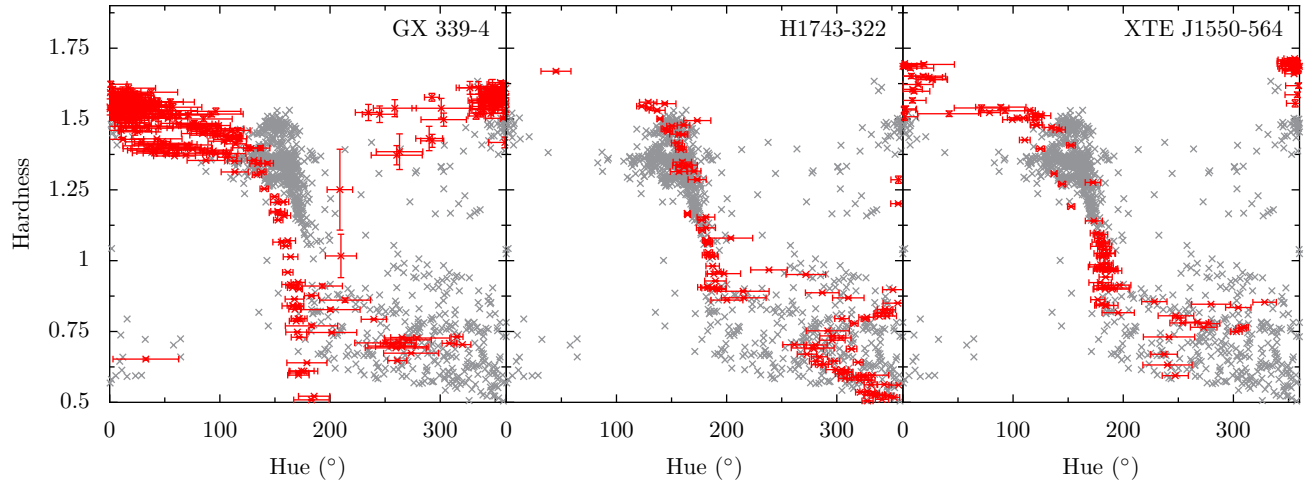


Figure 42: HH diagrams for black holes

f

HARDNESS-INTENSITY DIAGRAMS

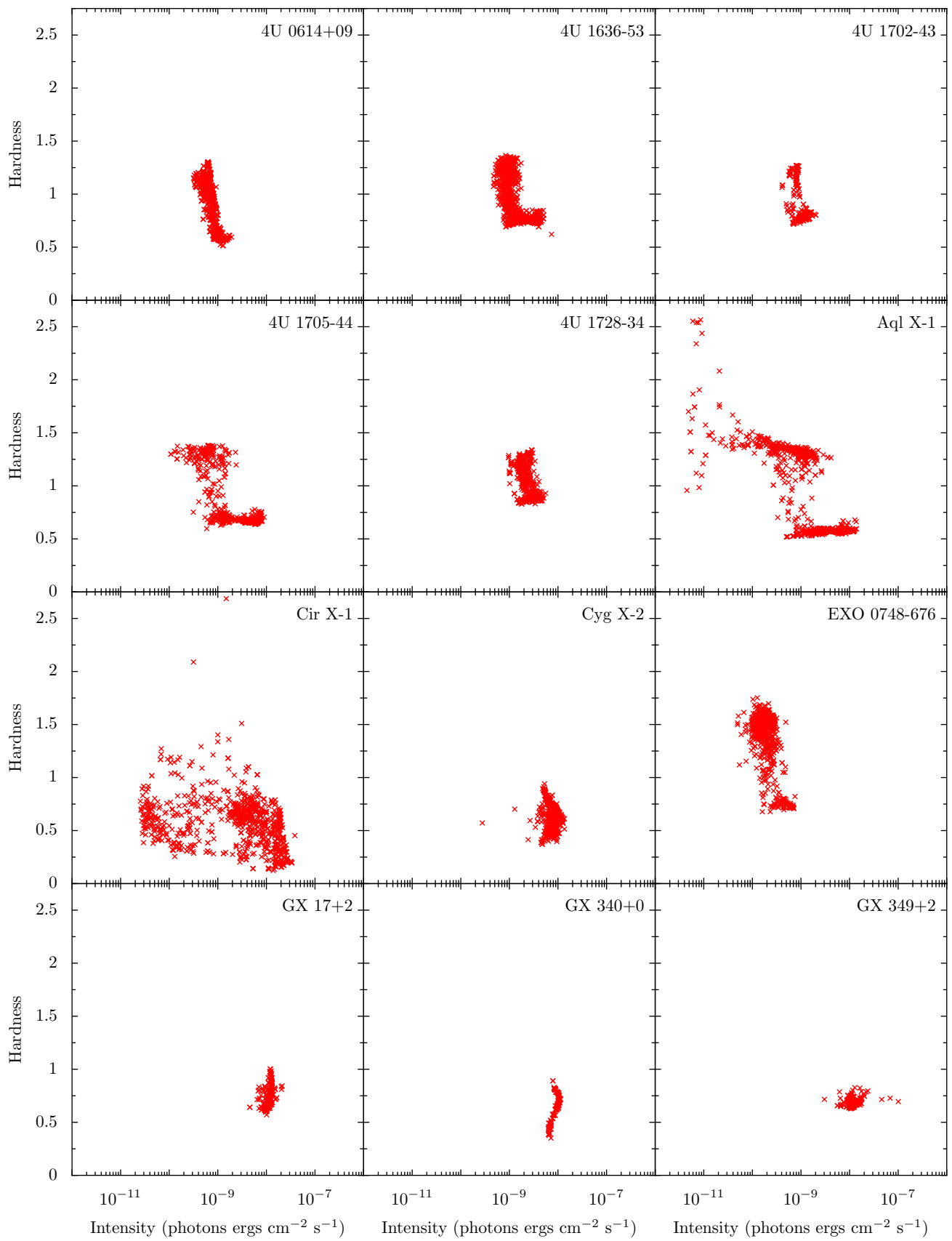


Figure 43: HI diagrams for 4U to GX

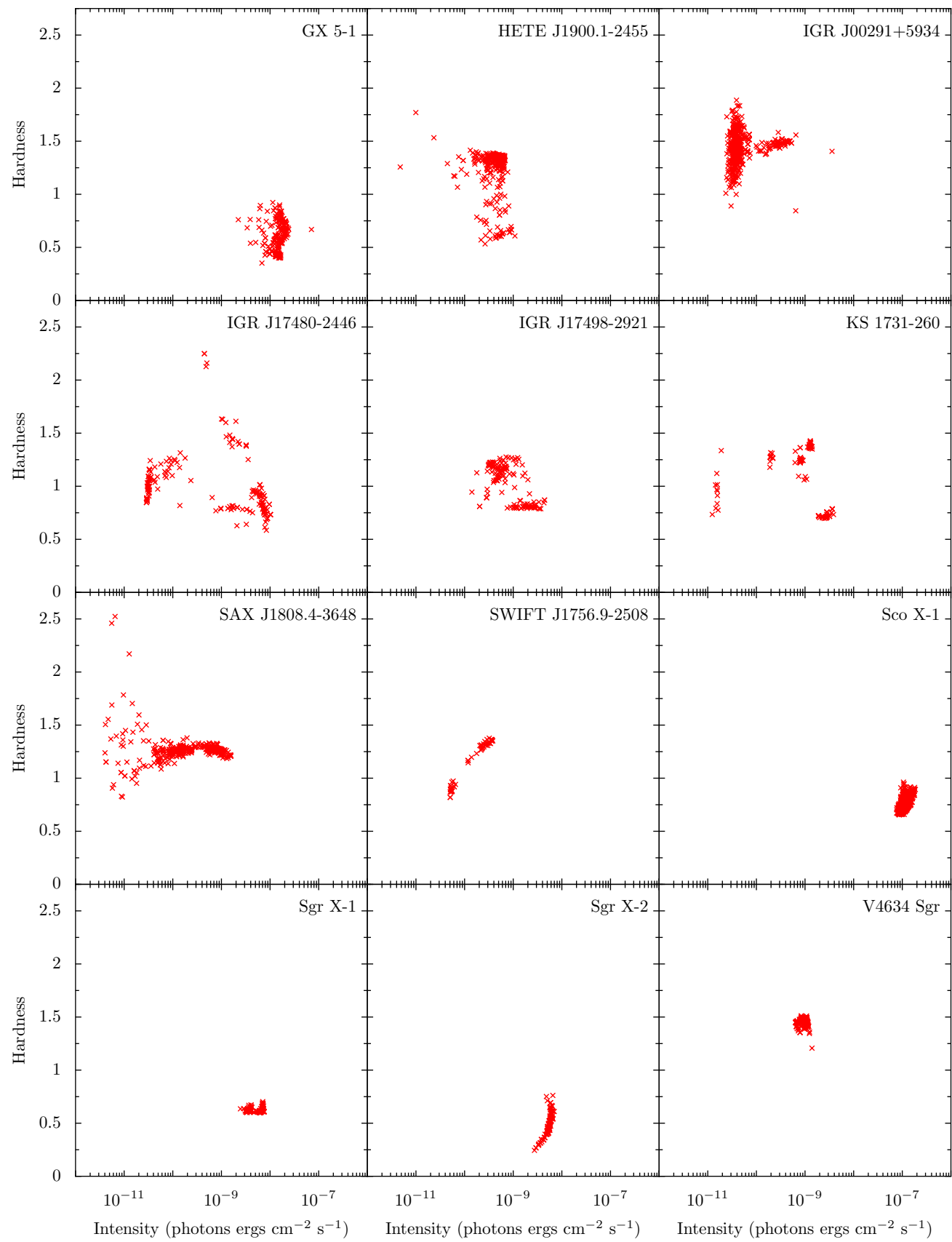


Figure 44: HI diagrams for GX to V4

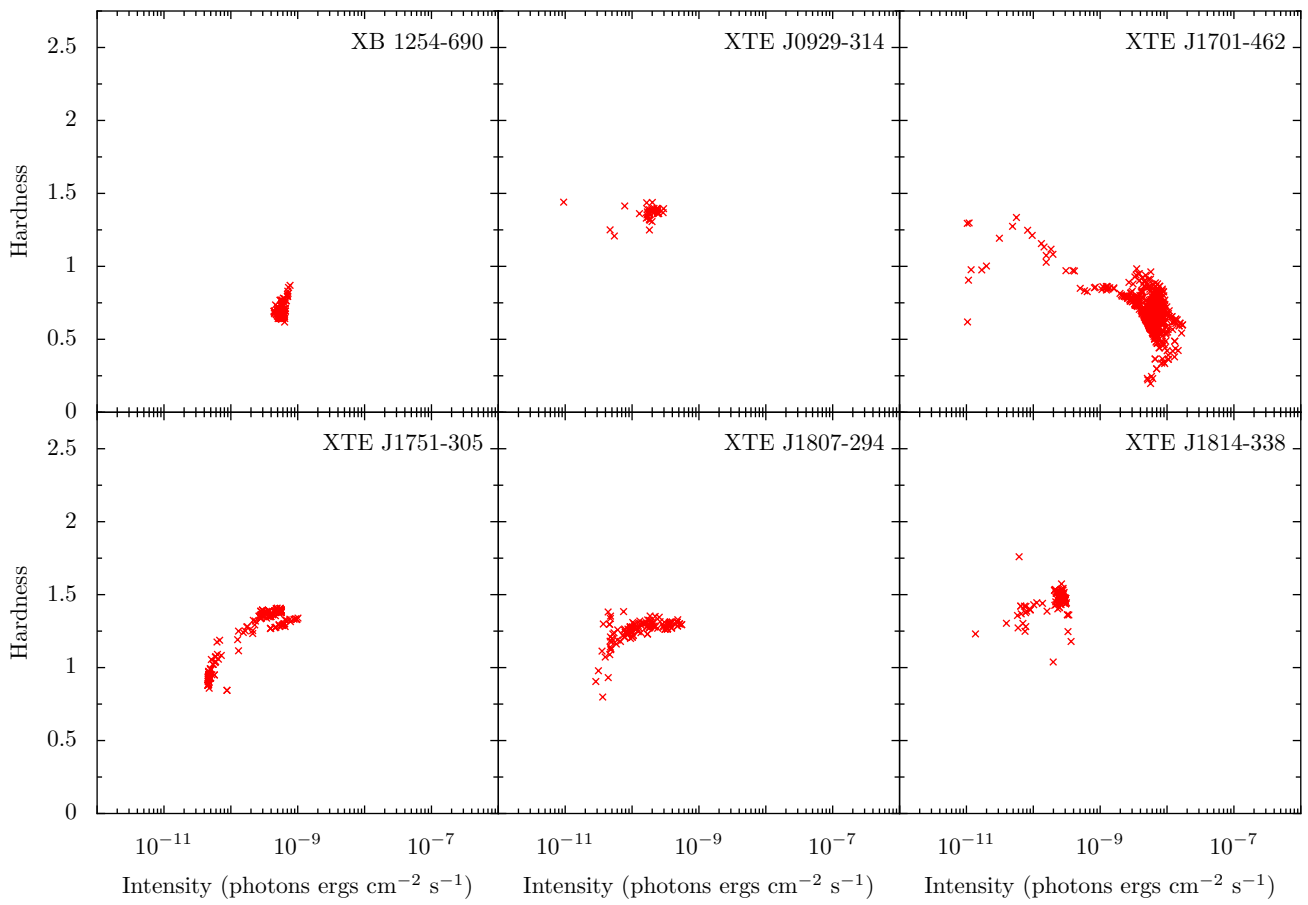


Figure 45: HI diagrams for XB to XTE

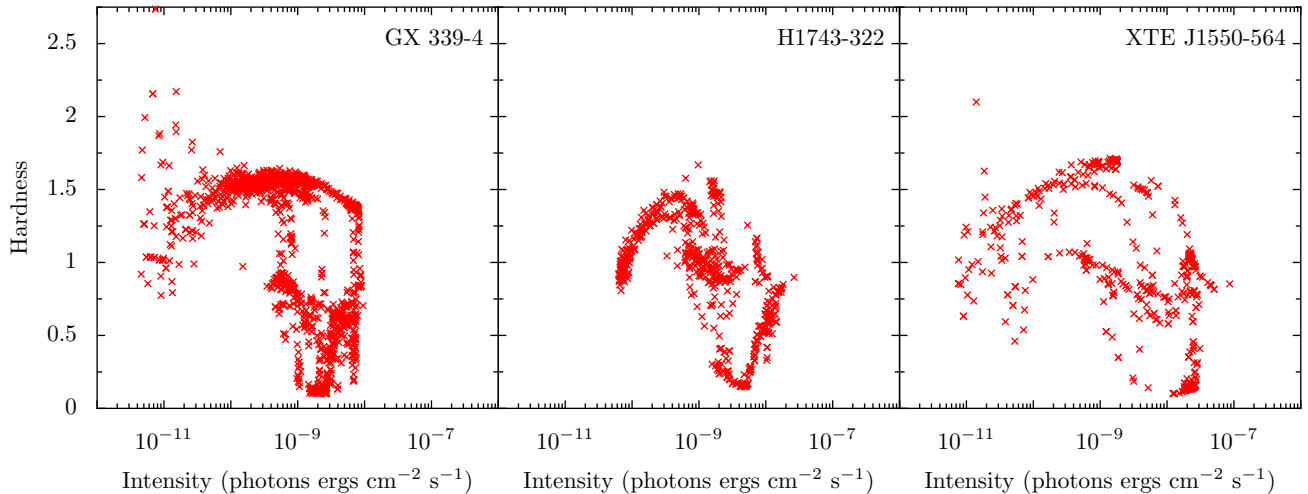


Figure 46: HI diagrams for black holes

BIBLIOGRAPHY

- Adams, (2002). *The Salmon of Doubt: Hitchhiking the Universe One Last Time*. Harmony.
- Altamirano, (2008). 'Different Manifestations of Accretion onto Compact Objects'. PhD thesis. University of Amsterdam.
- Arnaud, (1996). 'Astronomical data analysis software and systems V'. In: *ASP Conf. Ser.* Vol. 101. 1.
- Belloni, Hasinger and, (1990). 'Variability in the noise properties of Cygnus X-1'. In: *Astronomy and Astrophysics* 227, pp. L33–L36.
- Benacquista, (2012). *An introduction to the evolution of single and binary stars*. Springer Science & Business Media.
- Bhattacharyya, (2007). 'Timing properties of XB 1254- 690'. In: *Monthly Notices of the Royal Astronomical Society* 377.1, pp. 198–202.
- Bradt, Rothschild, Swank and, (1993). 'X-ray timing explorer mission'. In: *Astronomy and Astrophysics Supplement Series* 97, pp. 355–360.
- Cackett, Altamirano, Patruno, Miller, Reynolds, Linares, Wijnands and, (2009). 'Broad Relativistic Iron Emission Line Observed in SAX J1808. 4–3658'. In: *The Astrophysical Journal Letters* 694.1, p. L21.
- Chakrabarti, Molteni and, (1993). 'Smoothed particle hydrodynamics confronts theory: formation of standing shocks in accretion disks and winds around black holes'. In: *The Astrophysical Journal* 417, p. 671.
- Chakrabarty, Morgan, Muno, Galloway, Wijnands, van der Klis, Markwardt and, (2003). 'Nuclear-powered millisecond pulsars and the maximum spin frequency of neutron stars'. In: *Nature* 424.6944, pp. 42–44.
- Crampton, Cowley, Hutchings, Kaat and, (1976). 'Spectroscopic analysis of Scorpius X-1.' In: *The Astrophysical Journal* 207, pp. 907–913.
- Cumming, Zweibel, Bildsten and, (2001). 'Magnetic screening in accreting neutron stars'. In: *The Astrophysical Journal* 557.2, p. 958.
- Dennis, (2006). 'X-ray power density spectra of black hole binaries: a new deadtime model for the RXTE PCA'. PhD thesis. Massachusetts Institute of Technology.
- Di Salvo, et al. (2009). 'A relativistically smeared spectrum in the neutron star X-ray binary 4U 1705- 44: looking at the inner accretion disc with X-ray spectroscopy'. In: *Monthly Notices of the Royal Astronomical Society* 398.4, pp. 2022–2027.
- Done, Gierliński and, (2003). 'Observing the effects of the event horizon in black holes'. In: *Monthly Notices of the Royal Astronomical Society* 342.4, pp. 1041–1055.

- Done, Gierliński, Kubota and, (2007). 'Modelling the behaviour of accretion flows in X-ray binaries'. In: *The Astronomy and Astrophysics Review* 15.1, pp. 1–66.
- Frank, King, Raine and, (2002). *Accretion power in astrophysics*. Cambridge university press.
- Fridriksson, Homan, Remillard and, (2015). 'Common Patterns in the Evolution between the Luminous Neutron Star Low-Mass X-ray Binary Subclasses'. In: *The Astrophysical Journal* 809.1, p. 52.
- Galeev, Rosner, Vaiana and, (1979). 'Structured coronae of accretion disks'. In: *The Astrophysical Journal* 229, pp. 318–326.
- Galloway, Chakrabarty, Morgan, Remillard and, (2002). 'Discovery of a high-latitude accreting millisecond pulsar in an ultracompact binary'. In: *The Astrophysical Journal Letters* 576.2, p. L137.
- Galloway, Markwardt, Morgan, Chakrabarty, Strohmayer and, (2005). 'Discovery of the accretion-powered millisecond X-ray pulsar IGR J00291+ 5934'. In: *The Astrophysical Journal Letters* 622.1, p. L45.
- Galloway, Morgan, Krauss, Kaaret, Chakrabarty and, (2006). 'Intermittent pulsations in an accretion-powered millisecond pulsar'. In: *The Astrophysical Journal Letters* 654.1, p. L73.
- Galloway, Muno, Hartman, Psaltis, Chakrabarty and, (2008). 'Thermonuclear (type i) X-ray bursts observed by the rossi X-ray timing explorer'. In: *The Astrophysical Journal Supplement Series* 179.2, p. 360.
- Galloway, Lin, Chakrabarty, Hartman and, (2010). 'Discovery of a 552 Hz Burst Oscillation in the Low-Mass X-Ray Binary EXO 0748–676'. In: *The Astrophysical Journal Letters* 711.2, p. L148.
- Galloway, Ajamyan, Upjohn, Stuart and, (2016). 'Intermittent dipping in a low-mass X-ray Binary'. In: *Monthly Notices of the Royal Astronomical Society*, stw1576.
- Ghosh, Lamb and, (1978). 'Disk accretion by magnetic neutron stars'. In: *The Astrophysical Journal* 223, pp. L83–L87.
- Giacconi, Gursky, Paolini, Rossi and, (1962). 'Evidence for x Rays From Sources Outside the Solar System'. In: *Phys. Rev. Lett.* 9 (11), pp. 439–443.
- Gierlinski, Done and, (2002). 'A comment on the colour-colour diagrams of low-mass X-ray binaries'. In: *Monthly Notices of the Royal Astronomical Society* 331, pp. L47–L50.
- Gilfanov, (2010). 'X-ray emission from black-hole binaries'. In: *The Jet Paradigm*. Springer, pp. 17–51.
- Gilfanov, Merloni and, (2014). 'Observational appearance of black holes in X-ray binaries and AGN'. In: *Space Science Reviews* 183.1–4, pp. 121–148.
- Gladstone, Done, Gierliński and, (2007). 'Analysing the atolls: X-ray spectral transitions of accreting neutron stars'. In: *Monthly Notices of the Royal Astronomical Society* 378.1, pp. 13–22.

- Gleissner, Wilms, Pottschmidt, Uttley, Nowak, Staubert and, (2004). 'Long term variability of Cyg X-1-II. The rms-flux relation'. In: *Astronomy & Astrophysics* 414.3, pp. 1091–1104.
- Hasinger, van der Klis and, (1989). 'Two patterns of correlated X-ray timing and spectral behaviour in low-mass X-ray binaries'. In: *Astronomy and Astrophysics* 225, pp. 79–96.
- Heil, Uttley, Klein-Wolt and, (2015a). 'Inclination-dependent spectral and timing properties in transient black hole X-ray binaries'. In: *Monthly Notices of the Royal Astronomical Society* 448.4, pp. 3348–3353.
- Heil, Uttley, Klein-Wolt and, (2015b). 'Power colours: simple X-ray binary variability comparison'. In: *Monthly Notices of the Royal Astronomical Society* 448.4, pp. 3339–3347.
- Heil, Vaughan, Uttley and, (2012). 'The ubiquity of the rms–flux relation in black hole X-ray binaries'. In: *Monthly Notices of the Royal Astronomical Society* 422.3, pp. 2620–2631.
- Homan, (2012). 'A possible signature of Lense-Thirring precession in dipping and eclipsing neutron-star low-mass X-ray binaries'. In: *The Astrophysical Journal Letters* 760.2, p. L30.
- Homan, Fridriksson, Remillard and, (2015). 'On the Geometric Nature of Low-frequency Quasi-periodic Oscillations in Neutron-star Low-mass X-Ray Binaries'. In: *The Astrophysical Journal* 812.1, p. 80.
- Homan, Wijnands, van der Klis, Belloni, van Paradijs, Klein-Wolt, Fender, Mendez and, (2001). 'Correlated X-ray spectral and timing behavior of the black hole candidate XTE J1550–564: a new interpretation of black hole states'. In: *The Astrophysical Journal Supplement Series* 132.2, p. 377.
- Homan, Miller, Wijnands, van der Klis, Belloni, Steeghs, Lewin and, (2005). 'High-and Low-Frequency Quasi-periodic Oscillations in the X-Ray Light Curves of the Black Hole Transient H1743–322'. In: *The Astrophysical Journal* 623.1, p. 383.
- Homan, et al. (2007). 'Rossi X-Ray Timing Explorer Observations of the First Transient Z Source XTE J1701–462: Shedding New Light on Mass Accretion in Luminous Neutron Star X-Ray Binaries'. In: *The Astrophysical Journal* 656.1, p. 420.
- Iaria, D'Aí, Lavagetto, Di Salvo, Robba, Burderi and, (2008). 'Chandra Observation of Cir X-1 near the Periastron Passage: Evidence for an X-Ray Jet?' In: *The Astrophysical Journal* 673.2, p. 1033.
- Jahoda, Swank, Giles, Stark, Strohmayer, Zhang, Morgan and, (1996). 'In-orbit performance and calibration of the Rossi X-ray Timing Explorer (RXTE) Proportional Counter Array (PCA)'. In: *SPIE's 1996 International Symposium on Optical Science, Engineering, and Instrumentation*. International Society for Optics and Photonics, pp. 59–70.
- Jahoda, Markwardt, Radeva, Rots, Stark, Swank, Strohmayer, Zhang and, (2006). 'Calibration of the Rossi X-ray timing explorer pro-

- portional counter array'. In: *The Astrophysical Journal Supplement Series* 163.2, p. 401.
- Klein-Wolt, van der Klis and, (2008). 'Identification of black hole power spectral components across all canonical states'. In: *The Astrophysical Journal* 675.2, p. 1407.
- Klein-Wolt, (2004). 'Black Hole X-ray Binaries'. PhD thesis. University of Amsterdam.
- Krimm, et al. (2007). 'Discovery of the Accretion-powered Millisecond Pulsar SWIFT J1756. 9–2508 with a Low-Mass Companion'. In: *The Astrophysical Journal Letters* 668.2, p. L147.
- Kuulkers, van der Klis and, (1995). 'Detection of 26Hz quasi-periodic oscillations in the flaring branch of CygnusX-2.' In: *Astronomy and Astrophysics* 303, p. 801.
- Kuulkers, van der Klis, Oosterbroek, Asai, Dotani, van Paradijs, Lewin and, (1994). 'Spectral and correlated timing behaviour of GX 5-1'. In: *Astronomy and Astrophysics* 289, pp. 795–821.
- Kuulkers, Kuulkers, van der Klis, Oosterbroek, van Paradijs, Lewin and, (1997). 'GX 17+ 2: X-ray spectral and timing behaviour of a bursting Z source'. In: *Monthly Notices of the Royal Astronomical Society* 287.3, pp. 495–514.
- Lamb, Pethick, Pines and, (1973). 'A Model for Compact X-Ray Sources: Accretion by Rotating Magnetic Stars'. In: *The Astrophysical Journal* 184, pp. 271–290.
- Legg, Miller, Turner, Giustini, Reeves, Kraemer and, (2012). 'Direct measurement of the X-ray time-delay transfer function in active galactic nuclei'. In: *The Astrophysical Journal* 760.1, p. 73.
- Lin, Remillard, Homan and, (2007). 'Evaluating spectral models and the X-ray states of neutron star X-ray transients'. In: *The Astrophysical Journal* 667.2, p. 1073.
- Lin, Remillard, Homan and, (2009). 'Spectral States of XTE J1701–462: Link Between Z and Atoll Sources'. In: *The Astrophysical Journal* 696.2, p. 1257.
- Liu, van Paradijs, van den Heuvel and, (2001). 'A catalogue of low-mass X-ray binaries'. In: *Astronomy & Astrophysics* 368.3, pp. 1021–1054.
- Lyubarskii, (1997). 'Flicker noise in accretion discs'. In: *Monthly Notices of the Royal Astronomical Society* 292.3, pp. 679–685.
- Maccarone, Coppi, Poutanen and, (2000). 'Time domain analysis of variability in Cygnus X-1: constraints on the emission models'. In: *The Astrophysical Journal Letters* 537.2, p. L107.
- Markoff, Nowak, Wilms and, (2005). 'Going with the flow: can the base of jets subsume the role of compact accretion disk coronae?' In: *The Astrophysical Journal* 635.2, p. 1203.
- Markwardt, Smith, Swank and, (2003). 'Discovery of a Fourth Accreting Millisecond Pulsar, XTE J1807-294'. In: *The Astronomer's Telegram* 122.

- Markwardt, Swank and, (2003). 'XTE J1814-338'. In: *International Astronomical Union Circular* 8144, p. 1.
- Markwardt, Swank, Strohmayer, Marshall, et al. (2002). 'Discovery of a Second Millisecond Accreting Pulsar: XTE J1751-305'. In: *The Astrophysical Journal Letters* 575.1, p. L21.
- Méndez, van der Klis, van Paradijs, Lewin, Lamb, Vaughan, Kuulkers, Psaltis and, (1997). 'Kilohertz quasi-periodic oscillation and atoll source states in 4U 0614+ 09'. In: *The Astrophysical Journal Letters* 485.1, p. L37.
- Misner, Thorne, Wheeler and, (1973). *Gravitation*. Macmillan.
- Morgan, Kaaret, Vanderspek and, (2005). 'HETE J1900. 1-2455 is a millisecond pulsar.' In: *The Astronomer's Telegram* 523.
- Motta, Homan, Muñoz-Darias, Casella, Belloni, Hiemstra, Méndez and, (2012). 'Discovery of two simultaneous non-harmonically related quasi-periodic oscillations in the 2005 outburst of the black hole binary GRO J1655-40'. In: *Monthly Notices of the Royal Astronomical Society* 427.1, pp. 595–606.
- Motta, Casella, Henze, Muñoz-Darias, Sanna, Fender, Belloni and, (2015). 'Geometrical constraints on the origin of timing signals from black holes'. In: *Monthly Notices of the Royal Astronomical Society* 447.2, pp. 2059–2072.
- Muno, Remillard, Chakrabarty and, (2002). 'How do Z and atoll x-ray binaries differ?' In: *The Astrophysical Journal Letters* 568.1, p. L35.
- NASA, (2014). *Black Holes (Illustrations)*. Accessed: 11-07-2016. URL: <http://chandra.harvard.edu/resources/illustrations/blackholes.html>.
- NASA, (2015). *High Energy Astrophysics Science Archive Research Center*. Accessed: 23-06-2016. URL: <http://heasarc.gsfc.nasa.gov/cgi-bin/W3Browse/w3browse.pl>.
- OED, (1976). *The Concise Oxford Dictionary of Current English* (6th ed). Ely House, London: Oxford University Press.
- Oppenheimer, Volkoff and, (1939). 'On massive neutron cores'. In: *Physical Review* 55.4, p. 374.
- Orosz, Kuulkers and, (1999). 'The optical light curves of Cygnus X-2 (V1341 Cyg) and the mass of its neutron star'. In: *Monthly Notices of the Royal Astronomical Society* 305.1, pp. 132–142.
- Pahari, Neilsen, Yadav, Misra, Uttley and, (2013). 'Comparison of time/phase lags in the hard state and plateau state of GRS 1915+ 105'. In: *The Astrophysical Journal* 778.2, p. 136.
- Pandel, Kaaret, Corbel and, (2008). 'Relativistic iron line emission from the neutron star low-mass X-ray binary 4U 1636-536'. In: *The Astrophysical Journal* 688.2, p. 1288.
- Papitto, Bozzo, Ferrigno, Belloni, Burderi, Di Salvo, Riggio, D'Aì, Iaria and, (2011a). 'The discovery of the 401 Hz accreting millisecond pulsar IGR J17498-2921 in a 3.8 h orbit'. In: *Astronomy & Astrophysics* 535, p. L4.

- Papitto, D'Aì, Motta, Riggio, Burderi, Di Salvo, Belloni, Iaria and, (2011b). 'The spin and orbit of the newly discovered pulsar IGR J17480-2446'. In: *Astronomy & Astrophysics* 526, p. L3.
- Papitto, D'Aì, Di Salvo, Egron, Bozzo, Burderi, Iaria, Riggio, Menna and, (2013). 'The accretion flow to the intermittent accreting millisecond pulsar, HETE J1900. 1- 2455, as observed by XMM-Newton and RXTE'. In: *Monthly Notices of the Royal Astronomical Society*, sts605.
- Parmar, White, Giommi, Gottwald and, (1986). 'The discovery of 3.8 hour periodic intensity dips and eclipses from the transient low-mass X-ray binary EXO 0748-676'. In: *The Astrophysical Journal* 308, pp. 199–212.
- Patruno, Watts and, (2012). 'Accreting millisecond X-ray pulsars'. In: *arXiv preprint* 1206.2727.
- Payne, Melatos and, (2006). 'Magnetic burial and the harmonic content of millisecond oscillations in thermonuclear X-ray bursts'. In: *The Astrophysical Journal* 652.1, p. 597.
- Peille, Barret, Uttley and, (2015). 'The spectral-timing properties of upper and lower kHz QPOs'. In: *The Astrophysical Journal* 811.2, p. 109.
- Popham, Sunyaev and, (2001). 'Accretion disk boundary layers around neutron stars: X-ray production in low-mass X-ray binaries'. In: *The Astrophysical Journal* 547.1, p. 355.
- Psaltis, Lamb, Miller and, (1995). 'X-ray spectra of Z sources'. In: *The Astrophysical Journal Letters* 454.2, p. L137.
- ROSAT, (2002). *South Atlantic Anomaly*. Accessed: 29-06-2016. URL: http://heasarc.gsfc.nasa.gov/docs/rosat/gallery/misc_saad.html.
- RXTE, (1998a). *Maketime*. Accessed: 29-06-2016. URL: <https://heasarc.gsfc.nasa.gov/ftools/caldb/help/maketime.txt>.
- RXTE, (1998b). *Pcabackest*. Accessed: 30-06-2016. URL: <https://heasarc.gsfc.nasa.gov/ftools/caldb/help/pcabackest.txt>.
- RXTE, (1998c). *Pcarsp*. Accessed: 03-07-2016. URL: <https://heasarc.gsfc.nasa.gov/ftools/caldb/help/pcarsp.txt>.
- RXTE, (1998d). *Saextract*. Accessed: 01-07-2016. URL: <https://heasarc.gsfc.nasa.gov/ftools/caldb/help/saextract.txt>.
- RXTE, (1998e). *Seextract*. Accessed: 01-07-2016. URL: <https://heasarc.gsfc.nasa.gov/ftools/caldb/help/seextract.txt>.
- RXTE, (1999). *PCA Issues*. Accessed: 23-06-2016. URL: https://heasarc.gsfc.nasa.gov/docs/xte/abc/pca_issues.html.
- RXTE, (2000). *Archive*. Accessed: 28-06-2016. URL: <https://heasarc.gsfc.nasa.gov/docs/xte/recipes/archive.html>.
- RXTE, (2006a). *Proportional Counter Array (PCA)*. Accessed: 13-07-2016. URL: <https://heasarc.gsfc.nasa.gov/docs/xte/PCA.html>.

- RXTE, (2006b). *Reduction and Analysis of PCA Binned-Mode Data*. Accessed: 29-06-2016. URL: https://heasarc.gsfc.nasa.gov/docs/xte/recipes/pca_spectra.html.
- RXTE, (2012a). *Correcting for PCA Deadtime*. Accessed: 20-05-2016. URL: https://heasarc.gsfc.nasa.gov/docs/xte/recipes/pca_deadtime.html.
- RXTE, (2012b). *Energy-Channel Conversion Table*. Accessed: 09-06-2016. URL: https://heasarc.gsfc.nasa.gov/docs/xte/e-c_table.html.
- RXTE, (2012c). *PCA Digest: Recent Developments*. Accessed: 30-06-2016. URL: http://heasarc.gsfc.nasa.gov/docs/xte/pca_news.html.
- RXTE, (2012d). *Reduction and Analysis of PCA Event-Mode Data*. Accessed: 29-06-2016. URL: https://heasarc.gsfc.nasa.gov/docs/xte/recipes/pca_event_spectra.html.
- RXTE, (2013). *Standard Data Products*. Accessed: 29-06-2016. URL: https://heasarc.gsfc.nasa.gov/docs/xte/recipes/stdprod_guide.html.
- Rhoades Jr, Ruffini and, (1974). 'Maximum mass of a neutron star'. In: *Physical Review Letters* 32.6, p. 324.
- Rothschild, Blanco, Gruber, Heindl, MacDonald, Marsden, Pelling, Wayne, Hink and, (1998). 'In-flight performance of the high energy X-ray timing experiment on the Rossi X-ray Timing Explorer'. In: *The Astrophysical Journal* 496.1, p. 538.
- SIMBAD, (2016). *SIMBAD Astronomical Database*. Accessed: 01-06-2016. URL: <http://simbad.u-strasbg.fr/simbad/>.
- Schulz, Nowak, Chakrabarty, Canizares and, (2010). 'Dynamical K Edge and Line Variations in the X-ray Spectrum of the Ultra-compact Binary 4U 0614+ 091'. In: *The Astrophysical Journal* 725.2, p. 2417.
- Schwarzschild, (1916). 'Über das gravitationsfeld eines massenpunktes nach der einsteinschen theorie'. In: *Sitzungsberichte der Königlich Preußischen Akademie der Wissenschaften (Berlin)*, 1916, Seite 189-196 1, pp. 189–196.
- Shakura, Sunyaev and, (1976). 'A theory of the instability of disk accretion on to black holes and the variability of binary X-ray sources, galactic nuclei and quasars'. In: *Monthly Notices of the Royal Astronomical Society* 175, pp. 613–632.
- Shakura, Sunyaev and, (1988). 'The theory of an accretion disk/neutron star boundary layer'. In: *Advances in Space Research* 8, pp. 135–140.
- Shaposhnikov, Titarchuk and, (2002). 'The bursting behavior of 4U 1728-34: parameters of neutron star and geometry of NS-disk system.' In: *34th COSPAR Scientific Assembly*. Vol. 34.
- Strohmayer, Bildsten and, (2003). 'New views of thermonuclear bursts'. In: *arXiv preprint astro-ph/0301544*.

- Sunyaev, Revnivtsev and, (2000). 'Fourier power spectra at high frequencies: a way to distinguish a neutron star from a black hole'. In: *Astronomy and Astrophysics* 358, pp. 617–623.
- Tagger, Pellat and, (1999). 'An accretion-ejection instability in magnetized disks'. In: *arXiv preprint astro-ph/9907267*.
- Tauris, van den Heuvel and, (2006). 'Formation and evolution of compact stellar X-ray sources'. In: *Compact stellar X-ray sources* 39, pp. 623–665.
- Uttley, Cackett, Fabian, Kara, Wilkins and, (2014). 'X-ray reverberation around accreting black holes'. In: *The Astronomy and Astrophysics Review* 22.1, pp. 1–66.
- Uttley, McHardy and, (2001). 'The flux-dependent amplitude of broadband noise variability in X-ray binaries and active galaxies'. In: *Monthly Notices of the Royal Astronomical Society* 323.2, pp. L26–L30.
- Watts, (2012). 'Thermonuclear Burst Oscillations'. In: *Annual Review of Astronomy and Astrophysics* 50, pp. 609–640.
- Watts, et al. (2009). 'Discovery of burst oscillations in the intermittent accretion-powered millisecond pulsar HETE J1900. 1-2455'. In: *The Astrophysical Journal Letters* 698.2, p. L174.
- Wijnands, van der Klis and, (1998). 'A millisecond pulsar in an X-ray binary system'. In: *nature* 394.6691, pp. 344–346.
- Wijnands, van der Klis and, (1999). 'The broadband power spectra of X-ray binaries'. In: *The Astrophysical Journal* 514.2, p. 939.
- Wilms, Allen, McCray and, (2000). 'On the absorption of X-rays in the interstellar medium'. In: *The Astrophysical Journal* 542.2, p. 914.
- Zhang, Giles, Jahoda, Soong, Swank, Morgan and, (1993). 'Laboratory performance of the proportional counter array experiment for the X-ray Timing Explorer'. In: *SPIE's 1993 International Symposium on Optics, Imaging, and Instrumentation*. International Society for Optics and Photonics, pp. 324–333.
- van Doesburgh, (2014). 'Lense-Thirring Precession Around Neutron Stars With Known Spin'. MSc thesis. University of Amsterdam.
- van Straaten, van der Klis, Wijnands and, (2005). 'Relations between timing features and colors in accreting millisecond pulsars'. In: *The Astrophysical Journal* 619.1, p. 455.
- van den Eijnden, Ingram, Uttley and, (2016). 'Probing the origin of quasi-periodic oscillations: the short-time-scale evolution of phase lags in GRS 1915+ 105'. In: *Monthly Notices of the Royal Astronomical Society* 458.4, pp. 3655–3666.
- van der Klis, (1994). 'Similarities in neutron star and black hole accretion'. In: *The Astrophysical Journal Supplement Series* 92, pp. 511–519.
- van der Klis, (2000). 'Millisecond Oscillations in X-Ray Binaries'. In: *Annual Review of Astronomy and Astrophysics* 38.1, pp. 717–760.

van der Klis, (2006). 'Rapid X-ray variability'. In: *Compact stellar X-ray sources 1*, pp. 39–112.

